Natural Resources Research Institute

UNIVERSITY OF MINNESOTA DULUTH

Driven to Discover

NRRI TECHNICAL REPORT

PHASE I FUZZY-LOGIC GIS MODELING TO EVALUATE THE OCCURRENCES OF MINERAL SYSTEMS IN MINNESOTA

Submitted by:

George J. Hudak, Kristi Nixon, Joyashish Thakurta, Will Bartsch

Date: December 2022

Report Number: NRRI/TR-2022/24

Collaborators:

United States Geological Survey, Minnesota Geological Survey,
Minnesota Department of Natural Resources

Funding:

The United States Geological Survey via the FY 2021 National Geological and Geophysical Preservation Program (NGGDPP), the Minnesota Geological Survey, and the University of Minnesota Permanent University Trust Fund

Website: www.nrri.umn.edu/

NRRI Duluth // Laboratories and Admin // 5013 5013 Miller Trunk Highway, Duluth, MN 55811 // (218) 788-2694

NRRI Coleraine // Laboratories // P.O. Box 188 // One Gayley Avenue, Coleraine, MN 55722 // (218) 667-4201

Recommended Citation:
Hudak, G.J., Nixon, K., Thakurta, J., and Bartsch, W. 2022. Phase I fuzzy-logic GIS modeling to evaluate the occurrences of mineral systems in Minnesota. Natural Resources Research Institute, University of Minnesota Duluth, Technical Report NRRI/TR-2022/24. 108 p. + 8 appendices.

Keywords: fuzzy logic, GIS, critical minerals, mineral system, mineral potential

Natural Resources Research Institute
University of Minnesota, Duluth
5013 Miller Trunk Highway
Duluth, MN 55811-1442
Telephone: 218.788.2694
e-mail: nrri-reports@umn.edu

Visit our website for access to NRRI publications.

EXECUTIVE SUMMARY

Eight mineral systems potentially present in Minnesota have been evaluated using fuzzy-logic modeling utilizing ArcMap® software. Data used from the models was derived from the Natural Resources Research Institute Assembling Minnesota dataset. The eight mineral systems modeled include: 1) Placer; 2) Marine Chemocline; 3) Volcanogenic Seafloor; 4) Orogenic; 5) Metamorphic; 6) Alkalic Porphyry; 7) Magmatic REE; and 8) Mafic Magmatic. Inference nets have been developed to illustrate the fuzzy logic and components of each of the mineral system models.

Results of the modeling are summarized below by mineral systems:

Placer Mineral System: Based on the modeling, the highest probabilities for the presence of a Placer mineral system occur in northeastern Minnesota and in southwestern Minnesota. These regions correlate with the presence of the Biwabik Iron Formation, metasedimentary rocks associated with the Penokean Orogeny, and the margins of the Sioux Quartzite.

Marine Chemocline: Based on the modeling, the highest probabilities for the presence of Marine Chemocline mineral systems occur in northeastern and north-central Minnesota in rocks associated with the Animikie Basin and Penokean Orogeny strata. As well, the model indicates high probabilities for the presence of the Marine Chemocline mineral system in western and southwestern Stearns County associated with interlayered volcanic, volcaniclastic, sedimentary, and hypabyssal intrusive rocks that comprise the Mille Lacs Group, North and South Range Groups, and Glen Township Formation.

Volcanogenic Seafloor: High potential for the presence of Volcanogenic Seafloor mineral systems were identified in both the Abitibi-Wawa and Wabigoon subprovinces. In the Abitibi-Wawa subprovince, this includes the Vermilion district and the Wilson Lake sequence (Jirsa, 1990). Within the Wabigoon subprovince, enhanced potential for Volcanogenic Seafloor mineral systems occurs in east-central Lake of the Woods County and in northwestern Beltrami County. A single region of high potential for the presence of a Volcanogenic Seafloor mineral system also occurs in north-central Marshall County.

Orogenic: The highest probabilities for Orogenic mineral system-associated gold deposits occur within the Abitibi-Wawa and Wabigoon subprovinces within the northernmost one-third of Minnesota. These regions are closely-associated with regional-scale shear zones. The modeled regions correlate well with the six areas of gold exploration identified by Severson (2011), as well as a weights of evidence model developed by Hartley (2014).

Metamorphic: Several regions occur where elevated potential for Metamorphic mineral systems exist in Minnesota. The highest modeled potential for such a system exists in east-central St. Louis County and northwestern Lake County; however, this region of modeled high potential may be a false positive due to anomalously high contents of nickel (and perhaps vanadium) within Mesoproterozoic rocks in the area. Other areas with modeled high potential occur within northeastern Koochiching County and are associated with Quetico subprovince high-grade metamorphic rocks in proximity to the Rainy Lake – Seine River Fault, and in northeastern Itaca County, in proximity to the Coon Lake Pluton.

Alkalic Porphyry: Modeling conducted for this study indicates several regions where elevated potential for Alkalic Porphyry mineral systems exist. The areas with the highest modeled probability for having Alkalic Porphyry mineral systems occur in northeastern Minnesota with Lake, St. Louis, and Itasca counties.

Magmatic REE: Regions with the highest modeled potential for Magmatic REE mineral systems occur in south-central Lake County, north-central and northwestern St. Louis County, northeastern Itasca County, east-central Koochiching County, southeastern Marshall County, and east-central Stearns County. These are associated with Neoarchean syenite, monzodiorite, granodiorite, and diorite and granite-rich migmatites, Neoarchean gabbro, peridotite, pyroxenite, lamprophyre and metamorphic equivalents, and Paleoproterozoic porphyritic granites.

Mafic Magmatic: Fuzzy-logic modeling indicates the highest probability for the presence of Mafic Magmatic mineral systems occurs in northeastern Lake County, east-central St. Louis County, and within eastern Aitkin County. The model identified known disseminated-to-massive Cu-Ni-PGM deposits that occur in troctolitic rocks at the base of the Duluth Complex in Lake and St. Louis counties, as well as Ti-V-oxide deposits and prospects associated with oxide ultramafic intrusions (peridotites, pyroxenites) that occur along the western margin of the Duluth Complex in central St. Louis County. As well, the model identified the location of the Tamarack intrusion in eastern Itasca County, the host of the Tamarack Ni-Cu-Co deposit.

TABLE OF CONTENTS

LIST OF FIGURES

LIST OF TABLES

LIST OF APPENDICES

INTRODUCTION

As a component of National Geological and Geophysical Data Preservation Program (NGGDPP) fiscal year 2021 (FY21) and University of Minnesota Permanent University Trust Fund (PUTF) grants, researchers from the Natural Resources Research Institute (NRRI) at the University of Minnesota Duluth developed knowledge-driven fuzzy logic models for several United State Geological Survey (USGS) mineral systems (Hofstra and Kreiner, 2021) that may be present in the state. This report discusses the general characteristics of the eight mineral systems modeled, the methods utilized to develop the knowledge-based fuzzy logic models for each of the mineral systems, and the results of the geographic information system (GIS)-based mineral system modeling

Mineral systems incorporate a number of mineral deposit types and conceptualize how mineral deposit types form in relation to the "broader geological framework and tectonic history of the Earth" (Hofstra and Kreiner, 2021). They provide a framework to understand various relationships that are known or inferred to exist between mineral system types, mineral deposit environments, and mineral deposit types (Hofstra et al., 2021). Mineral systems with genetically related mineral deposits commonly form during a period involving magmatism, metamorphism, deformation, sedimentation, weathering, or erosions within individual geotectonic settings (Hofstra and Kreiner, 2021). According to Hofstra and Kreiner (2021), mineral systems encompass all the components necessary for mineral deposits genesis, including:

- Geotectonic setting
- Energy for development and maintenance of the system
- Source rocks for the chemical components (ligands, metals)
- Transport mechanisms
- Transport pathways
- Chemical and/or physical traps for concentrating metals to form mineral deposits
- Mineralogical, chemical, or thermal components of the system that extend to the limits of the system (e.g. alteration zones)

There have been fundamental changes in recent years from studying individual mineral deposit types (e.g. magmatic copper-nickel-platinum group element (PGE) deposits, volcanic-associated massive sulfide deposits, lode gold deposits, etc.) to studying mineral systems. This is fundamentally a result of the ability for geoscientists to develop and analyze large datasets.

Fuzzy-logic modeling has been used to model mineral potential in many studies (examples include but are not limited to Bonham-Carter et al., 1989; Bonham-Carter, 1994; Bonham-Carter et al., 1996; Peterson, 2001; Porwal et al., 2003; Galetakis and Vasiliou, 2012; Abedi et al., 2013; Lindsay et al., 2014; Saljoughi et al., 2018; Niiränen et al., 2019; Ma et al., 2020; Behera and Panigrahi, 2021). Many of these researchers utilize knowledge-driven models which apply geoscientists knowledge of a mineral system components to decide which components of the model are most important, and subsequently ranking the components in order of importance to the model by utilizing weights of evidence (W.O.E.) to develop the model (Peterson, 2001; Abedi et al., 2013).

Fuzzy-logic modeling has both advantages and disadvantages. Advantages include: 1) fuzzy logic models are similar in structure to human reasoning; 2) the structure of fuzzy logic generally can be easily understood; 3) computer memory can be minimized, as stems can be described with less data; 4) it can provide effective solutions to complex problems; 5) the concept is simple, as it is based on mathematical set theory; 6) development time for fuzzy logic models is relatively short; and 7) it is a flexible method. Disadvantages of fuzzy logic models include: 1) run times can take long periods of time to produce outputs; 2) the fuzzy logic method must be simple to be fully understood; 3) fuzzy logic models are not always accurate; 4) solutions may not be unique, as different modelers may use different fuzzy logic techniques; 5) fuzzy logic models are not applicable to solve problems that require a high degree of accuracy; and 6) verification and validation of fuzzy logic models requires significant testing.

Knowledge-driven fuzzy-logic modeling (Bonham-Carter et al., 1993; Peterson, 2001; Saljoughi et al., 2018; Behera and Panigrahi, 2021) was utilized in this study to evaluate eight potential mineral systems that may occur within Minnesota. The mineral systems modeled include:

- Placer
- Marine Chemocline
- Volcanogenic Seafloor
- Orogenic
- Metamorphic
- Alkali Porphyry
- Magmatic Rare Earth Element (REE)
- Mafic Magmatic

The originally proposed "Chemical Weathering" mineral system modeling could not be performed due to a lack of sufficient data. Budget and time limitations did not permit the Basin Brine Path mineral system model to be developed and performed. This mineral system also appears to have been active in Minnesota (Severson and Heine, 2003; Severson et al., 2003).

The NRRI GIS-database "Assembling Minnesota" (Bartsch et al., 2022; Peterson, 2018) was utilized for the GIS-based fuzzy-logic modeling. This database represents a robust compilation of government records available so far, as well as academic and industry geological studies into a seamless Minnesota state-wide GIS database. There are four main components and numerous subcomponents to this dataset, including (from Peterson, 2018):

- Geology
    - Precambrian Geology Map – a polygon theme that represents a seamless detailed Precambrian bedrock geology map of Minnesota. The map is based largely on Minnesota Geological Survey State Map Series S-22 (Jirsa et al., 2012) with additional detailed geological mapping from a variety of industry and academic sources.
    - Geolines – a polyline theme including geological contacts and faults
    - Geosymbols – a point theme indicating classified geologic features and structures
    - Outcrops – a polygon theme indicating the locations of exposed bedrock as well as numerous up-dip projections of geology present in diamond drill holes

    - Geochemisty – a point theme indicating the locations and analyses for a variety of geochemical analyses (bedrock outcrops, drill core, till, soil, seeps, and lake sediments)
    - Depth to Bedrock – an image representing the depth to bedrock statewide
- Geophysics
    - State Gravity – a georeferenced 500-meter gridded color .tif image (after Chandler and Lively, 2011)
    - State Magnetics – four 100-meter gridded shaded relief .tif images (after Chandler, 1982)
    - Airborne Electromagnetic (EM) Survey Boundary – a polyline theme with boundaries of airborne geophysical surveys obtained from the Minnesota Department of Natural Resources.
    - Airborne EM – a point theme of airborne electromagnetic (EM) anomalies obtained from the Minnesota Department of Natural Resources
    - Airborne EM Interpretations – a polyline theme containing digitized interpretations of airborne EM maps obtained from the Minnesota Department of Natural Resources
    - Helicopter EM Points – a point theme of helicopter EM survey data obtained from the Minnesota Department of Natural Resources
    - Helicopter EM Interpretation – a polyline theme containing digitized interpretations of helicopter EM maps obtained from the Minnesota Department of Natural Resources
    - Ground EM – a polyline theme digitized from exploration company maps obtained from the Minnesota Department of Natural Resources
- Mineral Occurrences
    - NRRI Mineral Occurrences – a polygon theme comprising rock-based mineral occurrences obtained from the NRRI_MinOccur_ datasets (rocks, drill core, prospects)
- Miscellaneous
    - NRRI Gold Potential Model – a polygon theme comprising the gold potential model of Peterson, 2001
    - DC Mineral Resources – a polygon theme of historic NI 43-101 compliant mineral resources associated with the Duluth Complex
    - NRRI Mesabi Tailings – a polygon theme illustrating Mesabi Range tailings basins
    - NRRI Mesabi Stockpiles – a polygon theme illustrating stockpiles on the Mesabi Range
    - NRRI Mesabi Mine Features – a polygon theme illustrating mine features associate with Minnesota's Mesabi Range

Individual mineral system models (including attributes of individual models, methods utilized for modeling individual mineral systems, and the results of the mineral system models) will be described in detail below.

MINERAL SYSTEMS POTENTIALLY PRESENT IN MINNESOTA

A General Summary of Minnesota Geology

The geology of Minnesota encompasses numerous bedrock geological terranes and unconsolidated sedimentary deposits that range from Paleoarchean to Quaternary in age (Ojakangas, 2009). A geological history of more than 3.5 billion years represented in Minnesota's geological materials encompasses a wide variety of geological processes and has enabled the potential for a diverse collection of mineral systems to be present in the state. Readers of this report are directed to the Minnesota Geological Survey website to obtain more information about the geology in the state.

Figure 1 illustrates the geological map of Minnesota, including major Precambrian subprovinces (labeled in dark red) and major Precambrian-age geological structures (in green). These subprovinces and geological terranes will be described below in terms of their geographic locations within the state.

Northwestern Minnesota: The northwestern one-third of Minnesota comprises Neoarchean-age granite greenstone terranes (Wabigoon Subprovince and Abitibi-Wawa Subprovince). These two subprovinces comprise Neoarchean-age, typically greenschist-facies metamorphosed volcanic, sedimentary, and plutonic rocks. Many of the supracrustal rocks are interpreted to have formed in submarine settings. These two subprovinces contain numerous shear zones interpreted to have formed from transpressional tectonic forces during the accretion of the Canadian Shield. The Wabigoon and Abitibi-Wawa subprovinces are separated by the Quetico Subprovince, which comprises medium- to high-grade metamorphosed metasedimentary rocks and associated granitoid intrusions.

Northeastern and Eastern Minnesota: Northeastern Minnesota as well as a region which trends south-southwest through southern Minnesota are regions of rocks formed during the 1.1-billion-year-old Midcontinent (Keweenawan) Rift. During this time, the North American continent underwent extension in regions that extend northeastward from Kansas to Lake Superior, and southeastward from Lake Superior through Michigan and Ohio. This geological event was associated with the Keweenawan Large Igneous Province (Nicholson et al., 1992), which produced enormous volumes of intrusive and volcanic rocks and associated rift-fill clastic sedimentary strata.

North-Central Minnesota: North-Central Minnesota comprises a sequence of low-grade metamorphosed chemical and clastic sedimentary rocks that are associated with the development of the Animikie Basin between approximately 1.8–2 billion years ago. This assemblage of rocks contains the Biwabik Iron Range, a region where the majority of iron ore produced in the United States has occurred over the past 120 years. To the southwest of the Animikie Basin, a series of structurally deformed metavolcanic, metasedimentary and associated intrusive rocks, also ranging in age from 1.8–1.9 billion years old, comprise the Penokean Orogen terrane.

Southwestern Minnesota: The southwestern part of Minnesota comprises high-grade metamorphosed supracrustal rocks (sedimentary, volcanic) and associated granitoid intrusions and gneisses. This region is referred to as the Minnesota River Valley subprovince. The high-grade metamorphosed rocks in the Minnesota River Valley subprovince are Paleoarchean in age (Boerboom, 2021) and represent the oldest rocks in Minnesota.

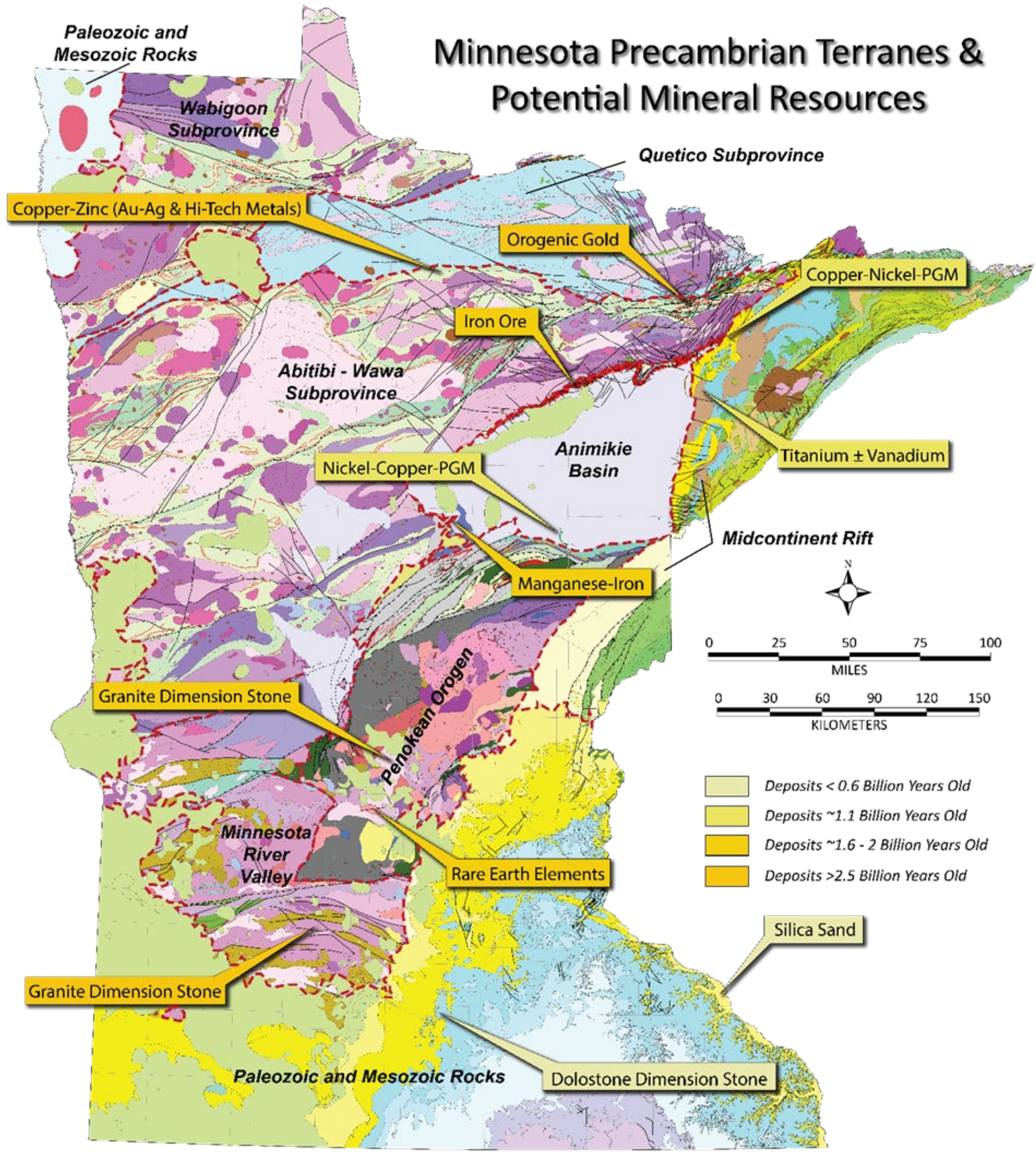

Figure 1. Generalized geological map of Minnesota indicating various prospective mineral deposits types (modified from Jirsa et al., 2011). Precambrian terranes are identified in dark red lines and black text. Modified after Jirsa et al. (2012) with terrane references from US Geology and Geomorphology website.

Potential Mineral Systems in Minnesota

The diverse geological history of Minnesota's geological terranes permits a wide variety of mineral systems to have been active at different time-intervals. Based on lithological associations, permissive mineral systems in Minnesota include:

- Wabigoon Subprovince: Volcanogenic Seafloor, Orogenic, Magmatic REE
- Abitibi-Wawa Subprovince: Volcanogenic Seafloor, Orogenic, Magmatic REE
- Quetico Subprovince: Metamorphic, Magmatic REE, Orogenic
- Midcontinent Rift Terrane: Mafic Magmatic
- Animikie Basin Terrane: Marine Chemocline, Placer
- Penokean Orogen Terrane: Volcanogenic Seafloor, Marine Chemocline, Basin Brine Path, Magmatic REE, Placer
- Minnesota River Valley Subprovince: Metamorphic, Magmatic REE

Mineral System Modeling

Eight mineral systems potentially present in Minnesota were evaluated using GIS-based, knowledge-based fuzzy-logic modeling. The eight mineral systems evaluated include: 1) Placer; 2) Marine Chemocline; 3) Volcanogenic Seafloor; 4) Orogenic; 5) Metamorphic; 6) Alkalic Porphyry ; 7) Magmatic REE; and 8) Mafic Magmatic.

Mineral system modeling was completed using ESRI ArcMap software. All mineral system models were completed using the North American Datum 1983 (NAD83) Zone 15 north projection. Details regarding each of the mineral system models produced for this report are presented below. Digital appendices 1-8 contain shapefiles and model calculations associated with each of the models.

Placer Mineral System

Deposit Types and Model

The Placer mineral system includes mineral deposits that form from the weathering, erosion, transportation, and ultimately, concentration of high specific gravity (>2.5 g/cm^3), chemically resistant minerals in sedimentary environments (Garnett and Bassett, 2005). These systems occur along shorelines or within fluvial systems associated with significant topographic relief (Garnett and Bassett, 2005; Hofstra and Kreiner, 2021). Water is the typical transporting agent, although wind currents may also allow separation of valuable minerals via size and/or gravity separation. The ultimate concentration of these heavy mineral deposits is commonly the result of a cyclic process involving both erosion and deposition (Patyk-Kara, 1976).

Table 1 indicates the various mineral deposit types associated with the Placer mineral system. For more detailed information on placer deposits, the reader is referred to Garnett and Bassett (2005), Van Gosen et al. (2014), Jones et al. (2017), and Dhinesh et al. (2021).

Table 1. Systems-Deposits-Commodities-Critical Minerals table for the ***Placer*** mineral system (modified after Hofstra and Kreiner, 2021). Explanation for table is as follows: ±, present (absent); --, not applicable; ?, maybe; Ag, silver; Al, aluminum; As, arsenic; Au, gold; B, boron; Ba, barium; Be, beryllium; Bi, bismuth; Br, bromine; Ca, calcium; Cd, cadmium; Co, cobalt; CO_2, carbon dioxide; Cs, cesium; Cr, chromium; Cu, copper; F, fluorine; Fe, iron; Ga, gallium; Ge, germanium; Hf, hafnium; Hg, mercury; I, iodine; IAEA, International Atomic Energy Agency; In, indium; IOA, iron oxide-apatite; IOCG, iron oxide-copper-gold; IS, intermediate sulfidation; K, potassium; LCT, lithium-cesium-tantalum; Li, lithium; Mg, magnesium; Mn, manganese; Mo, molybdenum; Na, sodium; Nb, niobium; Ni, nickel; NYF, niobium-yttrium-fluorine; P, phosphorus; Pb, lead; PGE, platinum group elements; R, replacement; Rb, rubidium; Re, rhenium; REE, rare earth elements; S, skarn; Sb, antimony; Sc, scandium; Se, selenium; Sn, tin; Sr, strontium; Ta, tantalum; Te, tellurium; Th, thorium; Ti, titanium; U, uranium; V, vanadium (in "Principal Commodities" column); V, vein (in "Deposit Types" column); W, tungsten; Y, yttrium; Zn, zinc; Zr, zirconium. In the "Critical Minerals" column, elements in **bold** have been produced from the deposit type, whereas elements in *italics* are enriched in the deposit type but have not been produced.

System Name	Deposit Types	Principal Commodities	Critical Minerals	References
Placer (riverine – marine-eluvial-alluvial-shoreline, paleo)	Gold	Au	--	Sloan, 1964; Levson, 1995; Van Gosen et al., 2014; Sengupta and Van Gosen, 2016; Jones et al., 2017; Wang et al., 2021
	Uraninite, autunite-group minerals	U	**U**	
	Platinum Group Elements (PGE)	PGE	**PGE**	
	Cassiterite	Sn	**Sn**, Sc	
	Wolframite/Scheelite	W	**W**, Sc	
	Barite	Barite ($BaSO_4$)	**Barite**	
	Fluorite	Flourite (CaF_2)	**Fluorite**	
	Monazite/Xenotime	REE, Y, Th	**REE**	
	Columbite/Tantalite	Nb, Ta	**Nb, Ta,** *Mn*	
	Zircon	Zr, Hf	**Zr, Hf**	
	Ilmenite/Rutile/Leucoxene	Ti	**Ti,** *Sc*	
	Magnetite/Hematite/Geothite	Fe	*V*	
	Diamond	Diamond gems and abrasives	--	
	Sapphire	Sapphire gems	--	
	Garnet	Garnet gems and abrasives	--	

Economically important features of placer deposits and mineral systems have been discussed by Garnett and Bassett (2005) and Hofstra and Kreiner (2021). Features that are considered economically important include, but are not limited to:

- bedrock lithology and morphology;
- the heavy minerals present and their physical characteristics;
- favored sites of mineral concentration which depend on transport medium energy levels;
- transport distance; and
- post-depositional processes.

Jones et al. (2017) note that understanding and identifying the distribution, geometry and evolution of paleoshorelines is a key component for exploration for new deposits.

Economically significant placer deposits can comprise a variety of mineral species, including native elements (diamonds, gold, silver, platinum group elements), oxides (sapphire, magnetite, hematite, wolframite, cassiterite, columbite, tantalite, uraninite, ilmenite, rutile, and associated leucoxene), hydroxides (goethite), phosphates (monazite, xenotime, autunite), tungstates (scheelite), sulfates (barite), fluorides (fluorite), and silicates (zircon, garnet). Principal commodities associated with placer deposits include Au, U, platinum group elements (PGE), tin, tungsten, rare earth elements (REE), yttrium, thorium, niobium, tantalum, zirconium, hafnium, titanium, and iron, as well as the minerals barite, fluorite, diamonds, corundum (sapphire), and garnet. Critical metals associated with placer deposits include uranium, PGE, tin, scandium, tungsten, niobium, tantalum, zirconium, hafnium, and titanium, as well as manganese, scandium, and vanadium (Hofstra and Kreiner, 2021).

Modeling Methods

It is difficult to evaluate paleotopography and paleoshoreline characteristics in generally steeply dipping, commonly poorly-exposed Precambrian environments such as those in Minnesota. As a result, the fuzzy-logic modeling methodology for this study included five components that could be ascertained from the Assembling Minnesota dataset (Bartsch et al., 2022; Peterson, 2018). These five components include: 1) bedrock geology; 2) mineral occurrences; 3) geochemistry; 4) geophysics; and 5) geologic structures. The inference net illustrating the various components used in the Placer Mineral System model are illustrated in Figure 2.

Bedrock geology focused on three main components. Permissible host rock type (conglomerate, sandstone/quartzite, and graywacke) polygons were extracted from the database and given a W.O.E. based on their prospectivity for hosting placer mineralization. Proximity to potential igneous heavy mineral source rocks was modeled by extracting intrusive rock – sedimentary rock contacts (lines), developing a 1-kilometer (1km) buffer for these contacts, and providing the resulting polygon a W.O.E. of 0.7. Locations of stratigraphic contacts were utilized as a proxy for changes in energy and/or source within depositional environments. These geologic features (lines) were classified and extracted from the database, given a 1km buffer, and the resulting polygons provided a W.O.E. of 0.6. This was done to indicate permissible regions where placer deposits may occur. Weights of evidence for the various lithological units utilized in the model are provided in Table 2. The various polygons values were added and normalized for the Geology Factor utilized in the model.

Mineral occurrences (point data) for mineral species commonly associated with placer deposits were extracted from the Assembling Minnesota mineral occurrence database. Based on the minerals present in this database, the following mineral species were utilized for the model: 1) ilmenite; 2) chromite; 3) magnetite; 4) oxides (not specifically identified); 5) gold (native); and 6) garnet. Each of these minerals was given a W.O.E. of 1, and the point locations were given a 1km buffer. The total number of overlapping mineral polygons present at any one site was summed and normalized to develop the mineral factor.

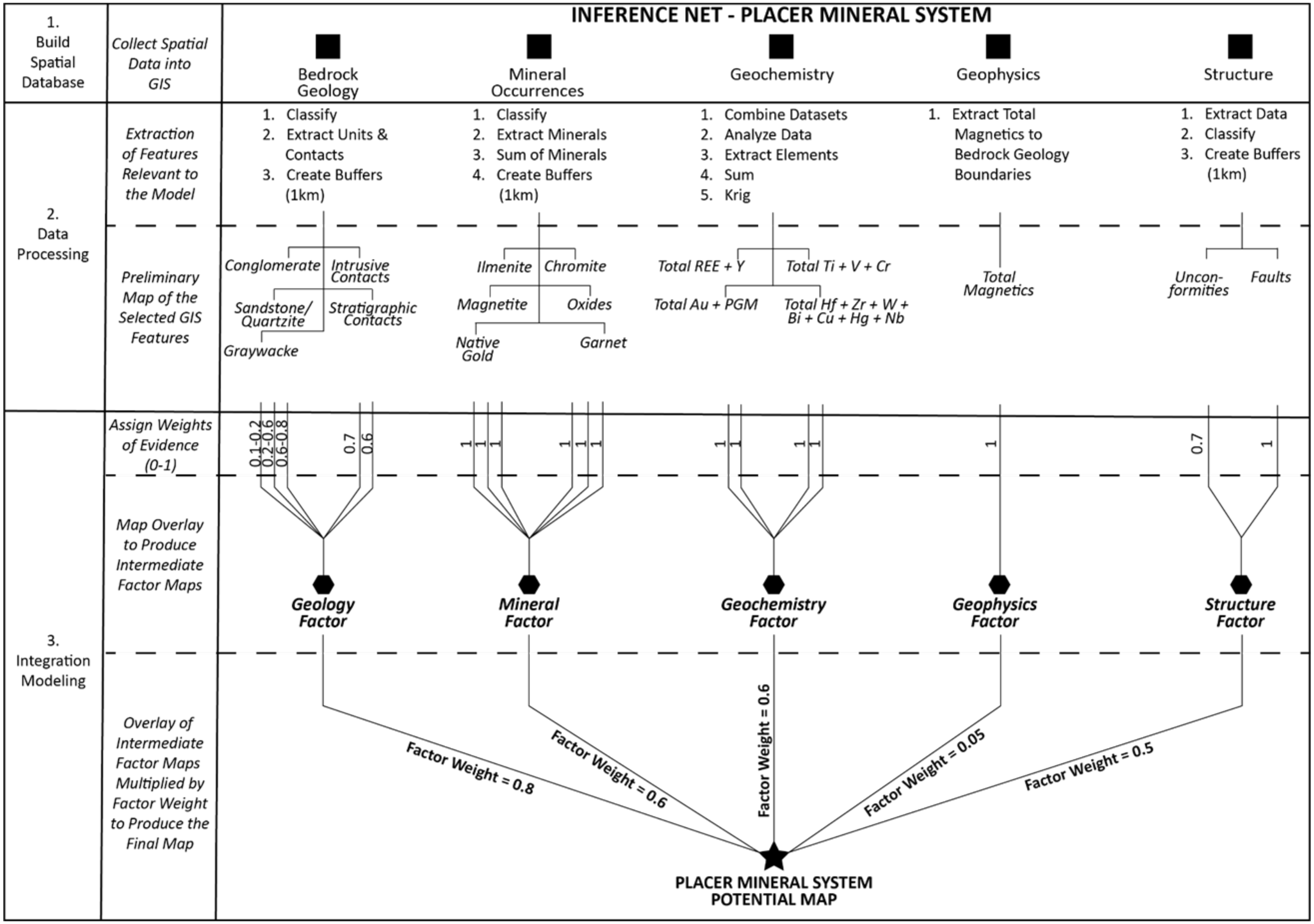

Figure 2. Inference Net for ***Placer*** Knowledge-based GIS model.

Table 2. Weights of evidence for geology polygons in the ***Placer*** mineral system model.

Map Label	Era	Rock Type	Model W.O.E.
Aas	Neoarchean	Arkosic and lithic sandstone	0.8
Mbss	Mesoproterozoic	Basal sandstone/quartzite	0.8
Acg	Neoarchean	Conglomerate	0.8
Acg	Neoarchean	Conglomerate and arkosic sandstone	0.8
Acg	Neoarchean	Conglomerate and lithic sandstone	0.8
Acg	Neoarchean	Conglomerate and related rocks, Timiskaming-Type	0.8
Acg	Neoarchean	Conglomerate and related rocks, Timiskaming-Type	0.8
Acg	Neoarchean	Conglomerate and volcaniclastic sandstones	0.8
Acg	Neoarchean	Conglomerate with arkosic and lithic sandstone	0.8
Pmq	Paleoproterozoic	Dam Lake Quartzite	0.8
Aas	Neoarchean	Lithic and arkosic sandstone	0.8
Ppq	Paleoproterozoic	Quartzite with siliceous mudstone and conglomeratic rocks	0.8
Psq	Paleoproterozoic	Quartzite, mudstone, conglomerate	0.8
Aszcgl	Neoarchean	Sheared and altered conglomerate	0.8
Aszcgl	Neoarchean	Sheared conglomerate	0.8
Aas	Neoarchean	Lithic sandstone, mudstone, and siliceous siltstone with detrital hbld and plag	0.6
Acg	Neoarchean	Conglomerate, lithic sandstone, graywacke, mudstone	0.6
Aas	Neoarchean	Lithic sandstone, mudstone, and siliceous siltstone with detrital hbld and plag	0.6
Aks	Neoarchean	Slate, siltstone, lithic sandstone, and conglomerate	0.6
Pvf	Paleoproterozoic	Greywacke, mudstone, and argillite	0.4
Prf	Paleoproterozoic	Greywacke, siltstone and argillite	0.4
Acgm	Neoarchean	Partially melted conglomerate	0.4
Acgm	Neoarchean	Partially melted conglomeratic rocks	0.4
Afvtb	Neoarchean	Dacitic to andesitic tuff, breccia, and epiclastic products	0.2
Afvu	Neoarchean	Dacitic tuff, lapilli tuff, and epiclastic deposits	0.2
Afve	Neoarchean	Dacitic volcanic conglomerate with stretched plag-phyric clasts	0.2
Pmd	Paleoproterozoic	Denham Formation; sandstone, marble, schist	0.2
Prfm	Paleoproterozoic	Disrupted and melted metasedimentary rocks	0.2
Pmda	Paleoproterozoic	Dolomitic arkose sandstone	0.2
Afve	Neoarchean	Epiclastic dacitic sediments and conglomerate	0.2
Afve	Neoarchean	Epiclastic Dacitic Volcanoclastic Rocks	0.2
Afvt	Neoarchean	Felsic Debris Flow Deposits	0.2
Afvt	Neoarchean	Felsic Debris Flow Deposits	0.2
Afve	Neoarchean	Felsic Epiclastic Rocks	0.2
Afvt	Neoarchean	Felsic tuff and epiclastic rocks	0.2
Afvt	Neoarchean	Felsic tuff and locally epiclastic rocks	0.2
Afvu	Neoarchean	Felsic volcanic and related tuffaceous and epiclastic rocks	0.2
Ags	Neoarchean	Graywacke and mudstone; typically greenschist facies metamorphism	0.2
Ags	Neoarchean	Greywacke and slate	0.2
Pag	Paleoproterozoic	Greywacke slate	0.2
Ags	Neoarchean	Greywacke-slate	0.2
Ags	Neoarchean	Greywacke-slate, mixed sourced	0.2
Ags	Neoarchean	Interbedded greywacke-slate	0.2
Mifs	Mesoproterozoic	Interflow conglomerate	0.2
Mifs	Mesoproterozoic	Interflow lithic-arkosic sandstone	0.2
Mifs	Mesoproterozoic	interflow sandstone	0.2
Mcc	Mesoproterozoic	Interflow sandstone, metamorphosed	0.2
Mifs	Mesoproterozoic	Interflow sandstone/shale	0.2
Mbx	Mesoproterozoic	Matrix supported volcanic breccia/conglomerate	0.2
Afve	Neoarchean	Mixed dacitic volcaniclastics, tuff-breccia-conglomerate	0.2
Pm	Paleoproterozoic	Mudstone, quartzite, graywacke, phyllite, graphitic argillite	0.2
Mifs	Mesoproterozoic	Sandstone	0.2
Afvt	Neoarchean	Siliceous sediment and/or felsic tuff	0.2
Pag	Paleoproterozoic	Slate, graywacke	0.2
Mcc	Mesoproterozoic	Thermally metamorphosed, cross-bedded, interflow sandstone	0.2
Afvtb	Neoarchean	Volcanic breccia/conglomerate, highly deformed	0.2
Mbx	Mesoproterozoic	Volcaniclastic conglomerate	0.2
Ams	Neoarchean	Biotite schist	0.1
Aqs	Neoarchean	Biotite schist, paragneiss, and schist-rich migmatite	0.1
Aqs	Neoarchean	Biotite-calcite-magnetite schist	0.1
Ams	Neoarchean	Biotitic metagreywacke-slate	0.1
Pgs	Paleoproterozoic	Graywacke, slate with graphitic and sulfidic zones	0.1
Amss	Neoarchean	Partially melted sandstone	0.1
Ams	Neoarchean	Schist of sedimentary protolith	0.1
Pac	Paleoproterozoic	Virginia Formation slate with thin limestone interbeds	0.1

Geochemical data (point data) were extracted from the Assembling Minnesota bedrock geology geochemistry and drillhole geochemistry databases. These databases were merged to develop the point data utilized in the model. Four sums were calculated from the datasets, including 1) total rare earth elements (REE) + yttrium (Y); 2) total titanium (Ti) + vanadium (V) + chromium (Cr); 3) total gold (Au) + platinum group metals (PGM; platinum, palladium, rhenium, osmium, ruthenium, iridium); and 4) total hafnium (Hf) + zirconium (Zr) + tungsten (W) + bismuth (Bi) + copper (Cu) + mercury (Hg) + niobium (Nb). Kriging of the normalized sums was performed to develop surface rasters, and the raster values were classified and converted to polygons for the Geochemistry Factor utilized in the model.

The geophysics factor was determined utilizing total magnetics data (Chandler, 1982). This data was extracted to the bedrock geology boundaries and subsequently normalized and reclassified into 10 quantile classes (1–10) to create the polygons for the Geophysics factor utilized in the model.

Two types of geological structures (lines) were utilized for the modeling. Unconformities were utilized in the model to locate potential erosional periods in geological history. These geologic features were classified and extracted from the database, provided a 1km buffer, and the resulting polygons were assigned a W.O.E. of 0.7. Faults were utilized as a proxy for paleotopographic relief. These geologic features (lines) were classified and extracted from the database, given a 1km buffer, and the resulting polygons were provided with a W.O.E. of 1. These two sets of polygons, with their respective W.O.E., were merged to develop the Structure Factor utilized in the model.

The final Placer Mineral System Potential Map was developed by multiplying each of the model factors by their assigned factor weights and then calculating the fuzzy algebraic sum by means of the following equation (Bonham-Carter, 1994; Peterson, 2001):

$$\mu_{\text{combination}} = 1 - \prod_{i=1}^{n}(\mu i)$$

where μi is the fuzzy membership value for the i^{th} map and i = 1. 2. 3, ….n maps are to be combined.

According to Peterson (2001), this operator is well suited for mineral potential mapping where evidence of economic mineralization is scarce. The fuzzy algebraic sum operator is consistent with the hypothesis that if two lines of evidence support one another, the combined evidence is more supportive than each line of evidence individually.

The factor weights assigned for each of the model factors are as follows:

- Geology Factor Weight = 0.8
- Mineral Factor Weight = 0.6
- Geochemistry Factor Weight = 0.6
- Geophysics Factor Weight = 0.05
- Structure Factor Weight = 0.5

Results

The Placer Mineral System Potential Map is illustrated in Figure 3 (with a Minnesota geology map underlay) and in Figure 4 (without the Minnesota geology map underlay). Shapefiles for the Placer Mineral System Potential Map can be found in Digital Appendix 1 in the subdirectory labeled “Shapefiles.” Model calculations can be found in Digital Appendix 1 in the subdirectory labeled “Model Calculations.”

Based on the modeling, the highest probabilities for the presence of a Placer mineral system occur in northeastern Minnesota and in southwestern Minnesota. In northeastern Minnesota, Placer mineral system probabilities are highest within footwall rocks to the Biwabik iron formation, along with rocks immediately up-section from the Biwabik iron formation in the Virginia formation. Elevated potential for Placer mineral systems occur in metasedimentary rocks associated with the Penokean orogeny in northern and southern Crow Wing County and the southwestern part of Aitkin County. In southwestern Minnesota, elevated potential for Placer mineral systems occurs in southern Lincoln county, southwestern Lyon county, southern Nobles county, and in Cottonwood, Watonwan, and Martin counties. These areas correspond to the margins of the Paleoproterozoic Sioux Quartzite (Jirsa et al., 2012).

Marine Chemocline Mineral System

Deposit Types and Model

The Marine Chemocline mineral system includes a variety of mineral deposit types that form as a result of deposition of metals from basin brines within the ocean (Hofstra and Kreiner, 2021). These include manganese- and iron-bearing mineral deposits that occur as a result of deposition on the margins of stable cratons as a result of redox reactions in various depositional sedimentary environments (Blatt and Tracy, 1997; Clout and Simonson, 2005; Trendall and Blockley, 2004; Cannon et al., 2017). Iron-rich deposits formed on the margins of stable cratons are believed to form in shallow-water, higher energy environments where oxidation of ferrous iron to ferric iron produces deposition of iron-bearing oxide, hydroxide, and carbonate minerals. Such iron-rich rocks commonly contain greater than 15% iron by weight and are referred to as iron formations (James, 1954). This type of iron-formation is characterized by a granular texture and is commonly referred to as granular iron formation (GIF) or Superior-type iron formation (Blatt and Tracy, 1997; Trendall and Blockley, 2004). GIF / Superior-type iron formations post-date the Great Oxidation Event. According to Gumsley et al. (2017), the Great Oxidation Event occurred between 2060 Ma and 2460Ma; Warke et al. (2020) have further constrained the age of the Great Oxidation Event to between 2434Ma and 2501Ma based on sulfur isotopic evidence. Manganese-bearing strata are commonly associated with iron-bearing strata such as GIF. According to Cannon et al. (2017), interlaying of iron-rich and manganese-rich clastic sedimentary deposits reflects deposition of these two metals in different physiochemical environments associated with a stratified ocean in which deeper waters are suboxic to anoxic (but not sulfidic) and shallow waters are oxidized. Manganese-rich deposits form in these deeper suboxic to anoxic environments and are often associated with black shale deposits, whereas the iron-rich deposits (e.g. GIF) form in shallower water, higher-energy, oxidized environments.

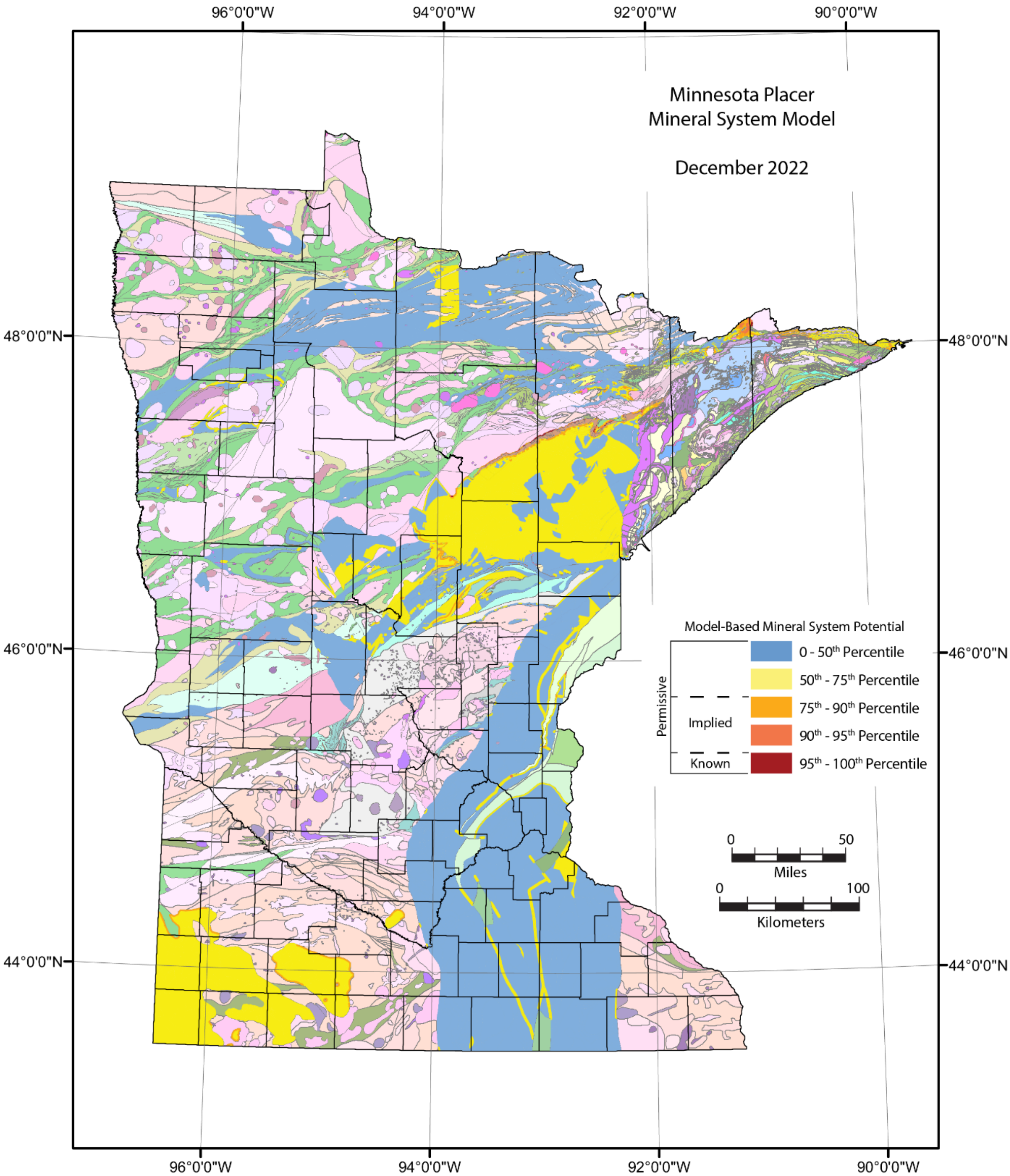

Figure 3. Results of ***Placer*** knowledge-based mineral system model with geology.

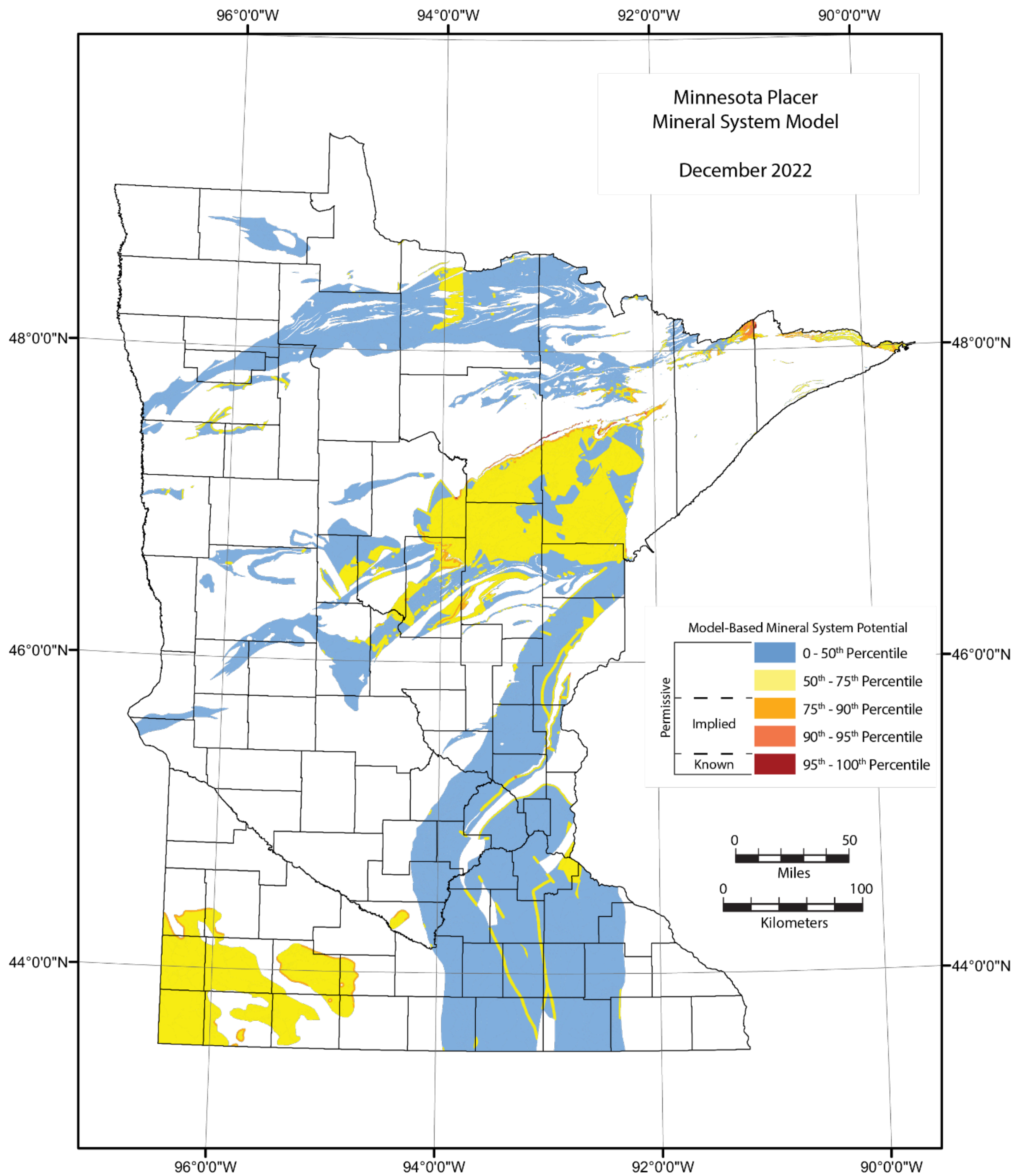

Figure 4. Results of ***Placer*** knowledge-based mineral system model without geology.

Table 3 indicates the various mineral deposit types associated with the Marine Chemocline mineral system. Minnesota's geology dictates that the fuzzy logic Marine Chemocline mineral system model developed for this study focus on iron-manganese and Superior iron deposits. Detailed descriptions and economically important features of these deposit types have been discussed by Blatt and Tracy (1997), McSwiggen et al. (1995), Trendall and Blockley (2004), Clout and Simonson (2005), Cannon et al. (2017), Hofstra and Kreiner (2021), and references therein.

Table 3. Systems-Deposits-Commodities-Critical Minerals table for the ***Marine Chemocline*** mineral system (modified after Hofstra and Kreiner, 2021). Explanation for table is as follows: ±, present (absent); --, not applicable; ?, maybe; Ag, silver; Al, aluminum; As, arsenic; Au, gold; B, boron; Ba, barium; Be, beryllium; Bi, bismuth; Br, bromine; Ca, calcium; Cd, cadmium; Co, cobalt; CO_2, carbon dioxide; Cs, cesium; Cr, chromium; Cu, copper; F, fluorine; Fe, iron; Ga, gallium; Ge, germanium; Hf, hafnium; Hg, mercury; I, iodine; IAEA, International Atomic Energy Agency; In, indium; IOA, iron oxide-apatite; IOCG, iron oxide-copper-gold; IS, intermediate sulfidation; K, potassium; LCT, lithium-cesium-tantalum; Li, lithium; Mg, magnesium; Mn, manganese; Mo, molybdenum; Na, sodium; Nb, niobium; Ni, nickel; NYF, niobium-yttrium-fluorine; P, phosphorus; Pb, lead; PGE, platinum group elements; R, replacement; Rb, rubidium; Re, rhenium; REE, rare earth elements; S, skarn; Sb, antimony; Sc, scandium; Se, selenium; Sn, tin; Sr, strontium; Ta, tantalum; Te, tellurium; Th, thorium; Ti, titanium; U, uranium; V, vanadium (in "Principal Commodities" column); V, vein (in "Deposit Types" column); W, tungsten; Y, yttrium; Zn, zinc; Zr, zirconium. In the "Critical Minerals" column, elements in **bold** have been produced from the deposit type, whereas element in *italics* are enriched in the deposit type but have not been produced.

System Name	Deposit Types	Principal Commodities	Critical Minerals	References
Marine chemocline (bathtub rim)	Black shale	Stone coal, petroleum, V, Ni, Mo, Au, PGE	**V,** *Re, PGE, Cr, U*	Lefebure and Coveney, 1995; Force et al., 1999; Emsbo, 2000; Emsbo et al., 2015; Cannon et al., 2017
	Phosphate	Phosphate fertilizer	***F, REE, Cr, U***	
	Iron-manganese	Fe, Mn, Co	**Mn, Co**	
	Superior iron	Fe	*Mn*	

Geologically important criteria for evaluating the presence of iron manganese and Superior iron deposits require geological, mineralogical, geochemical, and geophysical studies (Cannon et al., 2017). Key features that can be utilized to evaluate the potential presence of iron- and/or manganese deposits associated with the Marine Chemocline mineral system include:

- The presence of Proterozoic- or younger-age chemical sedimentary deposits formed along the margins of continental craton;
- The presence of iron- and manganese oxide, carbonate, and hydroxide minerals;
- Elevated lithogeochemical concentrations of iron and/or manganese; and
- An enhanced magnetic component of rocks associated with iron and/or manganese deposits due to the presence of magnetite in these deposits.

These features have been utilized in the development of the knowledge-based fuzzy logic model for the Marine Chemocline mineral system, and their utilization in the model is discussed below.

Modeling Methods

Based on Minnesota's geology, the fuzzy logic model developed for this study focused on two major types of Marine Chemocline associated mineral deposit types. These deposit types are iron-manganese and Superior iron as indicated above. The knowledge-based fuzzy-logic modeling methodology for this study included four components that could be ascertained from the Assembling Minnesota dataset (Bartsch et al., 2022; Peterson, 2018). These four components include: 1) bedrock geology; 2) mineral occurrences; 3) geochemistry; and 4) geophysics. The inference net illustrating the various components used in the Placer Mineral System model is illustrated in Figure 5.

The bedrock geology component (polygons) included two key geological features: 1) Superior-type iron formations; and 2) the presence of shelf environment sedimentary rocks. Superior-type iron formations were given W.O.E. ranging from 0.1–1 based on the composition of the iron formation (see Table 4). Shelf-environment-associated clastic sedimentary rocks were given W.O.E. ranging from 0.05–0.7 based on composition and characteristics indicating deposition in a shallow-water shelf environment.

Mineral occurrences (point data) for mineral species commonly associated with iron- and/or manganese-rich (e.g. Trendall and Blockley, 2004; Clout and Simonson, 2005; Cannon et al., 2017) mineral deposits were extracted from the Assembling Minnesota mineral occurrence database. The following mineral species were utilized for the model: 1) the presence of iron carbonates, iron oxides, and iron hydroxides; and 2) the presence of manganese carbonates, manganese oxides, and manganese hydroxides. Iron-bearing minerals utilized for modeling included magnetite, martite, limonite, and goethite. Manganese-bearing minerals used in the model included manganite and rhodochrosite. Each of these minerals was given a W.O.E. of 1, and the point locations were given a 1km buffer. The total number of overlapping mineral polygons was summed and normalized to develop the polygon layer for the mineral factor.

Geochemical data (point data) were extracted from the Assembling Minnesota bedrock geology geochemistry and drillhole geochemistry databases. These databases were merged to develop the point data utilized in the model. Total iron percent and total manganese percent were each given a W.O.E. of 1. Kriging of the normalized sums of the point data was performed to develop the surface raster, and the raster values were classified and converted to polygons for the Geochemistry Factor utilized in the model.

The geophysics factor for the Marine Chemocline mineral system model was determined utilizing total magnetics data (Chandler, 1982). This data was extracted to the bedrock geology boundaries, and subsequently normalized and reclassified into 10 quantile classes (1–10) to create the polygons for the Geophysics factor utilized in the model.

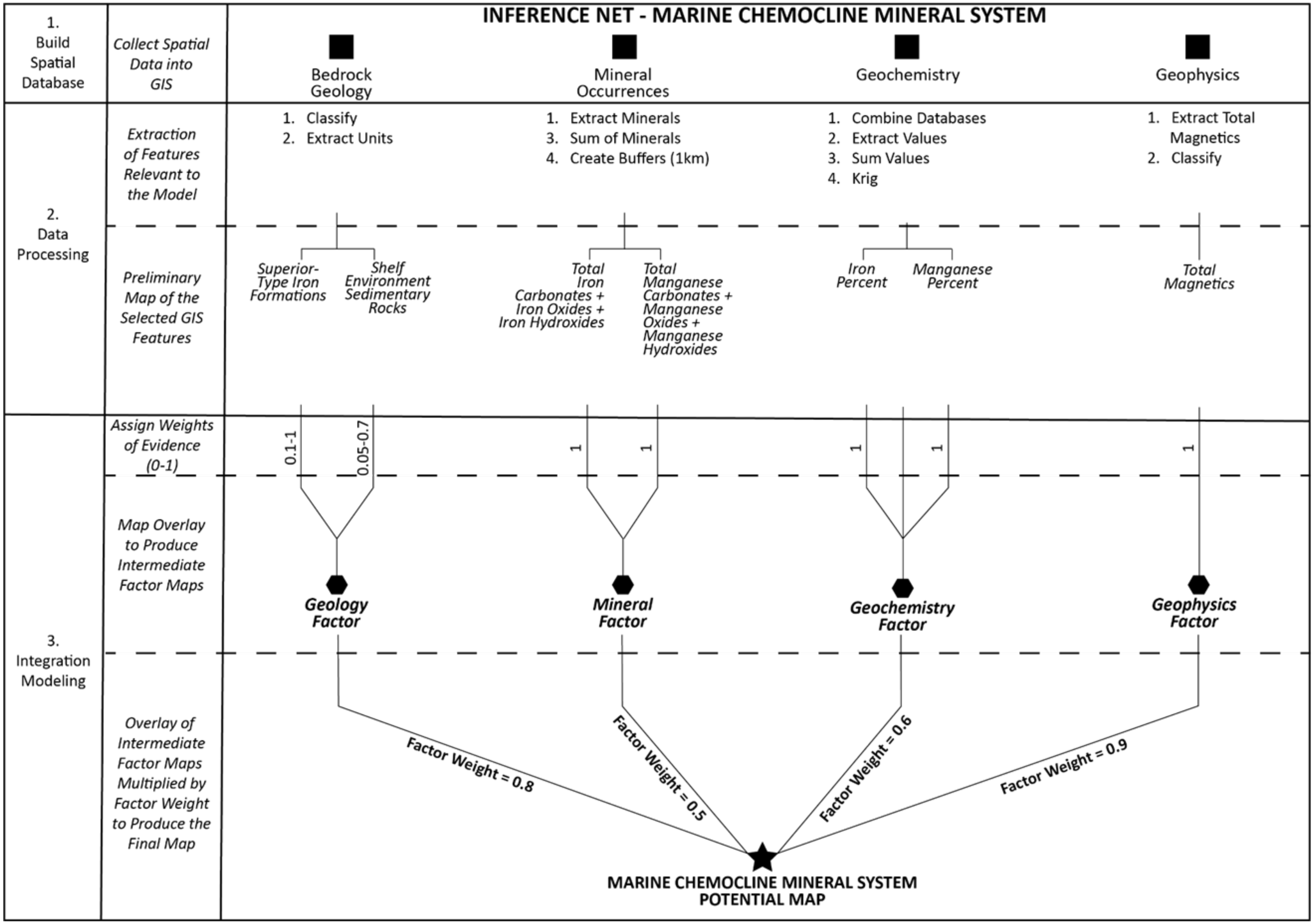

Figure 5. Inference net for ***Marine Chemocline*** knowledge-based mineral system model.

Table 4. Weights of evidence for geology polygons in the ***Marine Chemocline*** mineral system model.

Map Label	Era	Rock Type	W.O.E.
Pifa	Paleoproterozoic	Algoma-type iron formation	1
Pifs	Paleoproterozoic	Iron Formation	1
Pifs	Paleoproterozoic	Manganiferous, thin bedded Virginia Formation Iron Formation associated w/ graphitic argillites	1
Pifs	Paleoproterozoic	Manganiferous, thin bedded Virginia Formation Iron Formation associated w/ graphitic argillites	1
Pifs	Paleoproterozoic	Oxide facies iron-formation	1
Pifs	Paleoproterozoic	Superior type iron formation	1
Pvfg	Paleoproterozoic	Virginia Formation graphitic argillite w/ argillite, chert, and carbonate-silicate iron formation	0.7
Pac	Paleoproterozoic	Virginia Formation slate with thin limestone interbeds	0.7
Pmda	Paleoproterozoic	Dolomitic arkose sandstone	0.4
Pvs	Paleoproterozoic	Interlayered metasedimentary and metavolcanic rocks	0.4
Pvs	Paleoproterozoic	metasedimentary and metavolcanic rocks	0.4
Pmq	Paleoproterozoic	Dam Lake Quartzite	0.2
Pmd	Paleoproterozoic	Denham Formation; sandstone, marble, schist	0.2
Pag	Paleoproterozoic	Greywacke slate	0.2
Ppq	Paleoproterozoic	Quartzite with siliceous mudstone and conglomeratic rocks	0.2
Pvfg	Paleoproterozoic	Carbonaceous argillite	0.1
Pvfg	Paleoproterozoic	Graphitic argillite	0.1
Pgs	Paleoproterozoic	Graywacke, slate with graphitic and sulfidic zones	0.1
Pvf	Paleoproterozoic	Greywacke, mudstone, and argillite	0.1
Pmm	Paleoproterozoic	Mudstone, quartzite, graywacke, phyllite, graphitic argillite	0.1
Pmr	Paleoproterozoic	Mudstone, quartzite, graywacke, phyllite, graphitic argillite	0.1
Pmm	Paleoproterozoic	Mudstone, quartzite, graywacke, phyllite, graphitic argillite	0.1
Pm	Paleoproterozoic	Mudstone, quartzite, graywacke, phyllite, graphitic argillite	0.1
Pag	Paleoproterozoic	Slate, graywacke	0.1
Pgs	Paleoproterozoic	Sudbury Impact Layer	0.1
Psi	Paleoproterozoic	Sulfidic iron-formation	0.1
Pfv	Paleoproterozoic	felsic volcanic rocks	0.05
Prf	Paleoproterozoic	Greywacke, siltstone and argillite	0.05

The final Marine Chemocline Mineral System Potential Map was developed by multiplying each of the model factors by their assigned factor weights and then calculating the fuzzy algebraic sum by means of the following equation (Bonham-Carter, 1994; Peterson, 2001):

$$\mu_{\text{combination}} = 1 - \prod_{i=1}^{n}(\mu i)$$

where μi is the fuzzy membership value for the i^th map, and i = 1. 2. 3, ….n maps are to be combined.

The factor weights assigned for each of the model factors are as follows:

- Geology Factor Weight = 0.8
- Mineral Factor Weight = 0.5
- Geochemistry Factor Weight = 0.6
- Geophysics Factor Weight = 0.9

Results

The Marine Chemocline Mineral System Potential Map is illustrated in Figure 6 (with a Minnesota geology map underlay) and in Figure 7 (without the Minnesota geology map underlay). Shapefiles for the Marine Chemocline Mineral System Potential Map can be found in Digital Appendix 2 in the subdirectory labeled "Shapefiles." Model calculations can be found in Digital Appendix 2 in the subdirectory labeled "Model Calculations."

Based on the modeling, the highest probabilities for the presence of Marine Chemocline mineral systems occur in northeastern and north-central Minnesota in rocks associated with the Animikie Basin and Penokean Orogeny strata. This modeling is consistent with the presence of the Biwabik Iron Formation in St. Louis and Itasca counties as well as the various iron formations associated with Penokean Orogeny strata in Aitkin and Crow Wing counties. As well, the model indicates high probabilities for the presence of the Marine Chemocline mineral system in western and southwestern Stearns County associated with interlayered volcanic, volcaniclastic, sedimentary, and hypabyssal intrusive rocks that comprise the Mille Lacs Group, North and South Range Groups, and Glen Township Formation (Jirsa et al., 2011).

Volcanogenic Seafloor Mineral System

Deposit Types and Model

Table 5 indicates the various mineral deposit types associated with the Volcanogenic Seafloor mineral system (Hofstra and Kreiner, 2021). The Volcanogenic Seafloor mineral system comprises a variety of mineral deposit types associated with seafloor hydrothermal systems in both ancient and modern environments (Franklin et al., 2005).

Table 5. Systems-Deposits-Commodities-Critical Minerals table for the ***Volcanogenic Seafloor*** mineral system (modified after Hofstra and Kreiner, 2021). Explanation for table is as follows: ±, present (absent); --, not applicable; ?, maybe; Ag, silver; Al, aluminum; As, arsenic; Au, gold; B, boron; Ba, barium; Be, beryllium; Bi, bismuth; Br, bromine; Ca, calcium; Cd, cadmium; Co, cobalt; CO_2, carbon dioxide; Cs, cesium; Cr, chromium; Cu, copper; F, fluorine; Fe, iron; Ga, gallium; Ge, germanium; Hf, hafnium; Hg, mercury; I, iodine; IAEA, International Atomic Energy Agency; In, indium; IOA, iron oxide-apatite; IOCG, iron oxide-copper-gold; IS, intermediate sulfidation; K, potassium; LCT, lithium-cesium-tantalum; Li, lithium; Mg, magnesium; Mn, manganese; Mo, molybdenum; Na, sodium; Nb, niobium; Ni, nickel; NYF, niobium-yttrium-fluorine; P, phosphorus; Pb, lead; PGE, platinum group elements; R, replacement; Rb, rubidium; Re, rhenium; REE, rare earth elements; S, skarn; Sb, antimony; Sc, scandium; Se, selenium; Sn, tin; Sr, strontium; Ta, tantalum; Te, tellurium; Th, thorium; Ti, titanium; U, uranium; V, vanadium (in "Principal Commodities" column); V, vein (in "Deposit Types" column); W, tungsten; Y, yttrium; Zn, zinc; Zr, zirconium. In the "Critical Minerals" column, elements in **bold** have been produced from the deposit type, whereas element in *italics* are enriched in the deposit type but have not been produced.

System Name	Deposit Types	Principal Commodities	Critical Minerals	References
Volcanogenic Seafloor	Copper-zinc sulfide	Cu, Zn	*Co, Bi, Te, In, Sn, Ge, Ga, Sb*	Franklin et al., 1981; Levson, 1995; Franklin et al., 2005; Shanks and Thurston, 2012; Monecke et al., 2016; Cannon et al., 2017; DSM Observer, 2020
	Zinc-copper sulfide	Zn, Cu	***Ge, Ga, Sb, Co, Bi, Te, In, Sn***	
	Polymetallic sulfide	Cu, Zn, Pb, Ag, Au	***Sn, Bi, Te, In, Ge, Ga, Sb, As***	
	Barite	Barite	*Barite*	
	Manganese oxide (layers, crusts, nodules)	Mn, Fe, Ni	**Mn,** *Co, Ge, Te, REE, Sc*	
	Algoma iron	Fe	**?**	

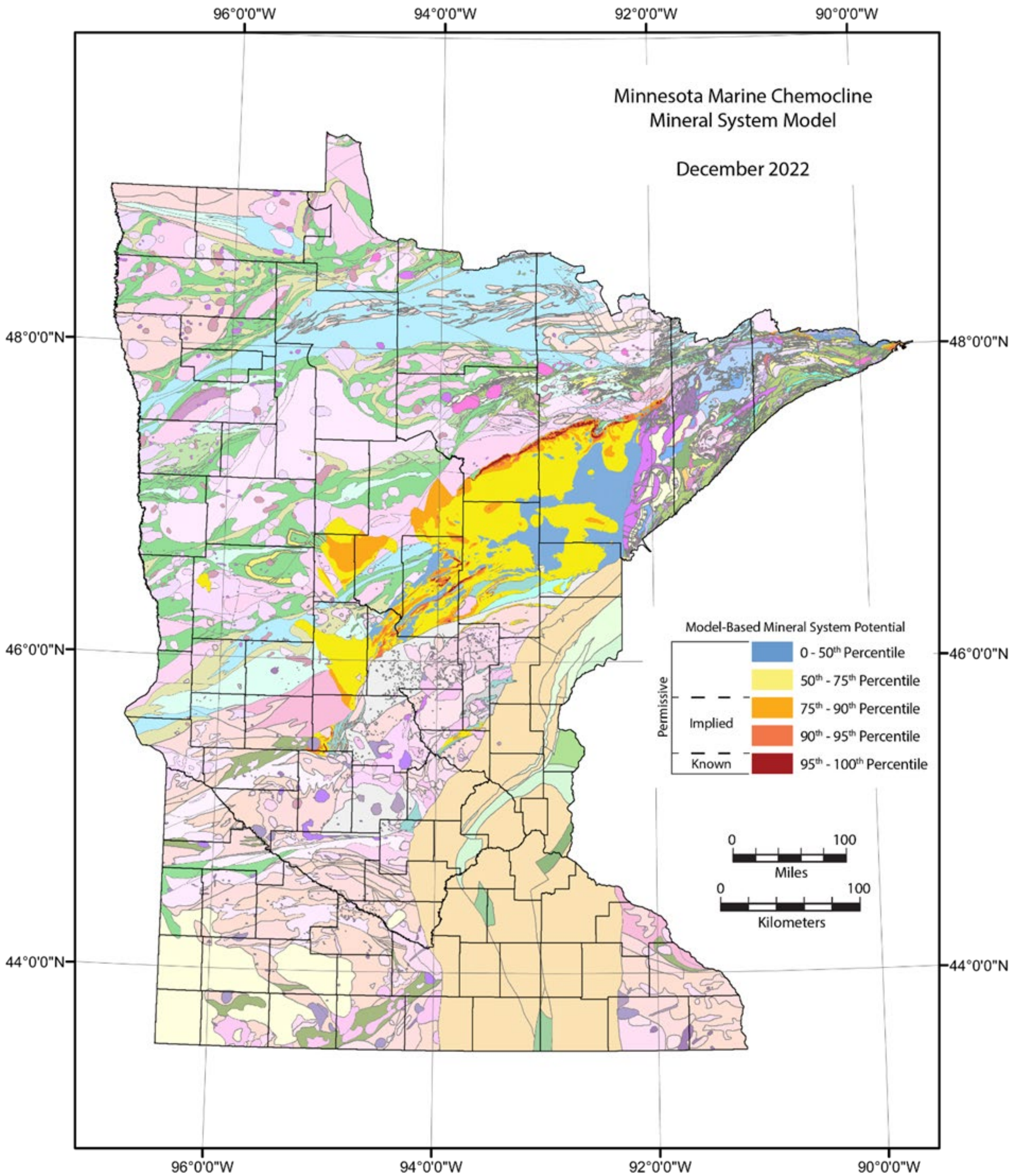

Figure 6. Results of ***Marine Chemocline*** knowledge-based mineral system model with geology.

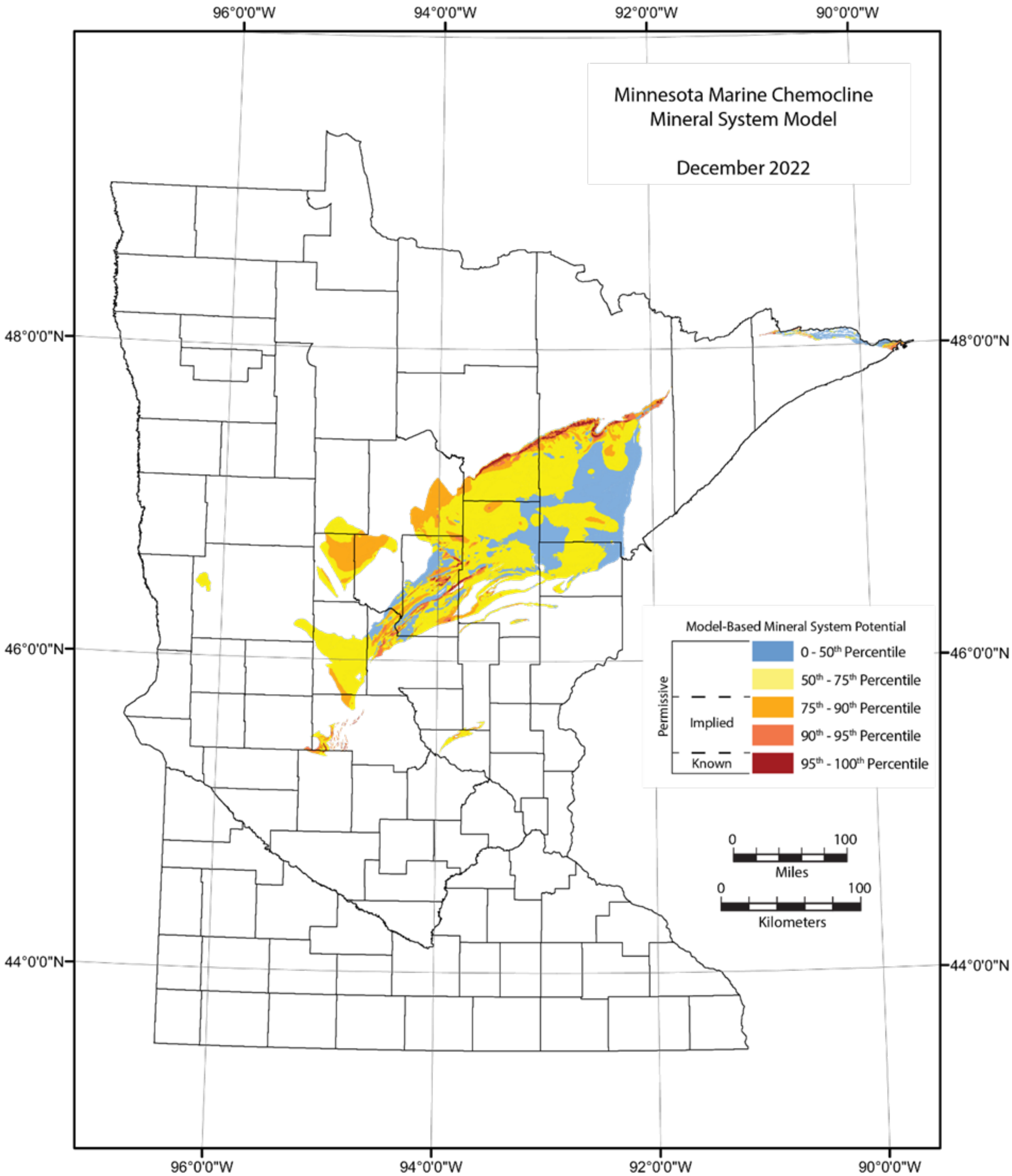

Figure 7. Results of ***Marine Chemocline*** knowledge-based mineral system model without geology.

The physical, chemical, and mineralogical characteristics of mineral deposits formed in the Volcanogenic Seafloor mineral system are, in part, dependent on the temperature of the hydrothermal fluid, the water depth at which the hydrothermal system is active, the physical characteristics of the host rocks, and the geotectonic environment in which the deposits formed (Franklin et al., 1981; Morton and Franklin, 1987; Gibson et al., 1999; Franklin et al., 2005; Hannington et al., 2005; Gibson et al., 2007; Shanks and Thurston, 2012; Monecke et al., 2016). Shallow-water Volcanic Seafloor-associated hydrothermal systems have many similarities with epithermal systems (e.g metals present and alteration mineralogy) and are commonly enriched in precious metals such as gold and silver (Franklin et al., 2005; Shanks and Thurston, 2012). These deposits are associated with low and moderate temperature (up to 350°C), are commonly zinc-rich and, and in modern oceanic settings, can contain significant quantities of barite. Deeper water depositional settings allow for more copper-rich deposits, and hydrothermal fluid temperatures greater than 400°C have been identified in such settings (Hannington et al., 2005). Distal low temperature hydrothermal fluids and/or waning of high temperature Volcanogenic Seafloor-associated hydrothermal systems may lead to the formation of Algoma-type banded iron formations (BIF; Trendall and Blockley, 2004) that are associated with and commonly are interlayered with or overlie massive sulfide mineralization (Zalenski and Peterson, 1995).

A schematic cross-section illustrating the key components of a Volcanogenic Seafloor hydrothermal system is presented in Figure 8. These key components (Gibson et al., 1999; Franklin et al., 2005; Gibson et al., 2007; Shanks and Thurston, 2012) include:

- An active submarine volcanic environment in an extensional tectonic environment;
- The presence of shallow, synvolcanic magma intrusions, some of which may provide magmatic hydrothermal fluids containing ore metals;
- Cross-stratal permeability represented by synvolcanic structures (synvolcanic faults);
- Quartz-epidote alteration zones deep in the subseafloor adjacent to synvolcanic intrusions that represent reservoir zones where high temperature seawater (evolved seawater) has interacted with the rocks to leach metals;
- Shallow sub-seafloor hydrothermal alteration zones that are commonly depleted in sodium and often contain mineral assemblages chlorite; and
- Semi-massive to massive sulfide mineralization at (in coherent-rock dominated settings) or near (in volcaniclastic-rock dominated settings) the seafloor comprising minerals such as chalcopyrite, sphalerite, galena, and pyrite.

Franklin et al. (1981) and Franklin et al. (2005) note that mineralization associated with Volcanic Seafloor mineral systems commonly occurs where abrupt changes in the chemical compositions of the volcanic rocks occur (for example, at or near contacts between mafic and felsic volcanic rocks).

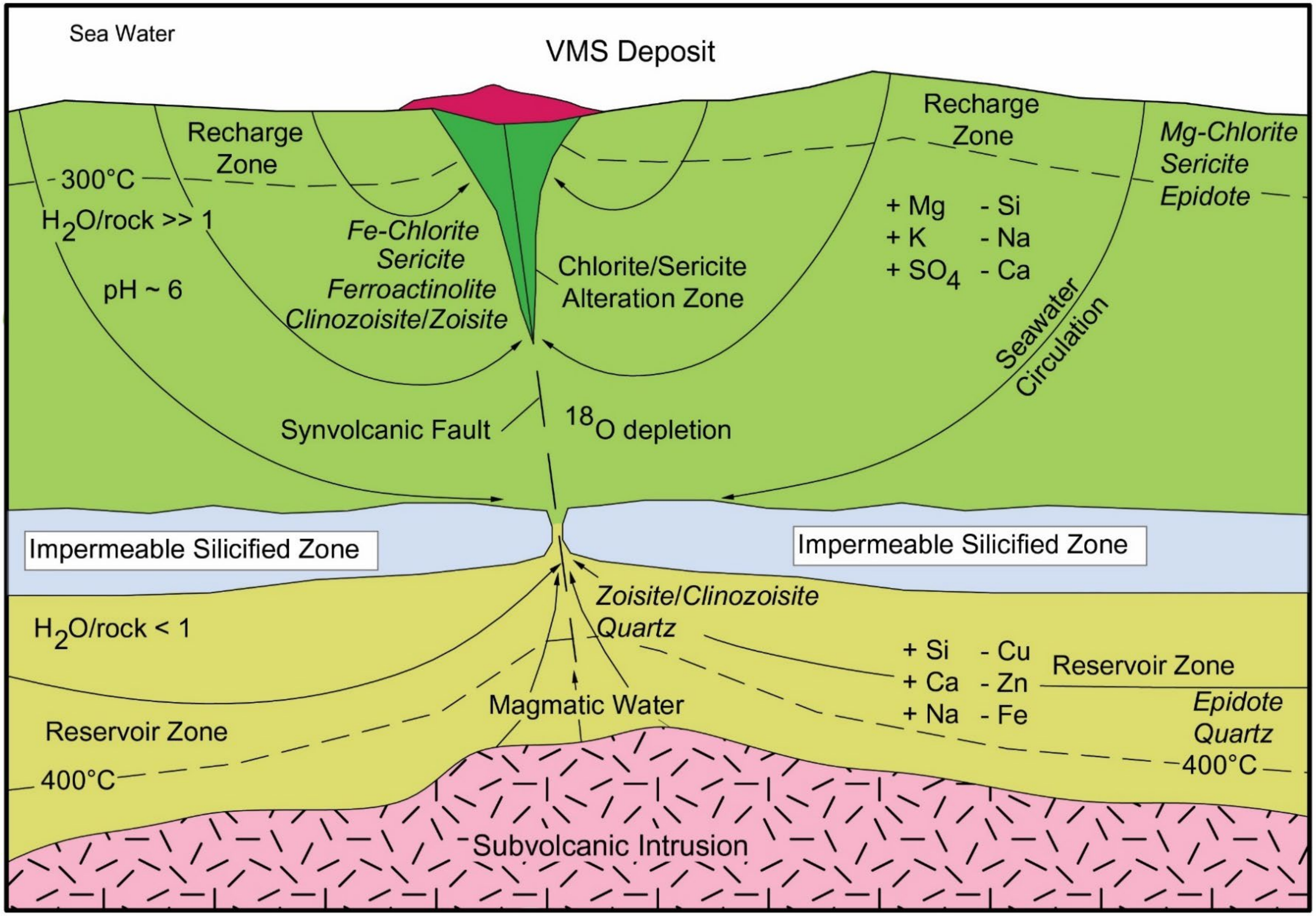

Figure 8. Generalized model of a volcanogenic massive sulfide deposit-producing hydrothermal system (modified after Franklin et al., 2005; Hudak and Peterson, 2014).

Modeling Methods

The knowledge-based fuzzy logic modeling methodology for the Volcanic Seafloor mineral system model included seven components that could be ascertained from the Assembling Minnesota dataset (Bartsch et al., 2022; Peterson, 2018). These seven components include: 1) bedrock geology; 2) geologic contacts; 3) synvolcanic intrusions; 4) mineral occurrence; 5) geochemistry; 6) geophysics; and 7) structure. The inference net illustrating the various components used in the Placer Mineral System model is illustrated in Figure 9. It is important to note that the modeling method for the Volcanogenic Seafloor model was developed to ascertain the potential for hydrothermal systems associated with Algoma-type iron formations (Blatt and Tracy, 1997) and Noranda-type (Morton and Franklin, 1987) volcanogenic massive sulfide deposits. The model does not evaluate the likelihood of Mattabi-type (Morton and Franklin, 1987; Gibson et al., 1999; Hudak et al., 2003; Franklin et al., 2005) volcanogenic massive sulfide systems as these systems are characterized by metamorphosed high sulfidation like alteration mineral assemblages containing mineral species such as andalusite, chloritoid, and iron carbonates that could not extracted from the Assembling Minnesota mineral occurrence database.

The bedrock geology component (polygons) included two geological features: 1) greenstone belt lithological units; and 2) synvolcanic intrusions. Greenstone belt-associated units were assigned W.O.E. ranging from 0.2 to 1 depending on the lithological associations with volcanic seafloor-type mineralization. Intrusive rocks identified as “synvolcanic” in the Assembling Minnesota geology database were assigned W.O.E. of 0.6. The W.O.E. of the various lithological units incorporated into the Volcanogenic Seafloor model are indicated in Table 6.

Three types of geological contacts (lines) were distinguished for this model and given W.O.E. based on their relationships with volcanic seafloor hydrothermal system mineralization. Contacts between felsic and mafic/ultramafic volcanic rocks, lava flows and fragmental rocks, and volcanic rocks and sedimentary rocks were each given buffers of 0.1km and assigned W.O.E. of 0.8, 0.7, and 0.4, respectively. The polygons with their respective W.O.E. were utilized as the contacts factor shapefile used in the final model.

Those rock units classified as “synvolcanic” intrusions in the Assembling Minnesota geology database were utilized in the Volcanogenic Seafloor model to develop a “Thermal Factor.” The thermal factor has been incorporated into the model to represent shallow seafloor heat sources that are required to drive submarine hydrothermal systems. Due to their larger size (and thus greater contained heat), plutons were assigned a W.O.E. of 1 and provided with a buffer equal to 4 km (a common depth where synvolcanic intrusions reside relative to volcanic seafloor-associated mineralization (Franklin et al., 2005). Synvolcanic dikes and sills were assigned a W.O.E. of 0.2 and provided with a buffer of 0.8 km. The polygons developed by these methods were utilized as the thermal factor in the model.

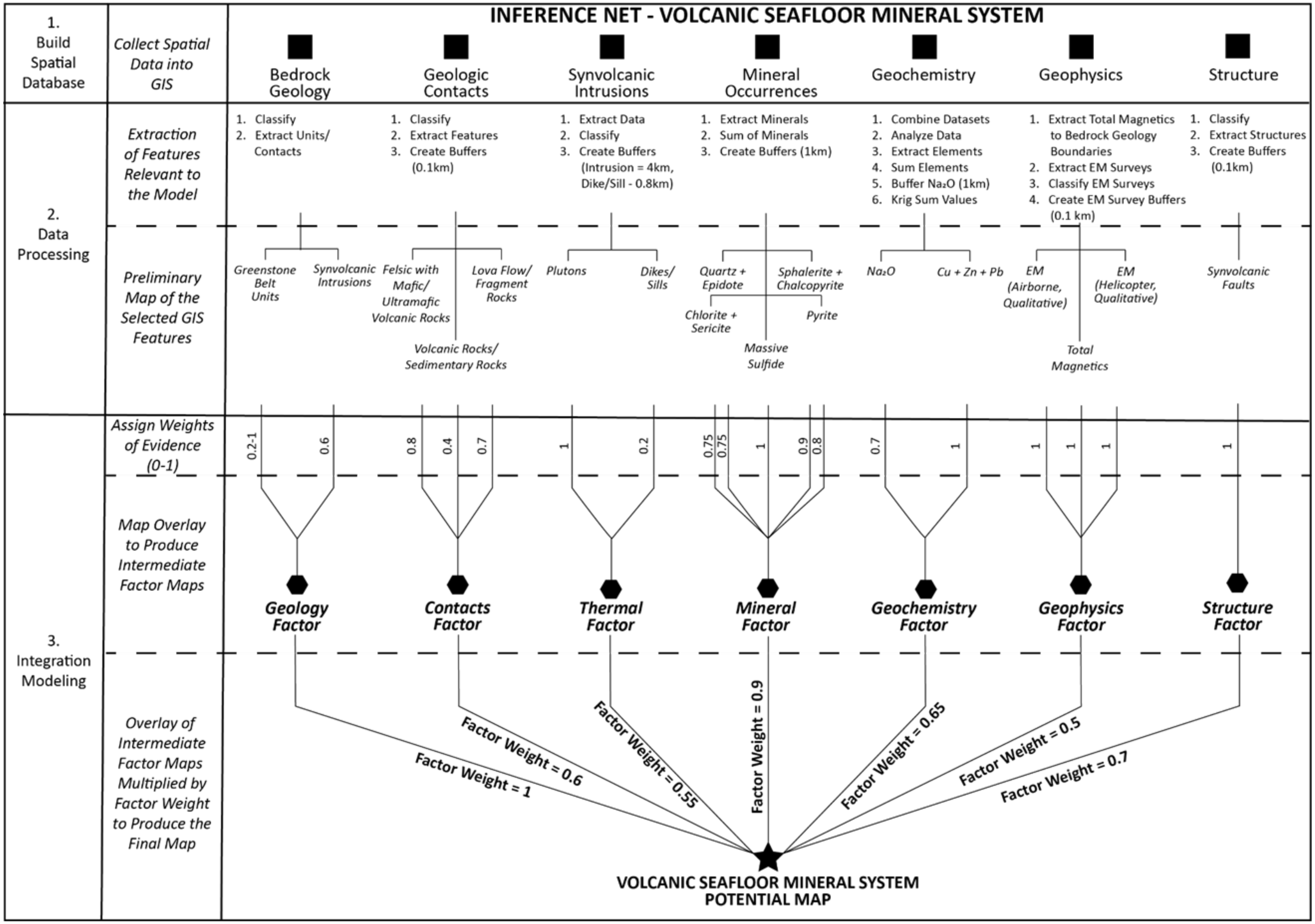

Figure 9. Inference net for ***Volcanogenic Seafloor*** knowledge-based mineral system model.

Table 6. Weights of evidence for geology polygons in the ***Volcanogenic Seafloor*** mineral system model.

Map Label	Era	Rock Type	W.O.E.
Pifa	Paleoproterozoic	Algoma-type iron formation	1
Avms	Neoarchean	Bedded massive sulfide	1
Aifs	Neoarchean	Bedded Pyrite-rich Exhalite	1
Aifo	Neoarchean	Iron Formation	1
Aifo	Neoarchean	Iron formation interlayered with green sandstone	1
Aifo	Neoarchean	Iron formation, defined magnetically	1
Aifo	Neoarchean	Iron Formation, defined via linear positive magnetic anomaly	1
Aifo	Neoarchean	Iron Formation, inferred from aeromagnetic data	1
Aifo	Neoarchean	Iron Formation, inferred from positive magnetic anomaly	1
Pms	Paleoproterozoic	Massive pyrite-pyrrhotite, locally saprolitic and siliceous	1
Avms	Neoarchean	Massive sulfide	1
Avms	Neoarchean	Massive sulfide (VMS-type)	1
Avms	Neoarchean	Massive sulfide is felsic breccias	1
Avms	Neoarchean	Massive sulfide to Semi-massive sulfide breccia with felsic fragments in flowed iron sulfide	1
Avms	Neoarchean	Massive sulfide, pyrite-rich	1
Aifo	Neoarchean	Oxide facies banded iron formation	1
Aifo	Neoarchean	Oxide Facies Iron Formation	1
Aifo	Neoarchean	Sheared Iron-formation	1
Aifs	Neoarchean	Sulfide facies iron formation	1
Avms	Neoarchean	Sulfide-facies iron fromation, ie., bedded massive sulfide	1
Psi	Paleoproterozoic	Sulfidic and graphitic iron-formation	1
Aifs	Neoarchean	Sulfidic interpillow exhalitive deposits	1
Psi	Paleoproterozoic	Sulfidic iron-formation	1
Aifo	Neoarchean	Thin BIF horizon in mafic tuff	1
Aifo	Neoarchean	Thin iron formation horizon in massive basalt	1
Avms	Neoarchean	Thin zones of massive sulfide in altered felsic tuff	1
Aifc	Neoarchean	Cherty interflow exhalite with pyrite	0.95
Avms	Neoarchean	Cherty interpillow exhalite	0.95
Aifc	Neoarchean	Cherty iron formation with pyrite	0.95
Amvm	Neoarchean	Basalt & BIF	0.9
Amvm	Neoarchean	Basalt sheet flow in small iron formation	0.9
Aifc	Neoarchean	Chert and lean iron formation	0.9
Aifc	Neoarchean	Chert-rich iron formation	0.9
Aifc	Neoarchean	Cherty iron formation	0.9
Aszc	Neoarchean	Metamorphosed VMS chlorite alteration pipe	0.8
Aifcb	Neoarchean	Carbonate facies iron formation	0.7
Aifc	Neoarchean	Cherty sedimentary rocks	0.7
Aifo	Neoarchean	Highly magnetic oxide-facies iron formation	0.7
Aifo	Neoarchean	Inferred iron formation	0.7
Aifo	Neoarchean	Inferred iron formation, defined magnetically	0.7
Avms	Neoarchean	Interflow chemical sediment, commonly with Mgt-Py-Cp	0.7
Pifs	Paleoproterozoic	Manganiferous, thin bedded Virginia Formation Iron Formation associated w/ graphitic argillites	0.7
Aifo	Neoarchean	Oxide-facies iron formatiom	0.7
Aifo	Neoarchean	Oxide-facies iron formation, highly magnetic	0.7
Afvm	Neoarchean	Quartz-eye rhyolite lava flow with sphalerite veining	0.7
Aifo	Neoarchean	Sheared iron formation, Quartz-calcite-magnetite schist	0.7
Aifo	Neoarchean	Sheared Iron-formation	0.7
Aifsl	Neoarchean	Silicate facies iron formation	0.7
Aifo	Neoarchean	Stretched iron formation	0.7
Aga	Neoarchean	Graphitic & pyritic argillite	0.65
Aga	Neoarchean	Graphitic and pyritic argillite	0.65
Aga	Neoarchean	Graphitic and pyritic sedimentary rocks intercalated with felsic tuffs	0.65
Aga	Neoarchean	Graphitic argillite with minor pyrite	0.65
Aga	Neoarchean	Graphitic sediment with 0.5-2% pyrite	0.65
Pgs	Paleoproterozoic	Graywacke, slate with graphitic and sulfidic zones	0.65
Aga	Neoarchean	Schistose graphitic argillite with 1-5% pyrite	0.65
Aga	Neoarchean	Sheared graphitic and pyritic argillite	0.65
Pvfg	Paleoproterozoic	Virginia Formation graphitic argillite w/ argillite, chert, and carbonate-silicate iron formation	0.65
Acv	Neoarchean	Andesitic to dacitic pillow bx, tuff breccia, lapilli tuff	0.6

Map Label	Era	Rock Type	W.O.E.
Amvpb	Neoarchean	Basaltic pillow breccia and hyaloclastite deposits	0.6
Acv	Neoarchean	Calc alkalic pillowed basalt and andesite	0.6
Aga	Neoarchean	Graphitic and tuffaceous metasediments	0.6
Pvfg	Paleoproterozoic	Graphitic argillite	0.6
Amvt	Neoarchean	Highly altered mafic tuffaceous rocks	0.6
Amvp	Neoarchean	Pillow basalt	0.6
Amvp	Neoarchean	Pillow basalt, thoeliitic and commonly glomeroporphyritic	0.6
Acv	Neoarchean	Pillow breccia and tuff	0.6
Apd	Neoarchean	Pillow dike	0.6
Amvp	Neoarchean	Pillowed andesite lavas	0.6
Amvp	Neoarchean	Pillowed basalt	0.6
Amvp	Neoarchean	Pillowed basalt flows	0.6
Amvp	Neoarchean	Pillowed basaltic lava flows	0.6
Amvpv	Neoarchean	Variolitic pillowed flows	0.6
Amvu	Neoarchean	Basaltic rocks, massive & pillowed undifferentiated	0.55
Amvm	Neoarchean	Andesitic volcanic rocks	0.5
Amvu	Neoarchean	Basaltic lava flows	0.5
Amvu	Neoarchean	Basaltic volcanic rocks	0.5
Acv	Neoarchean	Calc-alkalic volcanic and volcaniclastic rocks	0.5
Afvtb	Neoarchean	Dacite tuff breccia	0.5
Afvt	Neoarchean	Dacitic lapilli tuff with abundant pumice clasts	0.5
Afvt	Neoarchean	Dacitic lapilli tuff	0.5
Afvtb	Neoarchean	Dacitic to andesitic tuff, breccia, and epiclastic products	0.5
Afvt	Neoarchean	Dacitic tuff	0.5
Afvt	Neoarchean	Dacitic tuff and lapilli tuff	0.5
Afvtb	Neoarchean	Dacitic tuff breccia	0.5
Afvt	Neoarchean	Dacitic tuff to lapilli tuff	0.5
Afvu	Neoarchean	Dacitic tuff, lapilli tuff, and epiclastic deposits	0.5
Afvtb	Neoarchean	Dacitic tuff-breccia	0.5
Afvm	Neoarchean	Felsic Lava Flow	0.5
Afvt	Neoarchean	Felsic Tuff	0.5
Afvt	Neoarchean	Felsic tuff and crystal tuff	0.5
Afvt	Neoarchean	Felsic tuff and epiclastic rocks	0.5
Afvt	Neoarchean	Felsic tuff and lapilli tuff	0.5
Afvtb	Neoarchean	Felsic tuff and tuff breccia	0.5
Afvtb	Neoarchean	Felsic tuff breccia	0.5
Afvu	Neoarchean	Felsic volcanic and related tuffaceous and epiclastic rocks	0.5
Pfv	Paleoproterozoic	felsic volcanic rocks	0.5
Afvu	Neoarchean	Felsic volcanic rocks, undivided	0.5
Afvtb	Neoarchean	Fragmental Felsic Rocks	0.5
Akv	Neoarchean	Hornblende-bearing volcanic flows, breccia and tuff	0.5
Auv	Neoarchean	Komatiitic basalt lava flows	0.5
Auv	Neoarchean	Komatiitic metavolcanic rocks, strongly foliated to tremolitic schists	0.5
Afvtl	Neoarchean	Laminated ash tuff	0.5
Afvtl	Neoarchean	Laminated dacitic ash tuff	0.5
Afvtl	Neoarchean	Laminated mudstone/ash tuff	0.5
Amvu	Neoarchean	Mafic metavolcanic rocks	0.5
Amvu	Neoarchean	Mafic metavolcanic rocks and schistose equivalents	0.5
Auv	Neoarchean	Mafic to ultramafic volcanic rocks	0.5
Amvt	Neoarchean	Mafic Tuff	0.5
Amvt	Neoarchean	Mafic tuff and sediments	0.5
Amvu	Neoarchean	Mafic volcanic and associated rocks	0.5
Amvm	Neoarchean	Massive Basalt	0.5
Amvm	Neoarchean	Massive basalt flows	0.5
Amvm	Neoarchean	Massive basalt lava flows with thin iron formation horizons	0.5
Amvm	Neoarchean	Massive basalt sheet flow	0.5
Amvm	Neoarchean	Massive basalt with thin iron formation horizons	0.5
Amvm	Neoarchean	Massive basaltic lava flows	0.5
Afvm	Neoarchean	Massive dacite lava dome	0.5
Afvm	Neoarchean	Massive dacite, lava dome?	0.5
Afvm	Neoarchean	Massive felsic lava flows	0.5

Map Label	Era	Rock Type	W.O.E.
Amvm	Neoarchean	Massive metabasaltic rocks and/or metagabbroic sill-like intrusive	0.5
Amvu	Neoarchean	Metabasaltic rocks	0.5
Pmvm	Paleoproterozoic	Metabasaltic rocks metamorhhosed to amphibolite grade	0.5
Pmvm	Paleoproterozoic	Metabasaltic rocks metamorhhosed to amphibolite grade	0.5
Afvtb	Neoarchean	Polymict felsic tuff breccia	0.5
Afvm	Neoarchean	Rhyolite to latite lava flows	0.5
Afvt	Neoarchean	Rhyolitic to dacitic tuff and tuff breccia	0.5
Afvm	Neoarchean	Rhyolite to rhyodacite lava flows and fragmental rocks	0.5
Afvtl	Neoarchean	Thin-bedded to laminated dacitic ash tuff	0.5
Atv	Neoarchean	Trachyandesite	0.5
Auv	Neoarchean	Ultramafic to mafic volcanic and hypabyssal intrusive rocks	0.5
Amvu	Neoarchean	Undifferentiated Basalts	0.5
Avs	Neoarchean	Volcanic and volcaniclastic rocks; felsic to intermediate composition	0.5
Afvtb	Neoarchean	Volcanic breccia/conglomerate, highly deformed	0.5
Amvs	Neoarchean	Basaltic Scoria Deposit	0.45
Amvt	Neoarchean	Basaltic tuff	0.45
Amvt	Neoarchean	Basaltic tuff and epiclastic sediments	0.45
Amvs	Neoarchean	Bedded basaltic scoria deposits	0.45
Amvs	Neoarchean	Bedded scoria deposits	0.45
Aam	Neoarchean	Amphibolite	0.4
Ad	Neoarchean	Diorite	0.4
Ad	Neoarchean	Diorite, synvolcanic intrusion	0.4
Atf	Neoarchean	Foliated to gneissic tonalite	0.4
Amgb	Neoarchean	Gabbro	0.4
Agr	Neoarchean	Granite	0.4
Agd	Neoarchean	Granodiorite	0.4
Amgb	Neoarchean	Meta hornblende-gabbro sill	0.4
Amgb	Neoarchean	Meta hornblende-gabbro, amphibolite-grade	0.4
Pmv	Paleoproterozoic	Metabasaltic amphibolite	0.4
Amgb	Neoarchean	Meta-diabase sill	0.4
Pmdb	Paleoproterozoic	Metadiabase/metagabbro sill-like intrusive	0.4
Amgb	Neoarchean	Metadiorite/gabbro	0.4
Amgb	Neoarchean	Metagabbro	0.4
Amgb	Neoarchean	Metagabbro intrusion	0.4
Amgb	Neoarchean	Metagabbro sill	0.4
Agp	Neoarchean	Metagabbro, locally brecciated	0.4
Amgb	Neoarchean	Metagabbro/metadiabase	0.4
Amgb	Neoarchean	Metagabbroic sill	0.4
Amgp	Neoarchean	Porphyritic (opx) melagabbro	0.4
Ad	Neoarchean	Porphyritic diorite	0.4
Aqfp	Neoarchean	Quartz-feldspar porphyry	0.4
At	Neoarchean	Tonalite	0.4
At	Neoarchean	Tonalite, synvolcanic	0.4
Amvf	Neoarchean	Foliated Basalt	0.35
Amvf	Neoarchean	Foliated basaltic and related rocks	0.35
Amvf	Neoarchean	Foliated basaltic rocks	0.35
Amvf	Neoarchean	Foliated basaltic rocks, Pillowed?	0.35
Aszb	Neoarchean	BIF-Inclusion Schist	0.3
Afve	Neoarchean	Mixed dacitic volcaniclastics, tuff-breccia-conglomerate	0.3
Pmm	Paleoproterozoic	Mudstone, quartzite, graywacke, phyllite, graphitic argillite	0.3
Pifs	Paleoproterozoic	Oxide facies iron-formation	0.3
Aszp	Neoarchean	Pyrite-rich Phyllite / Schist	0.3
Aszu	Neoarchean	Sheared Felsic Tuff and Greywacke	0.3
Aas	Neoarchean	Arkosic and lithic sandstone	0.25
Aas	Neoarchean	Arkosic and lithic sandstone	0.25
Aszc	Neoarchean	Chlorite-Pyrite Schist	0.25
Avms	Neoarchean	Chlorite-pyrrhotite stockwork (chl-fragments in massive pyrrhotite)	0.25
APmvu	Neoarchean or Paleoproterozoic	Mafic volcanic and hypabyssal intrusive rocks of uncertain age	0.25
Aszs	Neoarchean	Quartz-Sericite Schist (+/- Pyrite)	0.25
Aszs	Neoarchean	Quartz-Sericite-Ankerite Schist (+/- Pyrite)	0.25

Map Label	Era	Rock Type	W.O.E.
Aszs	Neoarchean	Quartz-Sericite-Ankerite-Chlorite-Pyrite Schist	0.25
Aszs	Neoarchean	Quartz-Sericite-Ankerite-Pyrite Schist	0.25
Aszs	Neoarchean	Quartz-Sericite-Chlorite Schist (+/- Pyrite)	0.25
Aszs	Neoarchean	Quartz-Sericite-Chlorite-Pyrite Schist	0.25
Aszs	Neoarchean	Quartz-Sericite-Fuchsite-Pyrite Schist	0.25
Aszs	Neoarchean	Quartz-Sericite-Pyrite Schist	0.25
Aszu	Neoarchean	Sericite-ankerite-quartz-pyrite (1%) phyllite	0.25
Aszp	Neoarchean	Sericite-chlorite-ankerite-pyrite tectonite	0.25
Aszs	Neoarchean	Sericite-Chlorite-Pyrite Schist	0.25
Psz	Paleoproterozoic	Sericite-pyrite phyllite	0.25
Aam	Neoarchean	Amphibolite schist. Composed of hbld-bio-chl with thin magnetite-cherty layers	0.2
Aszc	Neoarchean	Ankerite-Chlorite schist shear zone	0.2
Aqs	Neoarchean	Biotite schist, paragneiss, and schist-rich migmatite	0.2
Aqs	Neoarchean	Biotite schist, paragneiss, and schist-rich migmatite	0.2
Aqs	Neoarchean	Biotite-calcite-magnetite schist	0.2
Ags	Neoarchean	Biotitic greywacke-slate	0.2
Ams	Neoarchean	Biotitic metagreywacke-slate	0.2
Aszf	Neoarchean	Carbonate-Fuchsite Schist (+/- Py & Qtz Veins)	0.2
Aszc	Neoarchean	Chlorite "mafic" schist, derived from basaltic flows and tuffaceous rocks	0.2
Aszc	Neoarchean	Chlorite schist	0.2
Aszc	Neoarchean	Chlorite schist, generally derived from pillow basalts	0.2
Aszc	Neoarchean	Chlorite schist, sheared basalt	0.2
Aszu	Neoarchean	Chlorite schist/phyllite with trace pyrite along foliation	0.2
Aszc	Neoarchean	Chlorite-Ankerite Schist	0.2
Aszc	Neoarchean	Chlorite-Ankerite-Pyrite Schist	0.2
Aszc	Neoarchean	Chlorite-calcite schist	0.2
Aszc	Neoarchean	Chlorite-dominant schist	0.2
Aszc	Neoarchean	Chlorite-dominate schist (shear zone)	0.2
Aszc	Neoarchean	Chlorite-dominate shear zone schist	0.2
Pmy	Paleoproterozoic	Chlorite-hornblende-tremolite schist, sheared metabasalt/metagabbro?	0.2
Aszc	Neoarchean	Chlorite-Quartz Schist	0.2
Aszc	Neoarchean	Chlorite-schist shear zone	0.2
Aszc	Neoarchean	Chlorite-sericite schist	0.2
Aszc	Neoarchean	Chlorite-sericite schist with flattened host-rock lozenges	0.2
Aszc	Neoarchean	Chlorite-sericite-ankerite-pyrite (5%) schist and phyllite	0.2
Aszu	Neoarchean	Chlorite-sericite-pyrite schist	0.2
Aszc	Neoarchean	Chloritic phyllite-schist	0.2
Aszc	Neoarchean	Crenulated chlorite phyllite	0.2
Pmi	Paleoproterozoic	Diabase dike	0.2
Afve	Neoarchean	Epiclastic dacitic sediments and conglomerate	0.2
Afve	Neoarchean	Epiclastic Dacitic Volcanoclastic Rocks	0.2
Afve	Neoarchean	Epiclastic felsic sediments and tuff	0.2
Afp	Neoarchean	Feldspar porphyry	0.2
Afvt	Neoarchean	Felsic Debris Flow Deposits	0.2
Afve	Neoarchean	Felsic Epiclastic Rocks	0.2
Afvt	Neoarchean	Felsic tuff and locally epiclastic rocks	0.2
Amvf	Neoarchean	Highly foliated basaltic rocks and schist	0.2
Pvs	Paleoproterozoic	Interlayered metasedimentary and metavolcanic rocks	0.2
Amm	Neoarchean	Interlayered volcanic and volcaniclastic rocks; amphibolite grade metamorphism	0.2
Pvs	Paleoproterozoic	metasedimentary and metavolcanic rocks	0.2
Aszu	Neoarchean	Poker-Chip Phyllonite	0.2
Aszs	Neoarchean	Quartz-sericite schist	0.2
Afvm	Neoarchean	Schistose meta-rhyolite and/or dacite	0.2
Afvm	Neoarchean	Schistose rhyolite with doubly terminated quartz phenocrysts	0.2
Aszu	Neoarchean	Sericite-chlorite phyllite with qtz-cal veinlets	0.2
Aszs	Neoarchean	Sericite-chlorite schist	0.2
Aszs	Neoarchean	Sericite-chlorite-ankerite schist and phyllite	0.2
Afvt	Neoarchean	Siliceous sediment and/or felsic tuff	0.2
Aks	Neoarchean	Slate, siltstone, lithic sandstone, and conglomerate	0.2
Acg	Neoarchean	Conglomerate	0.1
Acg	Neoarchean	Conglomerate and arkosic sandstone	0.1

Map Label	Era	Rock Type	W.O.E.
Acg	Neoarchean	Conglomerate and lithic sandstone	0.1
Acg	Neoarchean	Conglomerate and related rocks, Timiskaming-Type	0.1
Acg	Neoarchean	Conglomerate and volcaniclastic sandstones	0.1
Acg	Neoarchean	Conglomerate with arkosic and lithic sandstone	0.1
Acg	Neoarchean	Conglomerate, lithic sandstone, graywacke, mudstone	0.1
Acg	Neoarchean	Dacite Porphyry Conglomerate, Timiskaming-Type	0.1
Afve	Neoarchean	Dacitic volcanic conglomerate with stretched plag-phyric clasts	0.1
APd	Neoarchean or Paleoproterozoic	Dioritic to granodioritic intrusion of uncertain age	0.1
Ad	Neoarchean	Diorite	0.1
Atf	Neoarchean	Foliated to gneissic tonalite, diorite and granodiorite	0.1
Amgb	Neoarchean	Gabbro	0.1
Agp	Neoarchean	Gabbro, pyroxenite, peridotite, lamprophyre intrusion	0.1
Agan	Neoarchean	Gabbroic anorthosite	0.1
Pga	Paleoproterozoic	Gabbroic, noritic, and anorthositic intrusion	0.1
Agr	Neoarchean	Granite plug	0.1
Agrm	Neoarchean	Granite to granodiorite, variably magnetic	0.1
Agrm	Neoarchean	Granite to granodiorite, variably magnetic, locally magmatically foliated	0.1
Agrm	Neoarchean	Granite to granodiorite, variably magnetic, locally magmatically foliated	0.1
Agrm	Neoarchean	Granite to granodiorite, variably magnetic, locally magmatically foliated	0.1
Agrm	Neoarchean	Granite to granodiorite, variably magnetic, locally magmatically foliated	0.1
Agrm	Neoarchean	Granite to granodiorite, variably magnetic, locally magmatically foliated	0.1
Agrm	Neoarchean	Granite to granodiorite, variably magnetic, locally magmatically foliated	0.1
Agrm	Neoarchean	Granite to granodiorite, variably magnetic, locally magmatically foliated	0.1
Agrm	Neoarchean	Granite to granodiorite, variably magnetic, locally magmatically foliated	0.1
Agrm	Neoarchean	Granite to granodiorite, variably magnetic, locally magmatically foliated	0.1
Agrm	Neoarchean	Granite to granodiorite, variably magnetic, locally magmatically foliated	0.1
Agrm	Neoarchean	Granite to granodiorite, variably magnetic, locally magmatically foliated	0.1
Agrm	Neoarchean	Granite to granodiorite, variably magnetic, locally magmatically foliated	0.1
Agrm	Neoarchean	Granite to granodiorite, variably magnetic, locally magmatically foliated	0.1
Agrm	Neoarchean	Granite to granodiorite, variably magnetic, locally magmatically foliated	0.1
Agrm	Neoarchean	Granite to granodiorite, variably magnetic, locally magmatically foliated	0.1
Agrm	Neoarchean	Granite to granodiorite, variably magnetic, locally magmatically foliated	0.1
Agrm	Neoarchean	Granite to granodiorite, variably magnetic, locally magmatically foliated	0.1
Agr	Neoarchean	Granitic intrusion	0.1
APgr	Neoarchean or Paleoproterozoic	Granitic intrusion of uncertain age	0.1
Agru	Neoarchean	Granitoid intrusion, undifferentiated or poorly constrained by core and outcrop	0.1
Agd	Neoarchean	Granodiorite, foliated and synvolcanic	0.1
Agd	Neoarchean	Granodioritic intrusion	0.1
Ags	Neoarchean	Graywacke and mudstone; typically greenschist facies metamorphism	0.1
Ad	Neoarchean	Grey, fine to medium-grained, biotite-hornblende diorite	0.1
Ags	Neoarchean	Greywacke and slate	0.1
Pag	Paleoproterozoic	Greywacke slate	0.1
Ags	Neoarchean	Greywacke-slate, mixed sourced	0.1
Ags	Neoarchean	Interbedded greywacke-slate	0.1
Aas	Neoarchean	Lithic and arkosic sandstone	0.1
Aas	Neoarchean	Lithic sandstone, mudstone, and siliceous siltstone with detrital hbld and plag	0.1
Ami	Neoarchean	Mafic intrusion, defined magnetically	0.1
Ami	Neoarchean	Mafic intrusion, undifferentiated	0.1
Ami	Neoarchean or Paleoproterozoic	Mafic plug-like intrusion; typically magnetic	0.1
Aag	Neoarchean	Mafic to ultramafic hypabyssal intrusive complexes; gabbro, anorthosite	0.1
Ami	Neoarchean	Mafic to ultramafic intrusions	0.1
Agp	Neoarchean	Marginal oxide-rich gabbro	0.1
Asza	Neoarchean	Massive ankerite alteration zone	0.1
Amgps	Neoarchean	Melagabbro sill, locally sulfide-bearing	0.1
Pd	Paleoproterozoic	Mesocratic Diorite	0.1
Amgb	Neoarchean	Meta Orthopyroxene gabbro	0.1
Pmdb	Paleoproterozoic	Metadiabase hypabyssal intrusive rocks	0.1
Amgb	Neoarchean	Metagabbro	0.1

Map Label	Era	Rock Type	W.O.E.
Amgb	Neoarchean	Metagabbro sill	0.1
Amgb	Neoarchean	Metagabbro sill in basaltic rocks	0.1
Amgps	Neoarchean	Metagabbro sill, locally sulfide-bearing	0.1
Amgbs	Neoarchean	Metagabbro sill, weakly (0-3%) sulfide-bearing	0.1
Amgb	Neoarchean	Metagabbro sill, weakly sulfide-bearing	0.1
Aag	Neoarchean	Metagabbro, commonly chloritized	0.1
Amp	Neoarchean	Metaperidotite and pyroxenite sill	0.1
Amp	Neoarchean	Metaperidotite sill	0.1
Pml	Paleoproterozoic	Mille Lacs granite	0.1
Asd	Neoarchean	Monzodiorite and syenite	0.1
Am	Neoarchean	Monzonite	0.1
Agp	Neoarchean	Olivine-rich gabbro and peridotite	0.1
Amp	Neoarchean	Peridotite	0.1
Afp	Neoarchean	Plagioclase porphyritic dike	0.1
Amgps	Neoarchean	Porphyritic metagabbro sill, locally sulfide-bearing	0.1
Ampx	Neoarchean	Pyroxenite	0.1
Ampx	Neoarchean	Pyroxenite sill	0.1
Ampxs	Neoarchean	Pyroxenite, weakly sulfide-bearing	0.1
Aqfp	Neoarchean	Quartz feldspar porphyry	0.1
Aqm	Neoarchean	Quartz monzonite, monzonite, and granodiorite, non-magnetic	0.1
Aqmm	Neoarchean	Quartz monzonite, variably magnetic and magmatically foliated	0.1
Asza	Neoarchean	Quartz-Ankerite Schist (+/- Pyrite)	0.1
Agp	Neoarchean	Quartz-biotite gabbro	0.1
Aqfp	Neoarchean	Quartz-feldspar porphyry	0.1
Amgb	Neoarchean	Rusty, fine-grained chilled margin of gabbroic sills	0.1
Ags	Neoarchean	Schist and tonalite- to granodiorite-bearing paragneiss	0.1
Amp	Neoarchean	Serpentinized peridotite with chalcopyrite	0.1
Amp	Neoarchean	Serpentinized, strongly magnetic peridotite	0.1
Aszc	Neoarchean	Shear zone	0.1
Aqfp	Neoarchean	Sheared quartz-feldspar porphyry	0.1
Pls	Paleoproterozoic	Staurolite-garnet pelitic schist	0.1
Amqgs	Neoarchean	Sulfide-bearing to sulfide-rich, quartz gabbro	0.1
Amgbs	Neoarchean	Sulfide-bearing, microgabbro (chilled margin)	0.1
Amgbs	Neoarchean	Sulfidic metagabbro	0.1
Asd	Neoarchean	Syenite	0.1
Asd	Neoarchean	Syenitic, monzodioritic, or dioritic pluton	0.1
Amgbh	Neoarchean	Taxitic metagabbro	0.1
Pdt	Paleoproterozoic	Tonalite	0.1
Adt	Neoarchean	Tonalite to leucodiorite pluton	0.1
At	Neoarchean	Tonalite, diorite and granodiorite	0.1
At	Neoarchean	Tonalite, trondjehmite to leucogranite	0.1
Ags	Neoarchean	Tuffaceous metasediment (greywacke-slate?)	0.1
Almp	Neoarchean	Ultramafic Fragmental Rocks	0.1
Ampxs	Neoarchean	Weakly sulfide-bearing pyroxenite	0.1
Amps	Neoarchean	Weakly sulfide-bearing, serpentinized peridotite	0.1
Agr	Neoarchean	Granitic dike	0.05
Pvf	Paleoproterozoic	Greywacke, mudstone, and argillite	0.05
Pag	Paleoproterozoic	Slate, graywacke	0.05

Mineral occurrences (point data) for mineral species commonly associated with Volcanogenic Seafloor model-associated mineralization (Franklin et al., 2005) were extracted from the Assembling Minnesota mineral occurrence database. The following mineral species were utilized for the model: 1) quartz plus epidote, which represent broad regional semi-conformable alteration associated with subseafloor reservoir zones associated with volcanogenic seafloor-style mineralization; 2) chlorite plus sericite, which represent shallow seafloor, cross-stratal hydrothermal alteration that occurs in the footwall to and adjacent to Noranda-type volcanogenic massive sulfide deposits; 3) sphalerite plus chalcopyrite, which represents volcanogenic massive sulfide-associated ore minerals; 4) pyrite, which is associated with and commonly occurs proximal to volcanogenic massive sulfide mineralization; and 5) massive sulfide, a generic term for sulfide minerals associated with volcanogenic massive sulfide mineralization. W.O.E. assigned for the quartz plus epidote, chlorite plus sericite, sphalerite plus chalcopyrite, pyrite, and massive sulfide mineral occurrences were 0.75, 0.75, 0.9, 0.8, and 1, respectively. For each mineral group, the point locations were given a 1km buffer, and the total number of overlapping buffers was summed and normalized to develop the mineral factor polygon layers.

Geochemical data (point data) were extracted from the Assembling Minnesota bedrock geology geochemistry and drillhole geochemistry databases. These databases were merged to develop the point data utilized in the model. Where Na_2O values were greater than 1.0%, a W.O.E. of 0 was assigned. This was done to utilize only potentially sodium-depleted rocks in the model. Where Na_2O values were less than 1.0%, a W.O.E. of 0.7 was assigned, and a 1km buffer was created around the points and utilized as one of the geochemistry factor layers. The sum of copper (Cu in ppm), zinc (Sn in ppm) and lead (Pb, ppm) was calculated for each of the data points. Kriging of the normalized sums for each of the point data was performed to develop a surface raster, and the raster values were classified and converted to polygons as the second Geochemistry Factor layer.

The geophysics factor for the Volcanogenic Seafloor mineral system model combined total magnetics data (Chandler, 1982) to represent regions where Algoma-type iron formations may be present and electromagnetic data to indicate where conductive massive sulfide mineralization may potentially be present. The total magnetics data were extracted to the bedrock geology boundaries, and subsequently normalized and reclassified into 10 quantile classes (1–10) to create one of the polygon layers for the Geophysics factor utilized in the model. Airborne and Helicopter electromagnetic survey (EM) values (point data) were classified into three categories based on the number of channel responses indicated in the survey. Those points with 0 channel responses in both 6-channel surveys and 12-channel surveys were classified as “no conductor” and given a point value of 0. Those points indicating 1–2 channel responses in a 6-channel survey or 1–4 channel responses in a 12-channel survey were classified as “weak conductors” and given a point value of 0.33. Those points indicating 3–4 channel responses in a 6-channel survey or 5–8 channel responses in a 12-channel survey were classified as “moderate conductors” and assigned a point value of 0.67. Those points indicating 5–6 channel responses in a 6-channel survey or 9–12 channel responses in a 12-channel survey were classified as “good conductors” and were assigned a point value of 1. Both the airborne EM points and the helicopter EM points were buffered by 0.1km and utilized as the second polygon layer in the Geophysics Factor.

The structure component of the model included faults classified as “synvolcanic” in the Assembling Minnesota geology lines database. Synvolcanic faults were extracted from the database, provided a 0.1km buffer, and the resulting polygons were assigned a W.O.E of 1. The resulting layer was utilized as the Structure component in the calculation of the final Volcanogenic Seafloor mineral system model.

The Volcanogenic Seafloor Mineral System Potential Map was developed by multiplying each of the model factors by their assigned factor weights and then calculating the fuzzy algebraic sum by means of the following equation (Bonham-Carter, 1994; Peterson, 2001):

$$\mu_{\text{combination}} = 1 - \prod_{i=1}^{n}(\mu i)$$

where μi is the fuzzy membership value for the i^{th} map, and i = 1. 2. 3, ….n maps are to be combined.

The factor weights assigned for each of the model factors are as follows:

- Geology Factor Weight = 1
- Contacts Factor Weight = 0.6
- Thermal Factor Weight = 0.55
- Mineral Factor Weight = 0.9
- Geochemistry Factor Weight = 0.65
- Geophysics Factor Weight = 0.5
- Structure Factor Weight = 0.7

Results

The Volcanogenic Seafloor Mineral System Potential Map is illustrated in Figure 10 (with a Minnesota geology map underlay) and in Figure 11 (without the Minnesota geology map underlay). Shapefiles for the Volcanogenic Seafloor Mineral System Potential Map can be found in Digital Appendix 3 in the subdirectory labeled "Shapefiles." Model calculations can be found in Digital Appendix 3 in the subdirectory labeled "Model Calculations."

High potential for the presence of Volcanogenic Seafloor mineral systems was identified in both the Abitibi-Wawa and Wabigoon subprovinces. In the Abitibi-Wawa subprovince, this includes regions in St. Louis County associated with the Vermilion district and areas in northeastern Itasca County associated with the Wilson Lake sequence (Jirsa, 1990). Within the Wabigoon subprovince, enhanced potential for Volcanogenic Seafloor mineral systems occurs in east-central Lake of the Woods County and in northwestern Beltrami County. These findings are consistent with the presence of massive sulfide mineralization documented within the Assembling Minnesota database (Figure 12). A single region of high potential for the presence of a Volcanogenic Seafloor mineral system also occurs in north-central Marshall County.

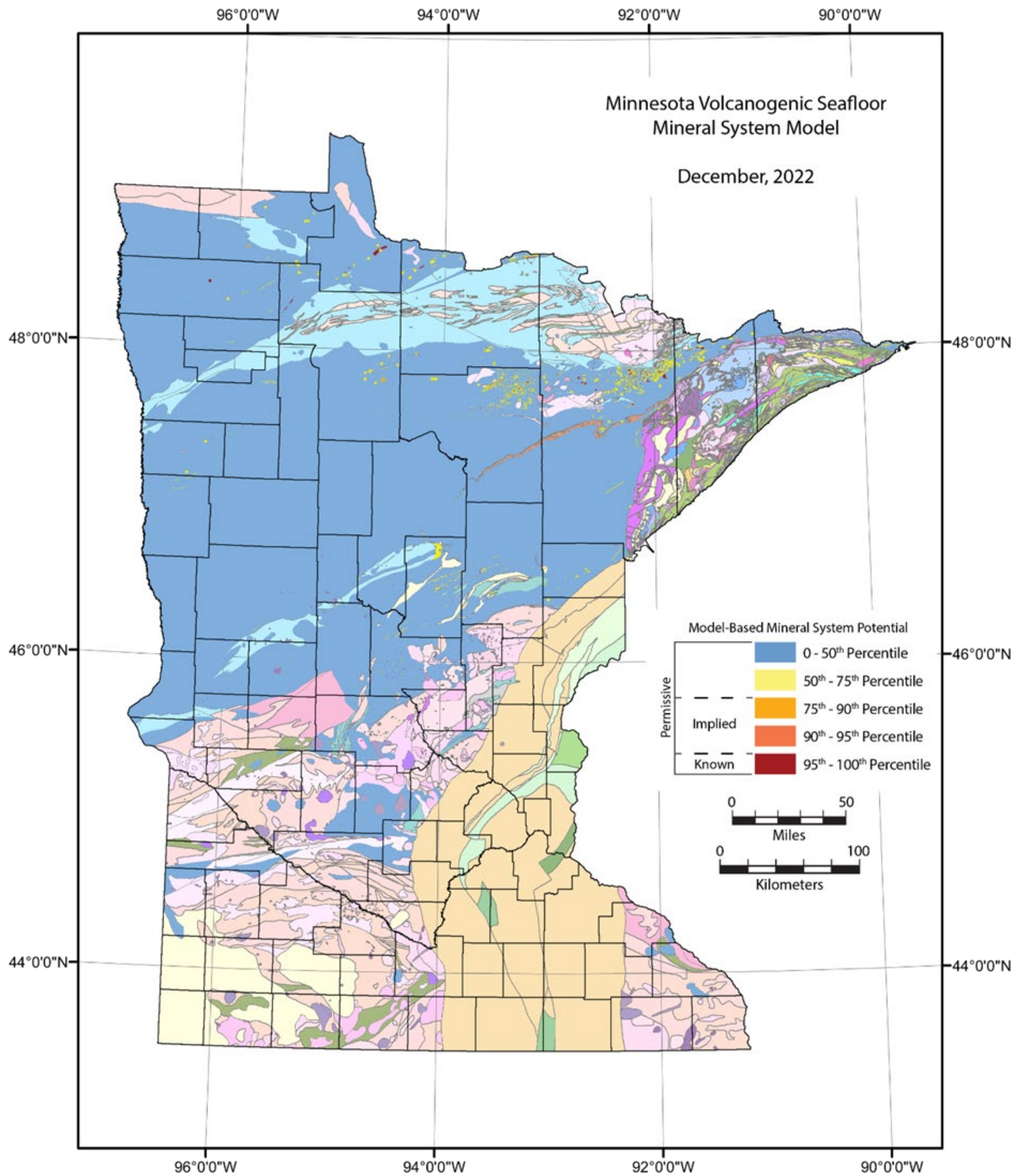

Figure 10. Results of ***Volcanogenic Seafloor*** knowledge-based mineral system model with geology.

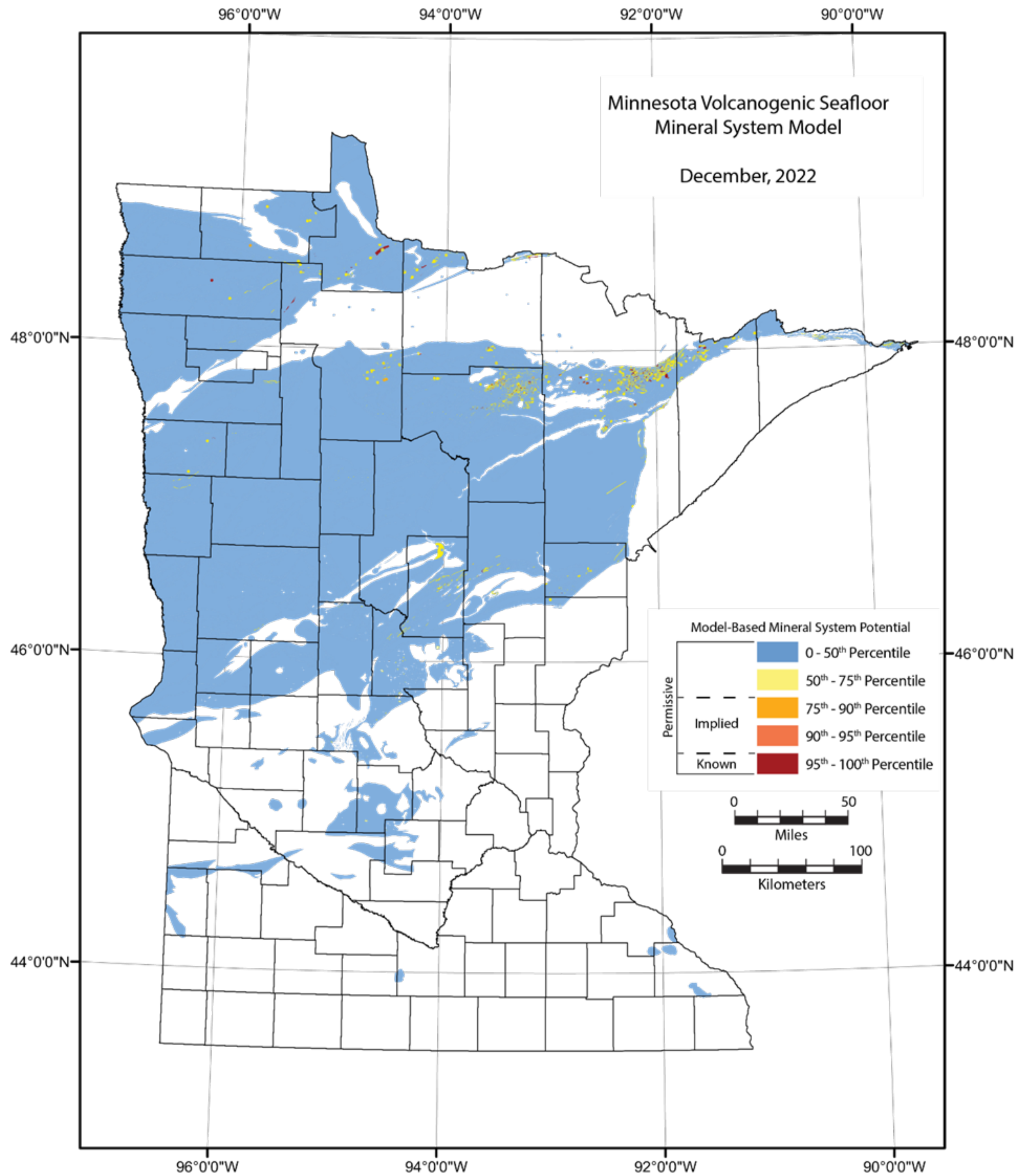

Figure 11. Results of ***Volcanogenic Seafloor*** knowledge-based mineral system model without geology.

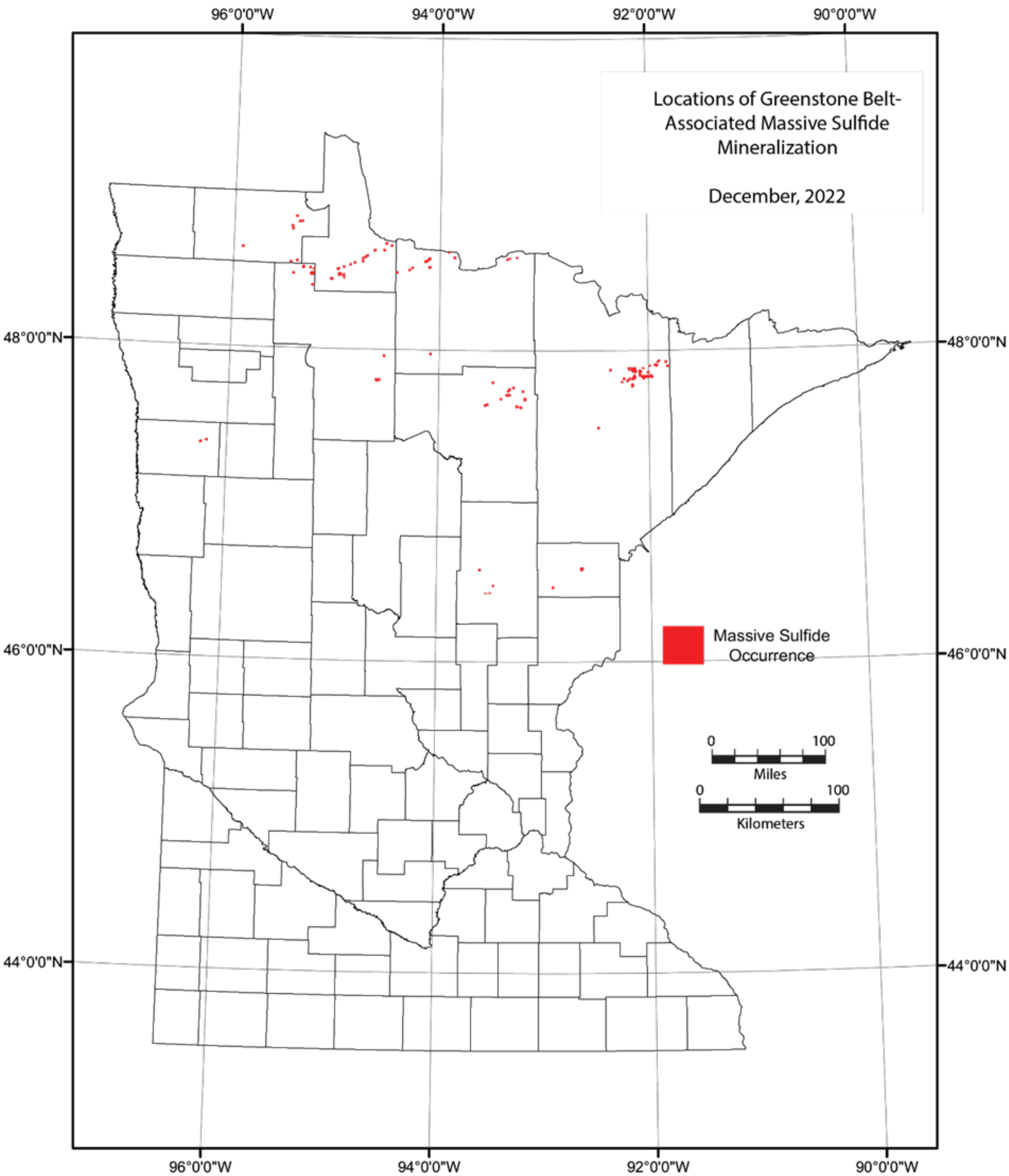

Figure 12. Occurrences of greenstone belt-associated volcanogenic massive sulfide derived from the Assembling Minnesota mineral occurrences database.

Orogenic Mineral System

Deposit Types and Model

Table 7 indicates the various mineral deposit types associated with the Orogenic mineral system (Hofstra and Kreiner, 2021). The Orogenic mineral system comprises a variety of mineral deposit types associated with first-, second- and third-order, deep-crustal fault zones that commonly have complex structural histories. These structures typically occur during compressional or transpressional deformation in greenschist-facies metamorphic terranes associated with Precambrian shields. They are commonly located in rocks of Neoarchean, Paleoproterozoic, and Neoproterozoic age (Goldfarb et al., 2005). The Orogenic mineral system model developed for this study is primarily focused on orogenic gold mineral deposits.

Table 7. Systems-Deposits-Commodities-Critical Minerals table for the ***Orogenic*** mineral system (modified after Hofstra and Kreiner, 2021). Explanation for table is as follows: ±, present (absent); --, not applicable; ?, maybe; Ag, silver; Al, aluminum; As, arsenic; Au, gold; B, boron; Ba, barium; Be, beryllium; Bi, bismuth; Br, bromine; Ca, calcium; Cd, cadmium; Co, cobalt; CO_2, carbon dioxide; Cs, cesium; Cr, chromium; Cu, copper; F, fluorine; Fe, iron; Ga, gallium; Ge, germanium; Hf, hafnium; Hg, mercury; I, iodine; IAEA, International Atomic Energy Agency; In, indium; IOA, iron oxide-apatite; IOCG, iron oxide-copper-gold; IS, intermediate sulfidation; K, potassium; LCT, lithium-cesium-tantalum; Li, lithium; Mg, magnesium; Mn, manganese; Mo, molybdenum; Na, sodium; Nb, niobium; Ni, nickel; NYF, niobium-yttrium-fluorine; P, phosphorus; Pb, lead; PGE, platinum group elements; R, replacement; Rb, rubidium; Re, rhenium; REE, rare earth elements; S, skarn; Sb, antimony; Sc, scandium; Se, selenium; Sn, tin; Sr, strontium; Ta, tantalum; Te, tellurium; Th, thorium; Ti, titanium; U, uranium; V, vanadium (in "Principal Commodities" column); V, vein (in "Deposit Types" column); W, tungsten; Y, yttrium; Zn, zinc; Zr, zirconium. In the "Critical Minerals" column, elements in **bold** have been produced from the deposit type, whereas element in *italics* are enriched in the deposit type but have not been produced.

System Name	Deposit Types	Principal Commodities	Critical Minerals	References
Orogenic	Gold	Au, Ag	**W,** *Te, As, Sb*	Groves et al., 1998; Goldfarb et al., 2005; Luque et al., 2014; Goldfarb et al., 2016
	Antimony	Sb, Au, Ag	**Sb**	
	Mercury	Hg, Sb	*Sb*	
	Graphite	Graphite (lump)	**Graphite (lump)**	

Geological controls related to orogenic gold mineral deposits are well-described in a number of summary papers (Goldfarb et al., 2005; Robert et al., 2005; Percival and Bleeker, 2019; Groves et al., 2020). Key components of genetic model for orogenic gold include:

- The presence of deep-crustal fault zones (shear zones; Groves et al., 2020) or lithosphere-scale structures that provide pathways from the upper mantle to the crust (Percival and Bleeker, 2019; Groves et al., 2020);
- A gold-enriched deep crustal source;
- An upward fluid flow (hydrothermal fluids and or magma) through these deep crustal structures;
- A depositional zone within or near the brittle-ductile transition zone within the crust; and
- Chemical traps for gold deposition (e.g. iron-rich or carbon-rich rocks along a hydrothermal flow path (Goldfarb et al., 2005).

Gold deposition appears to occur at late stages of orogenic events and can be closely associated with magmatic events that form intrusive rocks along these lithosphere-scale structures. Goldfarb et al. (2005) note that there are few gold-producing Archean greenstone belts without nearby intrusions of similar age to gold deposition. Hydrothermal fluids associated with gold mineralization are low salinity, mixed H_2O-CO_2 fluids (Percival and Bleeker, 2019), and therefore proximal alteration to gold mineralization commonly encompassed hydrous minerals such as sericite and chlorite, as well as carbonate minerals such as ankerite (Goldfarb et al., 2005). Alkaline magmatism associated with fault-bounded, Timiskiming-type clastic sedimentary strata may be a criterion for recognizing fault systems that can produce economic gold mineralization (Bleeker, 2012; Dube et al., 2015; Bleeker, 2015).

For further details regarding orogenic gold deposits, the reader is referred to Robert et al. (2005), Goldfarb et al. (2005), Dube et al. (2015), Groves et al. (2020, and references therein).

Modeling Methods

The knowledge-based fuzzy-logic modeling methodology for the Orogenic mineral system model included four components that could be ascertained from the Assembling Minnesota dataset (Bartsch et al., 2022; Peterson, 2018). These four components include: 1) geologic structures; 2) bedrock geology; 3) mineral occurrences; and 4) geochemistry. The inference net illustrating the various components used in the Placer Mineral System model is illustrated in Figure 13. Given Minnesota's geology, the model developed for this study focused on orogenic gold deposits.

The geologic structures component comprised first-order shear zones (primary shear zones) identified in the Assembling Minnesota dataset (Bartsch et al., 2022; Peterson, 2018). Each segment of these shear zones had been previously classified by Peterson (2001) as either pure shear, compressional, or extensional based on the sense of shear along the shear zone and the geometry of the shear zone. Peterson (2001) found that 100% of the mined gold in Canadian analogy mining camps occurred within a distance of 10 kilometers from a major shear zone. As well, he found that over 98% of the total ounces of gold mined occurred in compressional first-order structural settings. Given these relationships, primary shear zones were extracted from the Assembling Minnesota geology lines dataset and assigned a 10 kilometer buffer, with pure shear segments, extensional segments, and compressional segments of the primary shear zones assigned W.O.E. of 0.05, 0.1, and 0.9, respectively. The resulting structure factor polygon layer was utilized in the development of the final Orogenic mineral system model.

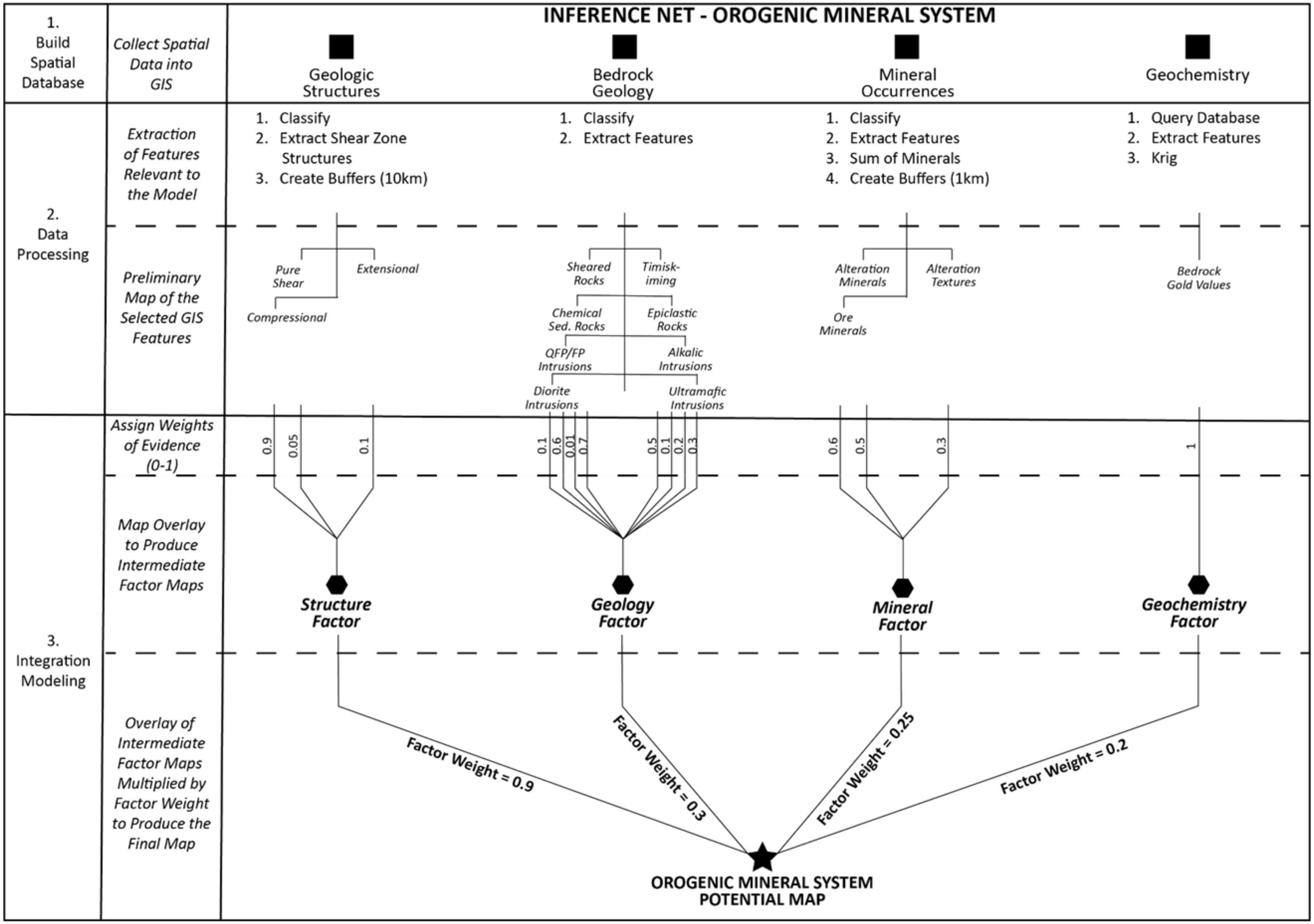

Figure 13. Inference net for ***Orogenic*** knowledge-based mineral system model.

Peterson's (2001) GIS analysis of analog Canadian orogenic gold mining camps indicated a relationship between gold mineralization and bedrock geology. Peterson found that felsic porphyries hosted approximately 36% of the total gold mined, Timiskiming-type sediments hosted approximately 30% of the total gold mined, ultramafic rocks hosted approximately 20% of the total gold mined, and alkalic intrusive rocks hosted approximately 14% of the total gold mined. Chemical sedimentary rocks did not host any of the gold mined. Given the apparent relationship between ounces mined and lithology, a bedrock geology component (polygons) was developed and included eight lithological units. These included: 1) sheared rocks; 2) Timiskiming-type sedimentary rocks; 3) chemical sedimentary rocks; 4) epiclastic rocks; 5) quartz feldspar porphyry (QFP) and feldspar porphyry (FP) intrusion; 6) alkalic intrusions; 7) diorite intrusions; and 8) ultramafic intrusions. W.O.E assigned to sheared rocks, Timiskiming-type sedimentary rocks, chemical sedimentary rocks, epiclastic rocks, QFP/FP intrusions, alkalic intrusions, and diorite intrusions were 0.7, 0.5, 0.01, 0.1, 0.6, 0.2, 0.1, and 0.3, respectively. Polygons of these units were extracted from the Assembling Minnesota dataset and were assigned their respective W.O.E. to develop the geology factor used in the model (Table 8).

Mineral occurrences and alteration textures (point data) commonly associated with orogenic gold-associated mineralization (Goldfarb et al., 2005; Robert et al., 2005) were extracted from the Assembling Minnesota mineral occurrence dataset. Mineral species utilized in the model were separated into three types: 1) alteration mineral (ankerite, sericite, chlorite and fuchsite); 2) ore minerals (gold and pyrite); and 3) alteration textures (including breccia and quartz veins). W.O.E. assigned for alteration minerals, ore minerals, and alteration textures were 0.5, 0.6, and 0.3, respectively. For each mineral group, the point locations were given a 1km buffer, and the total number of overlapping buffers was summed and normalized to develop the mineral factor polygon layers.

Geochemical data (point data) were extracted from the Assembling Minnesota bedrock and drillhole geochemistry databases. These databases were merged to develop the point data utilized in the model. Bedrock gold values were exclusively used in the model. Kriging of the normalized values of the point data was performed to develop a surface raster, and the raster values were classified and converted to polygons for the Geochemistry Factor utilized in the model.

The Orogenic Mineral System Potential Map was developed by multiplying each of the model factors by their assigned factor weights and then calculating the fuzzy algebraic sum by means of the following equation (Bonham-Carter, 1994; Peterson, 2001):

$$\mu_{\text{combination}} = 1 - \prod_{i=1}^{n}(\mu i)$$

where μi is the fuzzy membership value for the i^{th} map, and i = 1. 2. 3, ….n maps are to be combined.

The factor weights assigned for each of the model factors are as follows:

- Structure Factor = 0.9
- Geology Factor = 0.3
- Mineral Factor = 0.25
- Geochemistry Factor = 0.2

Table 8. Weights of evidence for geology polygons in the ***Orogenic*** mineral system model.

Map Label	Era	Rock Type	W.O.E
Am	Neoarchean	Monzonite	1
Aqfp	Neoarchean	Quartz-feldspar porphyry, gold bearing	1
Aam	Neoarchean	Amphibolite schist. Composed of hbld-bio-chl with thin magnetite-cherty layers	0.7
Aszc	Neoarchean	Ankerite-Chlorite schist shear zone	0.7
Aszs	Neoarchean	Ankerite-Sericite-Chlorite-Pyrite Schist	0.7
Aszu	Neoarchean	Banded ultramylonite with local heavy pyrite	0.7
Amvm	Neoarchean	Basalt & BIF	0.7
Aifs	Neoarchean	Bedded Pyrite-rich Exhalite	0.7
Aszb	Neoarchean	BIF-Inclusion Schist	0.7
Aszf	Neoarchean	Carbonate-Fuchsite Schist (+/- Py & Qtz Veins)	0.7
Aifc	Neoarchean	Chert-rich iron formation	0.7
Amvf	Neoarchean	Chlorite "mafic" schist, derived from basaltic flows and tuffaceous rocks	0.7
Aszc	Neoarchean	Chlorite Schist	0.7
Aszc	Neoarchean	Chlorite schist, generally derived from pillow basalts	0.7
Aszc	Neoarchean	Chlorite schist, sheared basalt	0.7
Aszu	Neoarchean	Chlorite schist/phyllite with trace pyrite along foliation	0.7
Aszc	Neoarchean	Chlorite-Ankerite Schist	0.7
Aszc	Neoarchean	Chlorite-Ankerite-Pyrite Schist	0.7
Aszc	Neoarchean	Chlorite-calcite schist	0.7
Aszc	Neoarchean	Chlorite-dominant schist	0.7
Aszc	Neoarchean	Chlorite-dominate schist (shear zone)	0.7
Aszc	Neoarchean	Chlorite-Pyrite Schist	0.7
Avms	Neoarchean	Chlorite-pyrrhotite stockwork (chl-fragments in massive pyrrhotite)	0.7
Aszc	Neoarchean	Chlorite-Quartz Schist	0.7
Aszc	Neoarchean	Chlorite-schist shear zone	0.7
Aszc	Neoarchean	Chlorite-sericite schist	0.7
Aszc	Neoarchean	Chlorite-sericite schist with flattened host-rock lozenges	0.7
Aszc	Neoarchean	Chlorite-sericite-ankerite-pyrite (5%) schist and phyllite	0.7
Aszu	Neoarchean	Chlorite-sericite-pyrite schist	0.7
Aszc	Neoarchean	Chloritic phyllite-schist	0.7
Aszc	Neoarchean	Crenulated chlorite phyllite	0.7
Amvf	Neoarchean	Foliated Basalt	0.7
Amvf	Neoarchean	Foliated basaltic and related rocks	0.7
Amvf	Neoarchean	Foliated basaltic rocks	0.7
Amvf	Neoarchean	Foliated basaltic rocks, Pillowed?	0.7
Agd	Neoarchean	Foliated granodioritic intrusion	0.7
Amvf	Neoarchean	Highly foliated basaltic rocks and schist	0.7
Aam	Neoarchean	Interlatered biotite schist and amphibolite	0.7
At	Neoarchean	Lt grey, fine to medium-grained, foliated biotite tonalite	0.7
Amgb	Neoarchean	Metagabbro - sheared	0.7
Aszu	Neoarchean	Poker-Chip Phyllonite	0.7
Aszp	Neoarchean	Pyrite-rich Phyllite / Schist	0.7
Asza	Neoarchean	Quartz-Ankerite Schist (+/- Pyrite)	0.7
Aqv	Neoarchean	Quartz-pyrite vein	0.7
Aszs	Neoarchean	Quartz-Sericite Schist	0.7
Aszs	Neoarchean	Quartz-Sericite Schist (+/- Pyrite)	0.7
Aszs	Neoarchean	Quartz-Sericite-Ankerite Schist (+/- Pyrite)	0.7
Aszs	Neoarchean	Quartz-Sericite-Ankerite-Chlorite-Pyrite Schist	0.7
Aszs	Neoarchean	Quartz-Sericite-Ankerite-Pyrite Schist	0.7
Aszs	Neoarchean	Quartz-Sericite-Chlorite Schist (+/- Pyrite)	0.7
Aszs	Neoarchean	Quartz-Sericite-Chlorite-Ankerite Schist	0.7
Aszs	Neoarchean	Quartz-Sericite-Chlorite-Pyrite Schist	0.7
Aszf	Neoarchean	Quartz-Sericite-Fuchsite Schist (+/- Pyrite)	0.7
Aszs	Neoarchean	Quartz-Sericite-Fuchsite-Pyrite Schist	0.7
Aszs	Neoarchean	Quartz-Sericite-Pyrite Schist	0.7
Afvm	Neoarchean	Schistose meta-rhyolite and/or dacite	0.7
Afvm	Neoarchean	Schistose rhyolite with doubly terminated quartz phenocrysts	0.7
Aszu	Neoarchean	Sericite-ankerite-quartz-pyrite (1%) phyllite	0.7
Aszu	Neoarchean	Sericite-chlorite phyllite with qtz-cal veinlets	0.7
Aszs	Neoarchean	Sericite-Chlorite Schist	0.7

Map Label	Era	Rock Type	W.O.E
Aszs	Neoarchean	Sericite-chlorite schist, sheared feldspathic arenite	0.7
Aszs	Neoarchean	Sericite-chlorite-ankerite schist and phyllite	0.7
Aszs	Neoarchean	Sericite-Chlorite-Pyrite Schist	0.7
Psz	Paleoproterozoic	Sericite-pyrite phyllite	0.7
Aszc	Neoarchean	Shear zone	0.7
Aszcgl	Neoarchean	Sheared and altered conglomerate	0.7
Aszcgl	Neoarchean	Sheared conglomerate	0.7
Aszu	Neoarchean	Sheared Felsic Tuff and Greywacke	0.7
Aga	Neoarchean	Sheared graphitic and pyritic argillite	0.7
Aifo	Neoarchean	Sheared iron formation, Quartz-calcite-magnetite schist	0.7
Aifo	Neoarchean	Sheared Iron-formation	0.7
Aifsl	Neoarchean	Silicate facies iron formation	0.7
Aifo	Neoarchean	Stretched iron formation	0.7
Afp	Neoarchean	Feldspar porphyry	0.6
Aqfp	Neoarchean	Quartz-feldspar porphyry	0.6
Aqfp	Neoarchean	Sheared quartz-feldspar porphyry	0.6
Acg	Neoarchean	Conglomerate	0.5
Acg	Neoarchean	Conglomerate and arkosic sandstone	0.5
Acg	Neoarchean	Conglomerate and lithic sandstone	0.5
Acg	Neoarchean	Conglomerate and related rocks, Timiskaming-Type	0.5
Acg	Neoarchean	Conglomerate and volcaniclastic sandstones	0.5
Acg	Neoarchean	Conglomerate with arkosic and lithic sandstone	0.5
Acg	Neoarchean	Conglomerate, lithic sandstone, graywacke, mudstone	0.5
Acg	Neoarchean	Dacite Porphyry Conglomerate, Timiskaming-Type	0.5
Afve	Neoarchean	Dacitic volcanic conglomerate with stretched plag-phyric clasts	0.5
Agd	Neoarchean	Granodiorite	0.5
Ami	Neoarchean	Mafic to ultramafic intrusions	0.5
Asza	Neoarchean	Massive ankerite alteration zone	0.5
Amvm	Neoarchean	Massive basaltic lava flows	0.5
Acgm	Neoarchean	Partially melted conglomeratic rocks	0.5
Afvtb	Neoarchean	Volcanic breccia/conglomerate, highly deformed	0.5
Aam	Neoarchean	Amphibolite, schistose to gneissic	0.4
Aam	Neoarchean	Amphibolitic schist and gneiss	0.4
Aga	Neoarchean	Graphitic & pyritic argillite	0.4
Aga	Neoarchean	Graphitic and pyritic argillite	0.4
Aga	Neoarchean	Graphitic and pyritic sedimentary rocks intercalated with felsic tuffs	0.4
Aga	Neoarchean	Graphitic argillite with minor pyrite	0.4
Aga	Neoarchean	Graphitic sediment with 0.5-2% pyrite	0.4
Aga	Neoarchean	Schistose graphitic argillite with 1-5% pyrite	0.4
Auv	Neoarchean	Komatiitic basalt lava flows	0.3
Auv	Neoarchean	Komatiitic metavolcanic rocks, strongly foliated to tremolitic schists	0.3
Aag	Neoarchean	Mafic to ultramafic hypabyssal intrusive complexes; gabbro, anorthosite	0.3
Ami	Neoarchean	Mafic to ultramafic intrusions	0.3
Pmi	Paleoproterozoic	Peridotite	0.3
Ampx	Neoarchean	Pyroxenite	0.3
Ampx	Neoarchean	Pyroxenite sill	0.3
Ampxs	Neoarchean	Pyroxenite, weakly sulfide-bearing	0.3
Afvt	Neoarchean	Qtz + Pl Phyric Tuff and Lapilli Tuff	0.3
Almp	Neoarchean	Ultramafic Fragmental Rocks	0.3
Asd	Neoarchean	Alkalic (syenitic, monzodioritic, dioritic), amphibole & pyroxene-bearing intrusions	0.2
Pdb	Paleoproterozoic	Diabase sill	0.2
Agp	Neoarchean	Gabbro, pyroxenite, peridotite, lamprophyre intrusion	0.2
Atv	Neoarchean	Hornblende trachyandesite lava flows	0.2
Almp	Neoarchean	Lamprophyre	0.2
Agp	Neoarchean	Lamprophyre dike	0.2
Agp	Neoarchean	Lamprophyre dike/plug	0.2
Agp	Neoarchean	Lamprophyre intrusion	0.2
Almp	Neoarchean	Lamprophyric to ultramafic intrusions	0.2
Auv	Neoarchean	Mafic to ultramafic volcanic rocks	0.2
Amgb	Neoarchean	Meta hornblende-gabbro sill	0.2
Amgb	Neoarchean	Meta hornblende-gabbro, amphibolite-grade	0.2

Map Label	Era	Rock Type	W.O.E
Asd	Neoarchean	Syenite	0.2
Asd	Neoarchean	Syenitic, monzodioritic, or dioritic pluton	0.2
Atv	Neoarchean	Trachyandesite	0.2
Auv	Neoarchean	Ultramafic to mafic volcanic and hypabyssal intrusive rocks	0.2
Avms	Neoarchean	Bedded massive sulfide	0.15
Avms	Neoarchean	Cherty interpillow exhalite	0.15
Pdg	Paleoproterozoic	Granodiorite; variably foliated	0.15
Avms	Neoarchean	Massive sulfide	0.15
Avms	Neoarchean	Massive sulfide (VMS-type)	0.15
Avms	Neoarchean	Massive sulfide is felsic breccias	0.15
Avms	Neoarchean	Massive sulfide to Semi-massive sulfide breccia with felsic fragments in flowed iron sulfide	0.15
Avms	Neoarchean	Massive sulfide, pyrite-rich	0.15
Avms	Neoarchean	Thin zones of massive sulfide in altered felsic tuff	0.15
Aam	Neoarchean	Amphibolite	0.1
Amn	Mesoarchean to Paleoarchean	Amphibolitic to dioritic gneiss	0.1
Afvu	Neoarchean	Andesitic and Dacitic volcanic and volcaniclastic rocks	0.1
Amvt	Neoarchean	Andesitic crystal and crystal-lithic tuff tuff	0.1
Amvm	Neoarchean	Andesitic volcanic rocks	0.1
Amvm	Neoarchean	Basalt sheet flow in small iron formation	0.1
Amvu	Neoarchean	Basaltic lava flows	0.1
Amvpb	Neoarchean	Basaltic pillow breccia and hyaloclastite deposits	0.1
Amvp	Neoarchean	Basaltic rocks, massive & pillowed undifferentiated	0.1
Amvs	Neoarchean	Basaltic Scoria Deposit	0.1
Amvt	Neoarchean	Basaltic tuff	0.1
Amvt	Neoarchean	Basaltic tuff and epiclastic sediments	0.1
Amvu	Neoarchean	Basaltic volcanic rocks	0.1
Amvs	Neoarchean	Bedded basaltic scoria deposits	0.1
Amvs	Neoarchean	Bedded scoria deposits	0.1
Ams	Neoarchean	Biotite schist	0.1
Ags	Neoarchean	Biotitic greywacke-slate	0.1
Ams	Neoarchean	Biotitic metagreywacke-slate	0.1
Acv	Neoarchean	Calc alkalic pillowed basalt and andesite	0.1
Pmy	Paleoproterozoic	Chlorite-hornblende-tremolite schist, sheared metabasalt/metagabbro?	0.1
Afvtb	Neoarchean	Dacite tuff breccia	0.1
Afvt	Neoarchean	Dacitic lapilli tuff	0.1
Afvt	Neoarchean	Dacitic lapilli tuff with abundant pumice clasts	0.1
Afvtb	Neoarchean	Dacitic to andesitic tuff, breccia, and epiclastic products	0.1
Afvt	Neoarchean	Dacitic tuff	0.1
Afvt	Neoarchean	Dacitic tuff and lapilli tuff	0.1
Afvt	Neoarchean	Dacitic tuff to lapilli tuff	0.1
Afvu	Neoarchean	Dacitic tuff, lapilli tuff, and epiclastic deposits	0.1
Afvtb	Neoarchean	Dacitic tuff-breccia	0.1
Ami	Neoarchean	Diabase plug	0.1
Ad	Neoarchean	Diorite	0.1
Ad	Neoarchean	Diorite, synvolcanic intrusion	0.1
APd	Neoarchean or Paleoproterozoic	Dioritic to granodioritic intrusion of uncertain age	0.1
Afve	Neoarchean	Epiclastic dacitic sediments and conglomerate	0.1
Afve	Neoarchean	Epiclastic Dacitic Volcanoclastic Rocks	0.1
Afve	Neoarchean	Epiclastic felsic sediments and tuff	0.1
Afvt	Neoarchean	Felsic Debris Flow Deposits	0.1
Afve	Neoarchean	Felsic Epiclastic Rocks	0.1
Afvm	Neoarchean	Felsic Lava Flow	0.1
Afvt	Neoarchean	Felsic Tuff	0.1
Afvt	Neoarchean	Felsic tuff and crystal tuff	0.1
Afvt	Neoarchean	Felsic tuff and epiclastic rocks	0.1
Afvt	Neoarchean	Felsic tuff and lapilli tuff	0.1
Afvt	Neoarchean	Felsic tuff and locally epiclastic rocks	0.1
Afvtb	Neoarchean	Felsic tuff and tuff breccia	0.1
Afvtb	Neoarchean	Felsic tuff breccia	0.1

Map Label	Era	Rock Type	W.O.E
Afvt	Neoarchean	Felsic tuff, xenolith in the Deer Lake Complex	0.1
Afvu	Neoarchean	Felsic volcanic and related tuffaceous and epiclastic rocks	0.1
Afvu	Neoarchean	Felsic volcanic rocks, undivided	0.1
Atf	Mesoarchean to Paleoarchean	Foliated to gneissic granodiorite to tonalite	0.1
Atf	Neoarchean	Foliated to gneissic tonalite	0.1
Atf	Neoarchean	Foliated to gneissic tonalite, diorite and granodiorite	0.1
Afvtb	Neoarchean	Fragmental Felsic Rocks	0.1
Amgb	Neoarchean	Gabbro	0.1
Agan	Neoarchean	Gabbroic anorthosite	0.1
Agan	Neoarchean	Gabbroic anorthosite	0.1
APgb	Neoarchean or Paleoproterozoic	Gabbroic to dioritic intrusion and metamorphic equivalent	0.1
Agr	Neoarchean	Granite	0.1
Aqpeg	Neoarchean	Granite pegmatite (Kspar-quartz-muscovite-plagioclase)	0.1
Agr	Neoarchean	Granite plug	0.1
Agrm	Neoarchean	Granite to granodiorite, variably magnetic	0.1
Agrm	Neoarchean	Granite to granodiorite, variably magnetic, locally magmatically foliated	0.1
Agr	Neoarchean	Granitic dike	0.1
APgr	Neoarchean or Paleoproterozoic	Granitic intrusion of uncertain age	0.1
Agr	Neoarchean	Granitoid	0.1
Agru	Neoarchean	Granitoid intrusion, undifferentiated or poorly constrained by core and outcrop	0.1
Agd	Neoarchean	Granodiorite cuts the conglomerate and sed	0.1
Agn	Neoarchean	Granodiorite gneiss	0.1
Agd	Neoarchean	Granodiorite to diorite	0.1
Agd	Neoarchean	Granodiorite, foliated and synvolcanic	0.1
Agd	Neoarchean	Granodioritic intrusion	0.1
Aga	Neoarchean	Graphitic and tuffaceous metasediments	0.1
Aga	Neoarchean	Graphitic argillite	0.1
Ags	Neoarchean	Graywacke and mudstone; typically greenschist facies metamorphism	0.1
Ad	Neoarchean	Grey, fine to medium-grained, biotite-hornblende diorite	0.1
Ags	Neoarchean	Greywacke and slate	0.1
Ags	Neoarchean	Greywacke-slate	0.1
Ags	Neoarchean	Greywacke-slate, mixed sourced	0.1
Amvt	Neoarchean	Highly altered mafic tuffaceous rocks	0.1
Ad	Neoarchean	Hornblende diorite	0.1
Am	Neoarchean	Hornblende monzonite	0.1
Akv	Neoarchean	Hornblende-bearing volcanic flows, breccia and tuff	0.1
Ags	Neoarchean	Interbedded greywacke-slate	0.1
Amm	Neoarchean	Interlayered volcanic and volcaniclastic rocks; amphibolite grade metamorphism	0.1
Aql	Neoarchean	Lac La Croix Granite; locally pegmatitic and magnetic	0.1
Afvtl	Neoarchean	Laminated ash tuff	0.1
Afvtl	Neoarchean	Laminated dacitic ash tuff	0.1
Afvtl	Neoarchean	Laminated mudstone/ash tuff	0.1
Aag	Neoarchean	Leucogabbro, amphibole-bearing	0.1
Agrl	Neoarchean	Leucogranite	0.1
Agr	Neoarchean	Leucogranite with 1/3 amphibolite fragments	0.1
Agr	Neoarchean	Leucogranite with 1/3 biotite schist and amphibolite fragments	0.1
Agr	Neoarchean	Leucogranite with 1/3 biotite schist fragments	0.1
Aas	Neoarchean	Lithic and arkosic sandstone	0.1
Aas	Neoarchean	Lithic sandstone, mudstone, and siliceous siltstone with detrital hbld and plag	0.1
Ami	Neoarchean	Mafic intrusion, defined magnetically	0.1
Ami	Neoarchean	Mafic intrusion, undifferentiated	0.1
Amvu	Neoarchean	Mafic metavolcanic rocks	0.1
Amvu	Neoarchean	Mafic metavolcanic rocks and schistose equivalents	0.1
Amvu	Neoarchean	Mafic metavolcanic rocks; minor volcaniclastic and hypabyssal intrusions	0.1
Aszc	Neoarchean	Mafic mylonite	0.1
Ami	Neoarchean or Paleoproterozoic	Mafic plug-like intrusion; typically magnetic	0.1
Amvt	Neoarchean	Mafic tuff	0.1
Amvt	Neoarchean	Mafic tuff and sediments	0.1

Map Label	Era	Rock Type	W.O.E
Amvu	Neoarchean	Mafic volcanic and associated rocks	0.1
APmvu	Neoarchean or Paleoproterozoic	Mafic volcanic and hypabyssal intrusive rocks of uncertain age	0.1
Amvm	Neoarchean	Massive basalt	0.1
Amvm	Neoarchean	Massive basalt flows	0.1
Amvm	Neoarchean	Massive basalt lava flows with thin iron formation horizons	0.1
Amvm	Neoarchean	Massive basalt lava flows with thin iron formation horizons	0.1
Amvm	Neoarchean	Massive basalt sheet flow	0.1
Amvm	Neoarchean	Massive basalt with thin iron formation horizons	0.1
Amvm	Neoarchean	Massive basaltic lava flows	0.1
Afvm	Neoarchean	Massive dacite lava dome	0.1
Afvm	Neoarchean	Massive dacite, lava dome?	0.1
Afvm	Neoarchean	Massive felsic lava flows	0.1
Amvm	Neoarchean	Massive metabasaltic rocks and/or metagabbroic sill-like intrusive	0.1
Amgps	Neoarchean	Melagabbro sill, locally sulfide-bearing	0.1
Amgb	Neoarchean	Meta Orthopyroxene gabbro	0.1
Amvu	Neoarchean	Metabasaltic rocks	0.1
Amgb	Neoarchean	Meta-diabase sill	0.1
Amgb	Neoarchean	Metadiorite/gabbro	0.1
Amgb	Neoarchean	Metagabbro	0.1
Amgb	Neoarchean	Metagabbro intrusion	0.1
Amgb	Neoarchean	Metagabbro sill	0.1
Amgps	Neoarchean	Metagabbro sill, locally sulfide-bearing	0.1
Amgbs	Neoarchean	Metagabbro sill, weakly (0-3%) sulfide-bearing	0.1
Amgb	Neoarchean	Metagabbro sill, weakly sulfide-bearing	0.1
Aag	Neoarchean	Metagabbro, commonly chloritized	0
Amgb	Neoarchean	Metagabbro/metadiabase	0.1
Amgb	Neoarchean	Metagabbroic sill	0.1
Aszc	Neoarchean	Metamorphosed VMS chlorite alteration pipe	0.1
Amp	Neoarchean	Metaperidotite and pyroxenite sill	0.1
Amp	Neoarchean	Metaperidotite sill	0.1
Afve	Neoarchean	Mixed dacitic volcaniclastics, tuff-breccia-conglomerate	0.1
Asd	Neoarchean	Monzodiorite and syenite	0.1
Agrl	Neoarchean	Muscovite-biotite leucogranite	0.1
Aszc	Neoarchean or Paleoproterozoic	Mylonite	0.1
Aszu	Neoarchean	Mylonite zone	0.1
Pmy	Paleoproterozoic	Mylonitic, gneissic, schistose rocks of plutonic and volcanic protolith	0.1
Amss	Neoarchean	Partially melted sandstone	0.1
Amvp	Neoarchean	Pillow basalt	0.1
Amvp	Neoarchean	Pillow basalt, thoeliitic and commonly glomeroporphyritic	0.1
Acv	Neoarchean	Pillow breccia and tuff	0.1
Apd	Neoarchean	Pillow dike	0.1
Amvp	Neoarchean	Pillowed andesite lavas	0.1
Amvp	Neoarchean	Pillowed basalt	0.1
Amvp	Neoarchean	Pillowed basalt flows	0.1
Amvp	Neoarchean	Pillowed basaltic lava flows	0.1
Afp	Neoarchean	Plagioclase porphyritic dike	0.1
Afvtb	Neoarchean	Polymict felsic tuff breccia	0.1
Amgp	Neoarchean	Porphyritic (opx) melagabbro	0.1
Ad	Neoarchean	Porphyritic diorite	0.1
Amgps	Neoarchean	Porphyritic metagabbro sill, locally sulfide-bearing	0.1
Aqfp	Neoarchean	Quartz feldspar porphyry	0.1
Aqm	Neoarchean	Quartz monzonite	0.1
Aqm	Neoarchean	Quartz monzonite, monzonite, and granodiorite, non-magnetic	0.1
Aqmm	Neoarchean	Quartz monzonite, variably magnetic and magmatically foliated	0.1
Afvm	Neoarchean	Quartz-eye rhyolite lava flow with sphalerite veining	0.1
Afvm	Neoarchean	Rhyolite to latite lava flows	0.1
Afvm	Neoarchean	Rhyolite to rhyodacite lava flows and fragmental rocks	0.1
Afvt	Neoarchean	Rhyolitic to dacitic tuff and tuff breccia	0.1
Amgb	Neoarchean	Rusty, fine-grained chilled margin of gabbroic sills	0.1
Ags	Neoarchean	Schist and tonalite- to granodiorite-bearing paragneiss	0.1

Map Label	Era	Rock Type	W.O.E
Ams	Neoarchean	Schist of sedimentary protolith	0.1
Amp	Neoarchean	Serpentinized peridotite with chalcopyrite	0.1
Amp	Neoarchean	Serpentinized, strongly magnetic peridotite	0.1
Afvt	Neoarchean	Siliceous sediment and/or felsic tuff	0.1
Aks	Neoarchean	Slate, siltstone, lithic sandstone, and conglomerate	0.1
Amqgs	Neoarchean	Sulfide-bearing to sulfide-rich, quartz gabbro	0.1
Amgbs	Neoarchean	Sulfidic metagabbro	0.1
Amgbh	Neoarchean	Taxitic metagabbro	0.1
Afvtl	Neoarchean	Thin-bedded to laminated dacitic ash tuff	0.1
At	Neoarchean	Tonalite	0.1
Adt	Neoarchean	Tonalite to leucodiorite pluton	0.1
At	Neoarchean	Tonalite, diorite and granodiorite	0.1
At	Neoarchean	Tonalite, synvolcanic	0.1
At	Neoarchean	Tonalite, trondjehmite to leucogranite	0.1
Ags	Neoarchean	Tuffaceous metasediment (greywacke-slate?)	0.1
Amvu	Neoarchean	Undifferentiated Basalts	0.1
Agru	Neoarchean	Undifferentiated granitoid pluton defined magnetically	0.1
Amvpv	Neoarchean	Variolitic pillowed flows	0.1
Avs	Neoarchean	Volcanic and volcaniclastic rocks; felsic to intermediate composition	0.1
Ampxs	Neoarchean	Weakly sulfide-bearing pyroxenite	0.1
Amps	Neoarchean	Weakly sulfide-bearing, serpentinized peridotite	0.1
Aqs	Neoarchean	Biotite schist	0.05
Aqs	Neoarchean	Biotite schist, paragneiss, and schist-rich migmatite	0.05
Aqs	Neoarchean	Biotite-calcite-magnetite schist	0.05
Pvfg	Paleoproterozoic	Carbonaceous argillite	0.05
Pmq	Paleoproterozoic	Dam Lake Quartzite	0.05
Pmd	Paleoproterozoic	Denham Formation; sandstone, marble, schist	0.05
Pfv	Paleoproterozoic	felsic volcanic rocks	0.05
Aqg	Neoarchean	Granite-rich migmatite, locally magnetic	0.05
Amg	Mesoarchean to Paleoarchean	Granitic orthogneiss and migmatite	0.05
Agn	Neoarchean	Granitic to granodioritic orthogneiss	0.05
Amd	Mesoarchean to Paleoarchean	Granitoid gneiss with amphibolitic to dioritic enclaves	0.05
Pag	Paleoproterozoic	Greywacke slate	0.05
Pvs	Paleoproterozoic	Interlayered metasedimentary and metavolcanic rocks	0.05
Pmv	Paleoproterozoic	Mafic metavolcanic and hypabyssal intrusive rocks	0.05
Pms	Paleoproterozoic	Massive pyrite-pyrrhotite, locally saprolitic and siliceous	0.05
Pmv	Paleoproterozoic	Metabasaltic amphibolite	0.05
Pmvm	Paleoproterozoic	Metabasaltic rocks metamorhhosed to amphibolite grade	0.05
Pmdb	Paleoproterozoic	Metadiabase/metagabbro sill-like intrusive	0.05
Pvs	Paleoproterozoic	metasedimentary and metavolcanic rocks	0.05
Pm	Paleoproterozoic	Mudstone, quartzite, graywacke, phyllite, graphitic argillite	0.05
Acgm	Neoarchean	Partially melted conglomerate	0.05
Aqs	Neoarchean	Schist-rich migmatite	0.05
Psi	Paleoproterozoic	Sulfidic and graphitic iron-formation	0.05
Psi	Paleoproterozoic	Sulfidic iron-formation	0.05
Aqt	Neoarchean	Tonalite- to granodiorite-rich migmatite	0.05
Pifa	Paleoproterozoic	Algoma-type iron formation	0.01
Aifcb	Neoarchean	Carbonate facies iron formation	0.01
Aifc	Neoarchean	Chert and lean iron formation	0.01
Aifc	Neoarchean	Cherty interflow exhalite with pyrite	0.01
Aifc	Neoarchean	Cherty iron formation	0.01
Aifc	Neoarchean	Cherty iron formation with pyrite	0.01
Aifc	Neoarchean	Cherty sedimentary rocks	0.01
Aifo	Neoarchean	Highly magnetic oxide-facies iron formation	0.01
Aifo	Neoarchean	Inferred iron formation	0.01
Aifo	Neoarchean	Inferred iron formation, defined magnetically	0.01
Avms	Neoarchean	Interflow chemical sediment, commonly with Mgt-Py-Cp	0.01
Avms	Neoarchean	Interflow chemical sediment, commonly with Mgt-Py-Cp	0.01
Aifo	Neoarchean	Iron Formation	0.01
Aifo	Neoarchean	Iron formation interlayered with green sandstone	0.01

Map Label	Era	Rock Type	W.O.E
Aifo	Neoarchean	Iron formation, defined magnetically	0.01
Aifo	Neoarchean	Iron Formation, defined via linear positive magnetic anomaly	0.01
Aifo	Neoarchean	Iron Formation, inferred from aeromagnetic data	0.01
Aifo	Neoarchean	Iron Formation, inferred from positive magnetic anomaly	0.01
Aifo	Neoarchean	Iron-formation	0.01
Aifo	Neoarchean	Oxide facies banded iron formation	0.01
Aifo	Neoarchean	Oxide Facies Iron Formation	0.01
Aifo	Neoarchean	Oxide-facies iron formation, highly magnetic	0.01
Aifsl	Neoarchean	Silicate facies iron formation	0.01
Aifs	Neoarchean	Sulfide facies iron formation	0.01
Aifs	Neoarchean	Sulfide-facies iron fromation, ie., bedded massive sulfide	0.01
Aifs	Neoarchean	Sulfidic interpillow exhalitive deposits	0.01
Pifs	Paleoproterozoic	Superior type iron formation	0.01
Aifo	Neoarchean	Thin BIF horizon in mafic tuff	0.01
Aifo	Neoarchean	Thin iron formation horizon in massive basalt	0.01
Aifo	Neoarchean	Thin iron formation in altered mafic tuff	0.01
Pvfg	Paleoproterozoic	Virginia Formation graphitic argillite w/ argillite, chert, and carbonate-silicate iron formation	0.01
Pifs	Paleoproterozoic	Virginia Formation Iron Formation associated w/ graphitic argillites	0.01
Pac	Paleoproterozoic	Virginia Formation slate with thin limestone interbeds	0.01
Pifs	Paleoproterozoic	Superior type iron formation	0.01

Results

The Orogenic Mineral System Potential Map is illustrated in Figure 14 (with a Minnesota geology map underlay) and in Figure 15 (without the Minnesota geology map underlay). Shapefiles for the Orogenic Mineral System Potential Map can be found in Digital Appendix 4 in the subdirectory labeled "Shapefiles." Model calculations can be found in Digital Appendix 4 in the subdirectory labeled "Model Calculations."

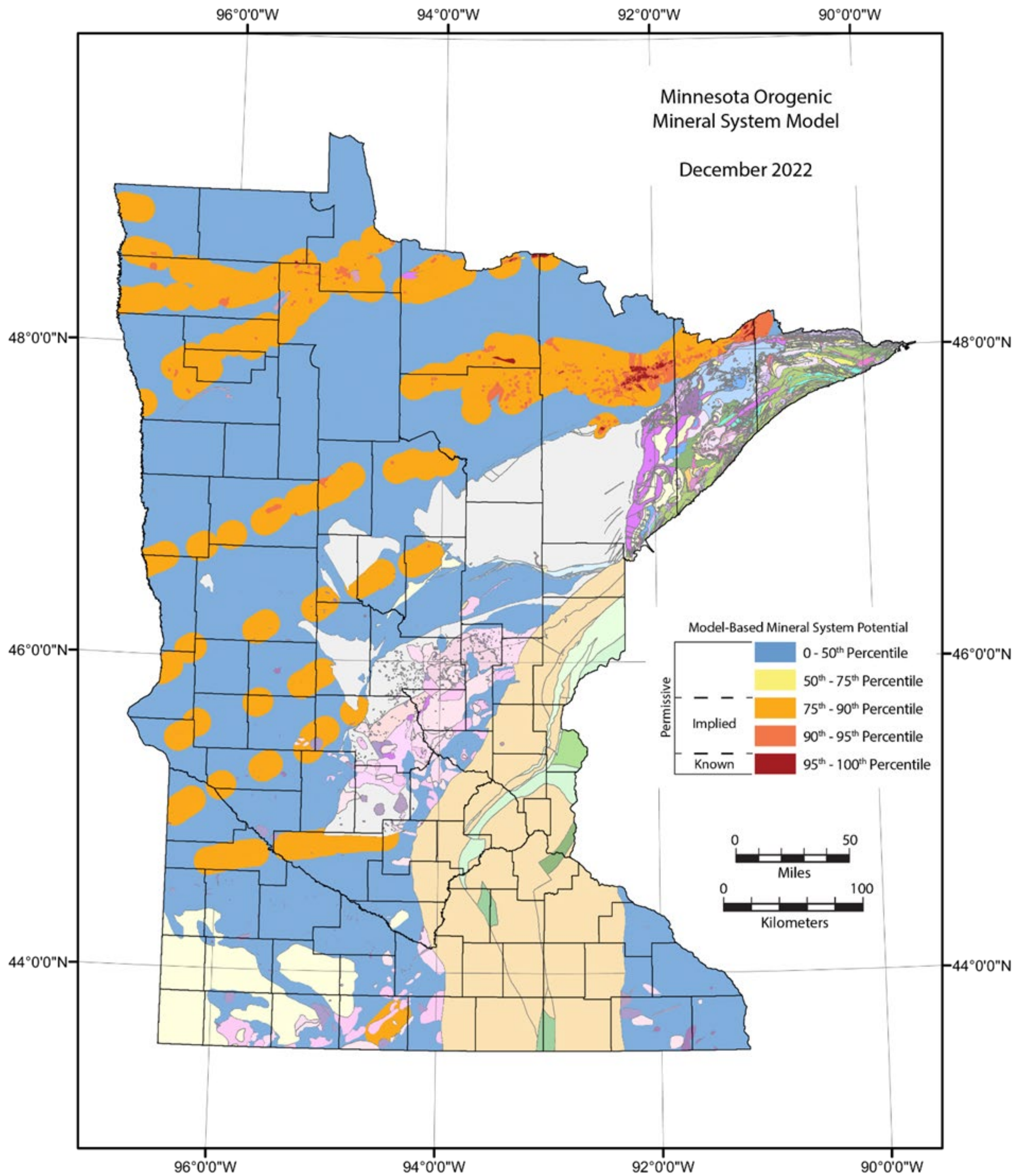

Figure 14. Results of ***Orogenic*** knowledge-based mineral system model with geology.

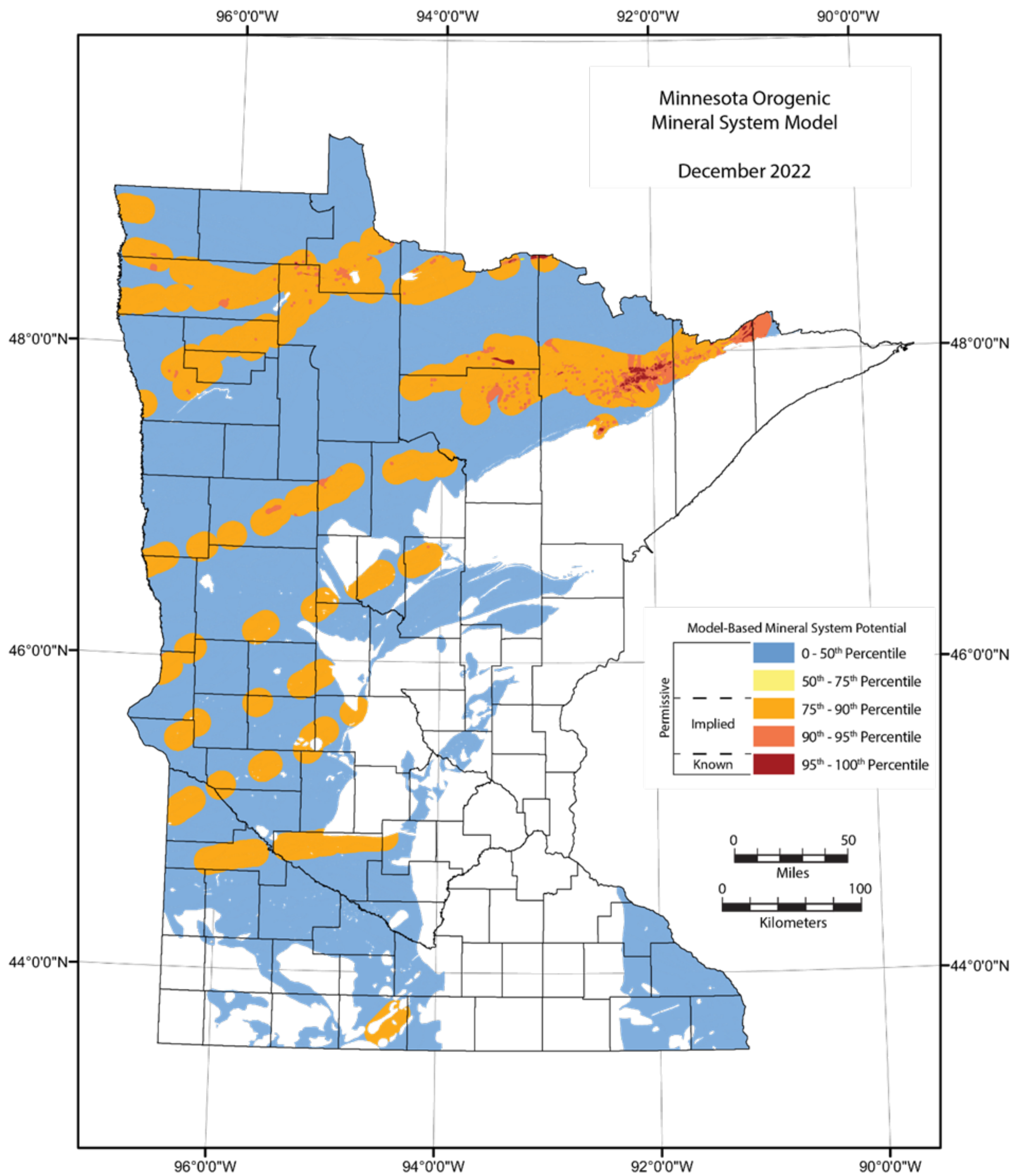

Figure 15. Results of ***Orogenic*** knowledge-based mineral system model without geology.

Based on the modeling, the highest probabilities for the presence of Orogenic mineral system-associated orogenic gold deposits occur within the Abitibi-Wawa and Wabigoon subprovinces within the northernmost one-third of Minnesota. Within the Abitibi-Wawa subprovince, the highest probabilities for Orogenic mineral systems occur in the nortwestern and east-central part of St. Louis County, the northern one-third of Itasca County, the southernmost part of Koochiching County, western Hubbard County, and east-central Becker County. Within the Wabigoon subprovince, the highest probabilities for Orogenic mineral system-related mineralization occur in the northwestern part of Koochiching County, the southern one-third of Lake of the Woods County, the northwestern part of Beltrami County, the west-central part of Polk County, and within the east-central and northwestern parts of Marshall County. The modeled regions correlate well with the six areas of gold exploration identified by Severson (2011), as well as a weights of evidence model developed by Hartley (2014).

Metamorphic Mineral System

Deposit Types and Model

Table 9 indicates the various mineral deposit types associated with the Metamorphic mineral system , which include amorphous or flake graphite, magnesite, gneiss-related REE deposits, and gneiss-related uranium deposits (Hofstra and Kreiner, 2021). Metasomatic processes can produce fluids that can mobilize and concentrate these commodities within such geological environments.

Table 9. Systems-Deposits-Commodities-Critical Minerals table for the ***Metamorphic*** mineral system (modified after Hofstra and Kreiner, 2021). Explanation for table is as follows: ±, present (absent); --, not applicable; ?, maybe; Ag, silver; Al, aluminum; As, arsenic; Au, gold; B, boron; Ba, barium; Be, beryllium; Bi, bismuth; Br, bromine; Ca, calcium; Cd, cadmium; Co, cobalt; CO_2, carbon dioxide; Cs, cesium; Cr, chromium; Cu, copper; F, fluorine; Fe, iron; Ga, gallium; Ge, germanium; Hf, hafnium; Hg, mercury; I, iodine; IAEA, International Atomic Energy Agency; In, indium; IOA, iron oxide-apatite; IOCG, iron oxide-copper-gold; IS, intermediate sulfidation; K, potassium; LCT, lithium-cesium-tantalum; Li, lithium; Mg, magnesium; Mn, manganese; Mo, molybdenum; Na, sodium; Nb, niobium; Ni, nickel; NYF, niobium-yttrium-fluorine; P, phosphorus; Pb, lead; PGE, platinum group elements; R, replacement; Rb, rubidium; Re, rhenium; REE, rare earth elements; S, skarn; Sb, antimony; Sc, scandium; Se, selenium; Sn, tin; Sr, strontium; Ta, tantalum; Te, tellurium; Th, thorium; Ti, titanium; U, uranium; V, vanadium (in “Principal Commodities” column); V, vein (in “Deposit Types” column); W, tungsten; Y, yttrium; Zn, zinc; Zr, zirconium. In the “Critical Minerals” column, elements in **bold** have been produced from the deposit type, whereas element in *italics* are enriched in the deposit type but have not been produced.

System Name	Deposit Types	Principal Commodities	Critical Minerals	References
Metamorphic	Graphite (coal or carbonaceous sediments/ sedimentary rocks)	Graphite (amorphous and flake)	Graphite (amorphous and flake)	Sutphin, 1991a, 1991b, 1991c; Hauck et al., 2014; Luque et al., 2014; McKinney et al., 2015; Sutherland and Cola, 2016; Robinson et al., 2017; Menzel et al., 2018; IAEA, 2020
	Magnesite	Mg	**Mg**	
	Gneiss REE	Th, U, REE, Y	**REE,** *U*	
	Gneiss Uranium	U	**U**	

The knowledge-based fuzzy logic model produced for this study is focused primarily on Metamorphic mineral system-associated graphite deposits. According to Robinson et al. (2017), most economically viable natural graphite deposits are mined from metamorphic rocks including marble, schist, and gneiss. Commercial deposits of natural graphite can be classified into three types:

- Amorphous graphite, which is genetically related to thermal metamorphism of coal;
- Flake graphite, which occurs in carbon-rich rock that have been subjected to amphibolite facies or higher grade regional metamorphism; and
- Lump graphite, which occurs as fracture fillings or veins withing igneous intrusions or metamorphic rocks that are commonly Precambrian in age. Luque et al. (2014) have completed a detailed study of vein graphite deposits and has shown that graphite mineralization in granulite-hosted vein deposits and igneous-hosted vein deposits are produced by different genetic processes.

Key exploration criteria for Metamorphic mineral system-associated graphite deposits include:

- Amphibolite-grade or higher metamorphic rocks;
- The presence of graphite associated with mineral assemblages indicative of amphibolite or higher grade metamorphism;
- The presence of geological contacts between rock types that can contain significant carbon contents;
- Geochemical correlations between rocks containing graphite deposits and vanadium, nickel, carbon, and uranium contents (Li et al., 1985 (referenced from Robinson et al., 2017); Tichy and Turnovec, 1978); and
- A strong response to electromagnetic survey due to the conductive property of graphite (Marjoribanks, 2010).

A detailed discussion of Metamorphic mineral system deposits is beyond the scope of this study. The reader is referred to Orris and Bliss (1991), Luque et al. (2014), McKinney et al. (2015), Robinson et al. (2017), and Menzel et al. (2018) for detailed discussions of mineral deposits associated with the Metamorphic mineral system.

Modeling Methods

The fuzzy logic modeling methodology for the Metamorphic mineral system included five components that could be ascertained from the Assembling Minnesota dataset (Bartsch et al., 2022; Peterson, 2018). These five components include: 1) bedrock geology; 2) mineral occurrences; 3) geological contacts; 4) geochemistry; and 5) geophysics. The inference net illustrating the various components used in the Placer Mineral System model are illustrated in Figure 16. This model focuses on graphite-bearing deposits associated with the Metamorphic mineral system.

Bedrock geology focused on six main components. Polygons of permissible host rock types (schist/gneiss/migmatite, felsic intrusions, graywacke/shale/slate, intermediate intrusions, graphitic argillite, and mafic/ultramafic intrusions) were extracted from the Assembling Minnesota gedrock and drillhole geology database and given W.O.E. based on their prospectivity for hosting metamorphic graphite mineralization. The W.O.E. for the various lithological units utilized in the model are provided in Table 10. The various polygons represented the Geology Factor utilized in the model.

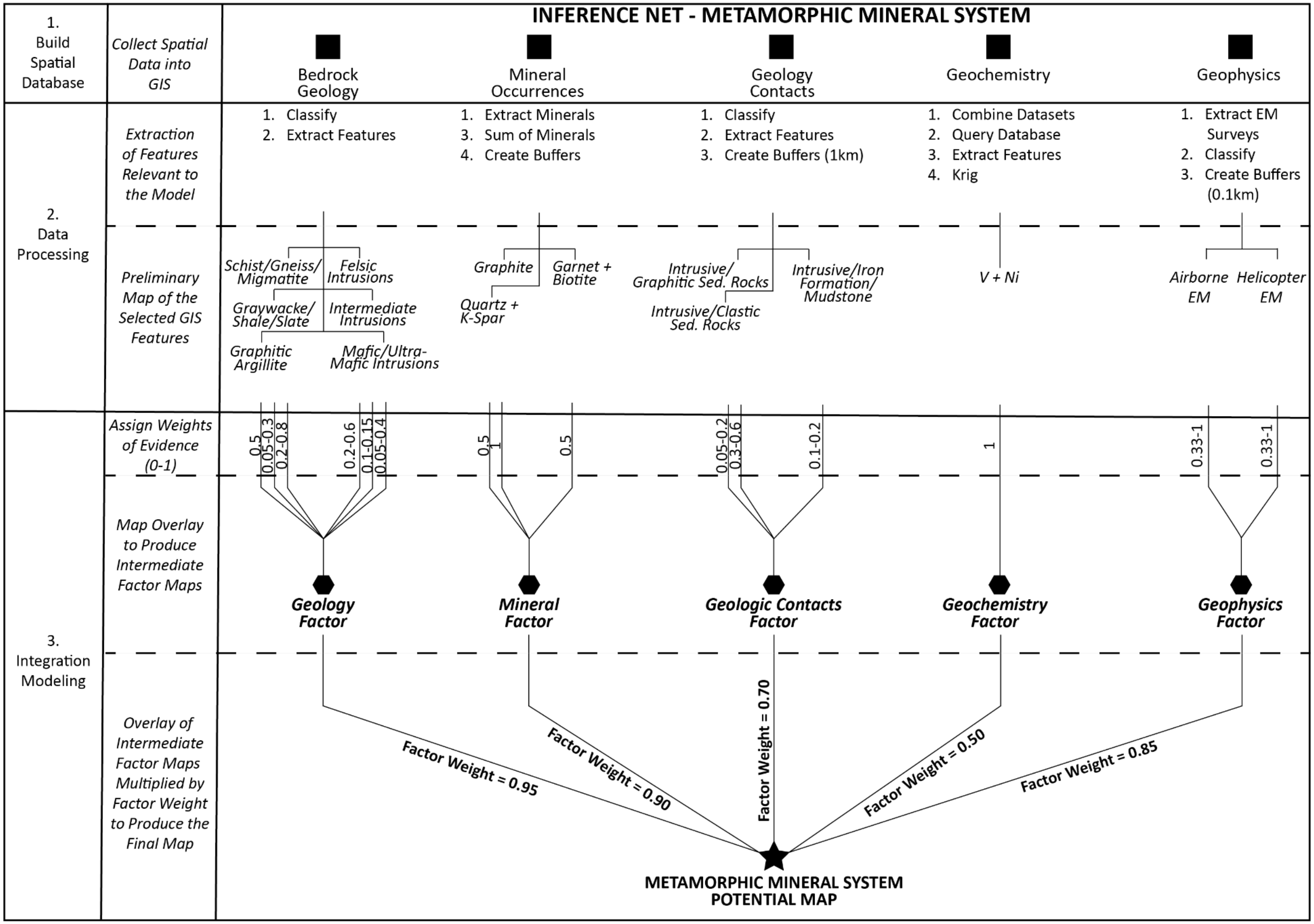

Figure 16. Inference net for ***Metamorphic*** knowledge-based mineral system model.

Table 10. Weights of evidence for geology polygons in the ***Metamorphic*** mineral system model.

Map Label	Era	Rock Type	W.O.E.
Ags	Neoarchean	Schist and tonalite- to granodiorite-bearing paragneiss	0.8
Aqs	Neoarchean	Schist-rich migmatite	0.7
Pls	Paleoproterozoic	Staurolite-garnet pelitic schist	0.7
Aqs	Neoarchean	Biotite schist, paragneiss, and schist-rich migmatite	0.6
Prfm	Paleoproterozoic	Disrupted and melted metasedimentary rocks	0.6
Aqg	Neoarchean	Granite-rich migmatite, locally magnetic	0.6
Ams	Neoarchean	Biotite schist	0.5
Ams	Neoarchean	Biotite schist	0.5
Ams	Neoarchean	Biotite schist	0.5
Ams	Neoarchean	Biotite schist	0.5
Ams	Neoarchean	Biotite schist	0.5
Aqs	Neoarchean	Biotite schist	0.5
Aqs	Neoarchean	Biotite schist	0.5
Pvfg	Paleoproterozoic	Carbonaceous argillite	0.5
Aga	Neoarchean	Graphitic & pyritic argillite	0.5
Aga	Neoarchean	Graphitic and pyritic argillite	0.5
Aga	Neoarchean	Graphitic and pyritic sedimentary rocks intercalated with felsic tuffs	0.5
Aga	Neoarchean	Graphitic and tuffaceous metasediments	0.5
Aga	Neoarchean	Graphitic argillite	0.5
Aga	Neoarchean	Graphitic argillite with minor pyrite	0.5
Aga	Neoarchean	Graphitic sediment with 0.5-2% pyrite	0.5
Aam	Neoarchean	Interlatered biotite schist and amphibolite	0.5
Aql	Neoarchean	Lac La Croix Granite; locally pegmatitic and magnetic	0.5
Aga	Neoarchean	Schistose graphitic argillite with 1-5% pyrite	0.5
Aga	Neoarchean	Sheared graphitic and pyritic argillite	0.5
Aqs	Neoarchean	Biotite-calcite-magnetite schist	0.4
Moui	Mesoproterozoic	Oxide Ultramafic Intrusion	0.4
Psi	Paleoproterozoic	Sulfidic and graphitic iron-formation	0.4
Avms	Neoarchean	Bedded massive sulfide	0.3
Avms	Neoarchean	Bedded massive sulfide	0.3
Avms	Neoarchean	Bedded massive sulfide	0.3
Ags	Neoarchean	Biotitic greywacke-slate	0.3
Ams	Neoarchean	Biotitic metagreywacke-slate	0.3
Pgs	Paleoproterozoic	Graywacke, slate with graphitic and sulfidic zones	0.3
Pms	Paleoproterozoic	Massive pyrite-pyrrhotite, locally saprolitic and siliceous	0.3
Avms	Neoarchean	Massive sulfide	0.3
Avms	Neoarchean	Massive sulfide (VMS-type)	0.3
Avms	Neoarchean	Massive sulfide is felsic breccias	0.3
Avms	Neoarchean	Massive sulfide to Semi-massive sulfide breccia with felsic fragments in flowed iron sulfide	0.3
Avms	Neoarchean	Massive sulfide, pyrite-rich	0.3
Pm	Paleoproterozoic	Mudstone, quartzite, graywacke, phyllite, graphitic argillite	0.3
Acgm	Neoarchean	Partially melted conglomerate	0.3
Acgm	Neoarchean	Partially melted conglomeratic rocks	0.3
Amss	Neoarchean	Partially melted sandstone	0.3
Agr	Neoarchean	Leucogranite with 1/3 biotite schist and amphibolite fragments	0.25
Agr	Neoarchean	Leucogranite with 1/3 biotite schist fragments	0.25
Psi	Paleoproterozoic	Sulfidic iron-formation	0.25
Pvfg	Paleoproterozoic	Virginia Formation graphitic argillite w/ argillite, chert, and carbonate-silicate iron formation	0.25
Mgr	Mesoproterozoic	Biotite granite	0.2
Mgr	Mesoproterozoic	Biotite granite	0.2
Mgr	Mesoproterozoic	Biotite granite	0.2
Mgr	Mesoproterozoic	Biotite granite	0.2
Mgr	Mesoproterozoic	Biotite granite	0.2
Mgr	Mesoproterozoic	Biotite granite	0.2
Mgr	Mesoproterozoic	Biotite granite	0.2
Mgr	Mesoproterozoic	Biotite granite	0.2
Mgr	Mesoproterozoic	Biotite granite	0.2
Mgr	Mesoproterozoic	Biotite granite	0.2

Map Label	Era	Rock Type	W.O.E.
Mgr	Mesoproterozoic	Biotite granite	0.2
Mgr	Mesoproterozoic	Biotite granite	0.2
Mgr	Mesoproterozoic	Biotite granite	0.2
Mgr	Mesoproterozoic	Biotite granite	0.2
Mgr	Mesoproterozoic	Biotite granite	0.2
Mgr	Mesoproterozoic	Biotite granite	0.2
Mgr	Mesoproterozoic	Biotite granite	0.2
Mgr	Mesoproterozoic	Granite	0.2
Mgr	Mesoproterozoic	Granite dike	0.2
Aqpeg	Neoarchean	Granite pegmatite (Kspar-quartz-muscovite-plagioclase)	0.2
Agr	Neoarchean	Granite plug	0.2
Agrm	Neoarchean	Granite to granodiorite, variably magnetic	0.2
Agrm	Neoarchean	Granite to granodiorite, variably magnetic, locally magmatically foliated	0.2
Mgr	Mesoproterozoic	Granite to quartz-monzodiorite	0.2
Mgr	Mesoproterozoic	Granite xenolith in the BRD	0.2
Pgr	Paleoproterozoic	Granite, red to pink, variably porphyritic, massive	0.2
Pgu	Paleoproterozoic	Granite, undifferentiated	0.2
Agr	Neoarchean	Granitic dike	0.2
Agr	Neoarchean	Granitic intrusion	0.2
APgr	Neoarchean or Paleoproterozoic	Granitic intrusion of uncertain age	0.2
Pgm	Paleoproterozoic	Granitic intrusion, variably magnetic	0.2
Amg	Neoarchean	Granitic orthogneiss and migmatite	0.2
Agn	Neoarchean	Granitic to granodioritic orthogneiss	0.2
Agr	Neoarchean	Granitoid	0.2
Amd	Mesoarchean to Paleoarchean	Granitoid gneiss with amphibolitic to dioritic enclaves	0.2
Agru	Neoarchean	Granitoid intrusion, undifferentiated or poorly constrained by core and outcrop	0.2
Mgr	Mesoproterozoic	Hornblende granite	0.2
Mgr	Mesoproterozoic	Leucogranite	0.2
Agr	Neoarchean	Leucogranite with 1/3 amphibolite fragments	0.2
Pml	Paleoproterozoic	Mille Lacs granite	0.2
Agrl	Neoarchean	Muscovite-biotite leucogranite	0.2
Pmy	Paleoproterozoic	Mylonitic, gneissic, schistose rocks of plutonic and volcanic protolith	0.2
Pgn	Paleoproterozoic	Quartzofeldspathic orthogneiss and schist	0.2
Asd	Neoarchean	Syenite	0.2
Asd	Neoarchean	Syenitic, monzodioritic, or dioritic pluton	0.2
Agru	Neoarchean	Undifferentiated granitoid pluton defined magnetically	0.2
Pifa	Paleoproterozoic	Algoma-type iron formation	0.15
Asd	Neoarchean	Alkalic (syenitic, monzodioritic, dioritic), amphibole & pyroxene-bearing intrusions	0.15
Aam	Neoarchean	Amphibolite, schistose to gneissic	0.15
Aam	Neoarchean	Amphibolitic schist and gneiss	0.15
Aifcb	Neoarchean	Carbonate facies iron formation	0.15
Pmd	Paleoproterozoic	Denham Formation; sandstone, marble, schist	0.15
Agd	Neoarchean	Foliated granodioritic intrusion	0.15
Atf	Mesoarchean to Paleoarchean	Foliated to gneissic granodiorite to tonalite	0.15
Atf	Neoarchean	Foliated to gneissic tonalite, diorite and granodiorite	0.15
Mgd	Mesoproterozoic	Granodiorite	0.15
Agd	Neoarchean	Granodiorite cuts the conglomerate and sed	0.15
Agn	Neoarchean	Granodiorite gneiss	0.15
Agd	Neoarchean	Granodiorite to diorite	0.15
Agd	Neoarchean	Granodiorite, foliated and synvolcanic	0.15
Pdg	Paleoproterozoic	Granodiorite; variably foliated	0.15
Agd	Neoarchean	Granodioritic intrusion	0.15
Pgd	Paleoproterozoic	Gray granodioritic to dioritic intrusion	0.15
Ad	Neoarchean	Grey, fine to medium-grained, biotite-hornblende diorite	0.15
Amvt	Neoarchean	Highly altered mafic tuffaceous rocks	0.15
Aifo	Neoarchean	Highly magnetic oxide-facies iron formation	0.15
Ad	Neoarchean	Hornblende diorite	0.15
Mgrd	Mesoproterozoic	Hornblende granodiorite	0.15

Map Label	Era	Rock Type	W.O.E.
Am	Neoarchean	Hornblende monzonite	0.15
Aifo	Neoarchean	Inferred iron formation	0.15
Aifo	Neoarchean	Inferred iron formation, defined magnetically	0.15
Avms	Neoarchean	Interflow chemical sediment, commonly with Mgt-Py-Cp	0.15
Pifs	Paleoproterozoic	Iron Formation	0.15
Aifo	Neoarchean	Iron formation interlayered with green sandstone	0.15
Aifo	Neoarchean	Iron formation, defined magnetically	0.15
Aifo	Neoarchean	Iron Formation, defined via linear positive magnetic anomaly	0.15
Aifo	Neoarchean	Iron Formation, inferred from aeromagnetic data	0.15
Aifo	Neoarchean	Iron Formation, inferred from positive magnetic anomaly	0.15
Aifo	Neoarchean	Iron-formation	0.15
Asd	Neoarchean	Monzodiorite and syenite	0.15
Mmd	Mesoproterozoic	Monzodiorite, granite, and granodiorite	0.15
Mmd	Mesoproterozoic	Monzodioritic rocks	0.15
Am	Neoarchean	Monzonite	0.15
Aifo	Neoarchean	Oxide facies banded iron formation	0.15
Aifo	Neoarchean	Oxide Facies Iron Formation	0.15
Aifo	Neoarchean	Oxide-facies iron formation	0.15
Aifo	Neoarchean	Oxide-facies iron formation, highly magnetic	0.15
Aifo	Neoarchean	Oxide-facies iron formation, highly magnetic	0.15
Mfm	Mesoproterozoic	Pyroxene-quartz ferromonzonite	0.15
Aqm	Neoarchean	Quartz monzonite	0.15
Aqm	Neoarchean	Quartz monzonite, monzonite, and granodiorite, non-magnetic	0.15
Aqmm	Neoarchean	Quartz monzonite, variably magnetic and magmatically foliated	0.15
Mfmd	Mesoproterozoic	Quartz-bearing ferromonzodiorite	0.15
Mmd	Mesoproterozoic	Quartz-bearing monzodiorite	0.15
Aifo	Neoarchean	Sheared iron formation, Quartz-calcite-magnetite schist	0.15
Aifo	Neoarchean	Sheared Iron-formation	0.15
Aifsl	Neoarchean	Silicate facies iron formation	0.15
Aifo	Neoarchean	Stretched iron formation	0.15
Aifs	Neoarchean	Sulfide facies iron formation	0.15
Aifs	Neoarchean	Sulfide-facies iron formation	0.15
Avms	Neoarchean	Sulfide-facies iron fromation, ie., bedded massive sulfide	0.15
Aifo	Neoarchean	Thin BIF horizon in mafic tuff	0.15
Aifo	Neoarchean	Thin iron formation horizon in massive basalt	0.15
Aifo	Neoarchean	Thin iron formation in altered mafic tuff	0.15
Avs	Neoarchean	Thin zones of massive sulfide in altered felsic tuff	0.15
Avms	Neoarchean	Thin zones of massive sulfide in altered felsic tuff	0.15
Aam	Neoarchean	Amphibolite	0.1
Aam	Neoarchean	Amphibolite schist. Composed of hbld-bio-chl with thin magnetite-cherty layers	0.1
Amn	Mesoarchean to Paleoarchean	Amphibolitic to dioritic gneiss	0.1
Md	Mesoproterozoic	Diorite	0.1
Ad	Neoarchean	Diorite, synvolcanic intrusion	0.1
APd	Neoarchean or Paleoproterozoic	Dioritic to granodioritic intrusion of uncertain age	0.1
Pmda	Paleoproterozoic	Dolomitic arkose sandstone	0.1
Pmdm	Paleoproterozoic	Dolomitic marble	0.1
Afp	Neoarchean	Feldspar porphyry	0.1
Afp	Neoarchean	Feldspar-hornblende porphyry	0.1
Atf	Neoarchean	Foliated to gneissic tonalite	0.1
Mgy	Mesoproterozoic	Granophyre	0.1
Pvf	Paleoproterozoic	Greywacke, mudstone, and argillite	0.1
Prf	Paleoproterozoic	Greywacke, siltstone and argillite	0.1
Ags	Neoarchean	Greywacke-slate	0.1
Ags	Neoarchean	Greywacke-slate, mixed sourced	0.1
Ags	Neoarchean	Interbedded greywacke-slate	0.1
At	Neoarchean	Lt grey, fine to medium-grained, foliated biotite tonalite	0.1
Mmgy	Mesoproterozoic	Melagranophyre	0.1
Pd	Paleoproterozoic	Mesocratic Diorite	0.1
Mpd	Mesoproterozoic	Porphyritic diorite	0.1
Mmd	Mesoproterozoic	Pyroxene-quartz Monzodiorite	0.1

Map Label	Era	Rock Type	W.O.E.
Mqd	Mesoproterozoic	Quartz diorite	0.1
Mfmd	Mesoproterozoic	Quartz ferromonzodiorite	0.1
Mfm	Mesoproterozoic	Quartz ferromonzonite to ferromonzodiorite	0.1
Afvm	Neoarchean	Quartz-eye rhyolite lava flow with sphalerite veining	0.1
Aqfp	Neoarchean	Quartz-feldspar porphyry	0.1
Aqfp	Neoarchean	Quartz-feldspar porphyry, gold bearing	0.1
Mfmd	Mesoproterozoic	Quartz-ferromonzodiorite	0.1
Aqfp	Neoarchean	Sheared quartz-feldspar porphyry	0.1
Mfmd	Mesoproterozoic	Sparsely porphyritic quartz-ferromonzodiorite	0.1
Mfmd	Mesoproterozoic	Sparsely porphyritic, amygduloidal quartz-ferromonzodiorite	0.1
Pifs	Paleoproterozoic	Superior type iron formation	0.1
At	Neoarchean	Tonalite	0.1
Aqt	Neoarchean	Tonalite- to granodiorite-rich migmatite	0.1
Adt	Neoarchean	Tonalite to leucodiorite pluton	0.1
Pgt	Paleoproterozoic	Tonalite with abundant biotite schist of graywacke protolith	0.1
At	Neoarchean	Tonalite, diorite and granodiorite	0.1
At	Neoarchean	Tonalite, synvolcanic	0.1
At	Neoarchean	Tonalite, trondjehmite to leucogranite	0.1
Aqt	Neoarchean	Tonalite-granodiorite-rich migmatite	0.1
Pac	Paleoproterozoic	Virginia Formation slate with thin limestone interbeds	0.1
Mpth	Mesoproterozoic	Altered troctolitic rocks	0.05
Man	Mesoproterozoic	Anorthosite	0.05
Maat	Mesoproterozoic	Anorthosite with troctolitic rocks	0.05
Mai	Mesoproterozoic	Anorthosite xenolith	0.05
Magh	Mesoproterozoic	Anorthosite, gabbro, and hornfels undivided	0.05
Mag	Mesoproterozoic	Anorthositic gabbro	0.05
Mag	Mesoproterozoic	Anorthositic gabbro to gabbro	0.05
Mags	Mesoproterozoic	Anorthositic gabbro, locally altered and sulfide-bearing	0.05
Mant	Mesoproterozoic	Anorthositic norite	0.05
Mau	Mesoproterozoic	Anorthositic rocks, undivided	0.05
Mat	Mesoproterozoic	Anorthositic troctolite	0.05
Mat	Mesoproterozoic	Anorthositic troctolite to troctolite	0.05
Mai	Mesoproterozoic	Anorthositic xenolith	0.05
Mfd	Mesoproterozoic	Apatite-bearing, ferrodiorite	0.05
Mfg	Mesoproterozoic	Apatitic ferrogabbro	0.05
feMD	Mesoproterozoic	Augite ferromonzodiorite, coarse-grained, prismatic ferromonzodiorite	0.05
Mpt	Mesoproterozoic	Augite troctolite	0.05
Mtpt	Mesoproterozoic	Augite troctolite to troctolite	0.05
Mg	Mesoproterozoic	Coarse-grained gabbro	0.05
Mgg	Mesoproterozoic	Coarse-grained, granophyric gabbro	0.05
Mprs	Mesoproterozoic	Coarse-grained, Ni-Cu sulfide-bearing peridotite	0.05
Mai	Mesoproterozoic	Coarse-grained, ophitic gabbroic anorthosite	0.05
Mxn	Mesoproterozoic	Contaminated, oxide-rich, noritic contact zone	0.05
Mfg	Mesoproterozoic	Cumulate-textured ferrogabbro	0.05
Mbrd	Mesoproterozoic	Diabase	0.05
Mdb	Mesoproterozoic	Diabase dike	0.05
Mdbm	Mesoproterozoic	Diabase dike, highly magnetic	0.05
Mdbn	Mesoproterozoic	Diabase Dike, normally polarized	0.05
Mdbr	Mesoproterozoic	Diabase dike, reversely polarized	0.05
Mdb	Mesoproterozoic	Diabase dike, sill	0.05
Mdb	Mesoproterozoic	Diabase dike, sill and/or plug-like intrusion	0.05
Ami	Neoarchean	Diabase plug	0.05
Pdb	Paleoproterozoic	Diabase sill	0.05
Mbrd	Mesoproterozoic	Diabase-gabbro	0.05
Mdbx	Mesoproterozoic	Diatreme breccia	0.05
Mpth	Mesoproterozoic	Eastern heterogeneous troctolite zone	0.05
Mdb	Mesoproterozoic	Ferrodiabase	0.05
Mfd	Mesoproterozoic	Ferrodiorite	0.05
Mfg	Mesoproterozoic	Ferrogabbro	0.05
Mfg	Mesoproterozoic	Ferrogabbro to ferromonzonite	0.05
Mfg	Mesoproterozoic	Ferrogabbro to quartz ferromonzodiorite	0.05
Mfd	Mesoproterozoic	Ferrogranodiorite	0.05

Map Label	Era	Rock Type	W.O.E.
Mfmd	Mesoproterozoic	Ferromonzodiorite to ferrogabbro	0.05
Mfmd	Mesoproterozoic	Ferromonzodiorite to granodiorite	0.05
Mfm	Mesoproterozoic	Ferromonzonite	0.05
feM	Mesoproterozoic	Ferromonzonite hybrid	0.05
Mfm	Mesoproterozoic	Ferromonzonite to ferrogranite	0.05
feMD	Mesoproterozoic	Ferromonzonite to ferromonzodiorite	0.05
Mdb	Mesoproterozoic	Fine to medium-grained, locally plag-phyric, ophitic olivine diabase	0.05
Mpt	Mesoproterozoic	Fine to medium-grained, poorly to moderately foliated, subophitc augite troctolite to troctolite	0.05
Mg	Mesoproterozoic	Fine-grained, foliated gabbro	0.05
Mmg	Mesoproterozoic	Fine-medium-grained, oxide-bearing microgabbro	0.05
Mfd	Mesoproterozoic	Foliated ferrodiorite	0.05
Mg	Mesoproterozoic	Foliated gabbro	0.05
Mxg	Mesoproterozoic	Foliated, oxide-bearing (lenses), gabbro	0.05
Amgb	Neoarchean	Gabbro	0.05
PMm	Paleoproterozoic or Mesoproterozoic	Gabbro and anorthosite	0.05
Mg	Mesoproterozoic	Gabbro sill	0.05
Pgp	Paleoproterozoic	Gabbro, pyroxenite, diorite, and lamprophyre intrusion	0.05
Mgd	Mesoproterozoic	Gabbro-diorite	0.05
Mga	Mesoproterozoic	Gabbroic anorthosite	0.05
Mga	Mesoproterozoic	Gabbroic anorthosite pegmatite	0.05
Mfg	Mesoproterozoic	Gabbroic rock with mottled granophyric zones	0.05
Mg	Mesoproterozoic	Gabbroic rocks	0.05
APgb	Neoarchean or Paleoproterozoic	Gabbroic to dioritic intrusion and metamorphic equivalent	0.05
Pga	Paleoproterozoic	Gabbroic, noritic, and anorthositic intrusion	0.05
Mgn	Mesoproterozoic	Gabbronorite	0.05
Mgn	Mesoproterozoic	Gabbronorite hornfels, highly magnetic	0.05
Mg	Mesoproterozoic	Granogabbro	0.05
Mdb	Mesoproterozoic	Granophyric, ophitic, poikilitic olivine-diabase	0.05
Mpth	Mesoproterozoic	Heterogeneous Augite Troctolite	0.05
Mpth	Mesoproterozoic	Heterogeneous troctolite to augite troctolite	0.05
Mht	Mesoproterozoic	Heterogeneous troctolitic rocks	0.05
Mpth	Mesoproterozoic	Heterogeneous troctolitic to gabbroic rocks	0.05
Mpth	Mesoproterozoic	Heterogeneous, augite troctolite	0.05
Mpth	Mesoproterozoic	Heterogeneous, inclusion-rich troctolite to olivine-oxide gabbro	0.05
Mhtgs	Mesoproterozoic	Heterogeneous, locally sulfide-bearing, gabbroic to troctolitic rocks	0.05
Mpt	Mesoproterozoic	Homogeneous augite troctolite with pegmatoidal oxide-augite patches	0.05
Mdb	Mesoproterozoic	Inclusion-rich diabase dike	0.05
Mird	Mesoproterozoic	Inclusion-rich diorite	0.05
Mdb	Mesoproterozoic	Intergranular diabase	0.05
Mdb	Mesoproterozoic	Intergranular diabase sill	0.05
Mltg	Mesoproterozoic	Interlayered gabbro and troctolite	0.05
Amm	Neoarchean	Interlayered volcanic and volcaniclastic rocks; amphibolite grade metamorphism	0.05
Mltmt	Mesoproterozoic	Latered troctolite	0.05
Mdn	Mesoproterozoic	Layered dunite	0.05
Mmt	Mesoproterozoic	Layered melatroctolite	0.05
Pxgl	Paleoproterozoic	Layered oxide-rich melaggabbro	0.05
Mcr_t	Mesoproterozoic	Layered troctolite and chromitite	0.05
Mltmt	Mesoproterozoic	Layered troctolite to melatroctolite	0.05
Mt	Mesoproterozoic	Layered, fine-grained troctolite dike	0.05
Mxog	Mesoproterozoic	Layered, oxide-olivine gabbro	0.05
Aag	Neoarchean	Leucogabbro, amphibole-bearing	0.05
Mdb	Mesoproterozoic	Mafic intrusion ?	0.05
Mdb	Mesoproterozoic	Mafic intrusion inferred	0.05
Ami	Neoarchean	Mafic intrusion, defined magnetically	0.05
Ami	Neoarchean	Mafic intrusion, undifferentiated	0.05
Pmi	Paleoproterozoic	Mafic intrusion; pyroxenite, peridotite, gabbro, lamprophyre	0.05
Mmi	Mesoproterozoic	Mafic intrusive stock; diabase, diorite, pyroxenite, gabbro	0.05

Map Label	Era	Rock Type	W.O.E.
Ami	Neoarchean	Mafic plug-like intrusion; typically magnetic	0.05
Ami	Neoarchean	Mafic to ultramafic intrusions	0.05
Mai	Mesoproterozoic	Magnetic Anorthosite and Gabbroic rocks, Magnetic	0.05
Agp	Neoarchean	Marginal oxide-rich gabbro	0.05
Mfmd	Mesoproterozoic	Medium- to fine-grained, nonfoliated ferromonzodiorite to ferrodiorite.	0.05
Mltg	Mesoproterozoic	Medium-grained, layered gabbro	0.05
Mgd	Mesoproterozoic	Medium-grained, well-foliated, apatitic olivine oxide gabbro/diorite	0.05
Mxog	Mesoproterozoic	Medium-to coarse-grained, well-foliated and modally layered, intergranular olivine oxide gabbro	0.05
Mmlg	Mesoproterozoic	Melagabbro	0.05
Amgps	Neoarchean	Melagabbro sill, locally sulfide-bearing	0.05
Amgb	Neoarchean	Meta hornblende-gabbro sill	0.05
Amgb	Neoarchean	Meta hornblende-gabbro, amphibolite-grade	0.05
Amgb	Neoarchean	Meta Orthopyroxene gabbro	0.05
Amgb	Neoarchean	Meta-diabase sill	0.05
Pmdb	Paleoproterozoic	Metadiabase/metagabbro sill-like intrusive	0.05
Amgb	Neoarchean	Metadiorite/gabbro	0.05
Amgb	Neoarchean	Metagabbro	0.05
Amgb	Neoarchean	Metagabbro intrusion	0.05
Amgb	Neoarchean	Metagabbro sill	0.05
Amgb	Neoarchean	Metagabbro sill in basaltic rocks	0.05
Amgps	Neoarchean	Metagabbro sill, locally sulfide-bearing	0.05
Amgbs	Neoarchean	Metagabbro sill, weakly (0-3%) sulfide-bearing	0.05
Amgb	Neoarchean	Metagabbro sill, weakly sulfide-bearing	0.05
Aag	Neoarchean	Metagabbro, commonly chloritized	0.05
Agp	Neoarchean	Metagabbro, locally brecciated	0.05
Amgb	Neoarchean	Metagabbro/metadiabase	0.05
Amgb	Neoarchean	Metagabbroic sill	0.05
Mhb	Mesoproterozoic	Metamorphosed basalt inclusion	0.05
Aszc	Neoarchean	Metamorphosed VMS chlorite alteration pipe	0.05
Amp	Neoarchean	Metaperidotite and pyroxenite sill	0.05
Amp	Neoarchean	Metaperidotite sill	0.05
Mg	Mesoproterozoic	Mg - Gabbroic rocks	0.05
Mmg	Mesoproterozoic	Microgabbro	0.05
Mmg	Mesoproterozoic	Micro-gabbro	0.05
Mdb	Mesoproterozoic	Mixed diabase and granophyre	0.05
Mmzg	Mesoproterozoic	Mixed monzogabbro, gabbronorite, and gabbro	0.05
Mpth	Mesoproterozoic	Mixed troctolitic and anorthositic rocks	0.05
Mdb	Mesoproterozoic	Monker Lake diabase	0.05
Mog	Mesoproterozoic	Olivine (oxide) gabbro and troctolite transition zone	0.05
Mdb	Mesoproterozoic	Olivine diabase	0.05
Mog	Mesoproterozoic	Olivine gabbro	0.05
Mga	Mesoproterozoic	Olivine-bearing gabbroic anorthosite	0.05
Mog	Mesoproterozoic	Olivine-bearing gabbroic rocks	0.05
Agp	Neoarchean	Olivine-rich gabbro and peridotite	0.05
Mgas	Mesoproterozoic	Ophitic anorthositic rocks, locally altered and sulfide-bearing	0.05
Mdb	Mesoproterozoic	Ophitic diabase	0.05
Mdb	Mesoproterozoic	Ophitic diabase dike	0.05
Mg	Mesoproterozoic	Ophitic gabbro	0.05
Mag	Mesoproterozoic	Ophitic gabbroic anorthosite	0.05
Mdb	Mesoproterozoic	Ophitic olivine diabase	0.05
Mgn	Mesoproterozoic	Ophitic olivine gabbronorite	0.05
Mdb	Mesoproterozoic	Ophitic olivine-diabase	0.05
Mdb	Mesoproterozoic	Ophitic olvine gabbro to diabase	0.05
Mbn	Mesoproterozoic	Ophitic to intergranular pigeonitic basalt	0.05
Mbn	Mesoproterozoic	Ophitic to pigeonitic basaltic rocks	0.05
Mdb	Mesoproterozoic	Ophitic troctolitic diabase	0.05
Mdbg	Mesoproterozoic	Ophitic, olivine-bearing diabase-gabbro sill	0.05
Mxog	Mesoproterozoic	Oxide and altered-oliving bearing ophitic gabbro	0.05
Mxg	Mesoproterozoic	Oxide gabbro	0.05
Mxg	Mesoproterozoic	Oxide gabbro of the Tamarack Intrusion Bowl	0.05
Mxt	Mesoproterozoic	Oxide rich troctolite	0.05

Map Label	Era	Rock Type	W.O.E.
Mxog	Mesoproterozoic	Oxide-bearing, olivine gabbro	0.05
Mxog	Mesoproterozoic	Oxide-olivine leucogabbro / leucotroctolite	0.05
Moui	Mesoproterozoic	Oxide-rich pyroxenite	0.05
Mxt	Mesoproterozoic	Oxide-rich troctolite	0.05
Mxog	Mesoproterozoic	Oxide-rich, coarse-grained, gabbro to olivine gabbro	0.05
Mxmts	Mesoproterozoic	Oxide-rich, sulfide-bearing, melatroctolite	0.05
Mgpeg	Mesoproterozoic	Pegmatitic gabbro	0.05
Mtpeg	Mesoproterozoic	Pegmatitic troctolite, locally sulfide-bearing	0.05
APgb	Neoarchean or Paleoproterozoic	Peridotite	0.05
Mpr	Mesoproterozoic	Peridotite of the Tamarack Bowl	0.05
Mdb	Mesoproterozoic	Plagioclase-porphyritic diabase	0.05
feD	Mesoproterozoic	Plagioclase-porphyritic ferrodiorite	0.05
Mtap	Mesoproterozoic	Poikilitic troctolitic anorthosite	0.05
Mtap	Mesoproterozoic	Poikilitic troctolitic anorthosite with pegmatoidal oxide-augite patches	0.05
Amgp	Neoarchean	Porphyritic (opx) melagabbro	0.05
Mdb	Mesoproterozoic	Porphyritic diabase	0.05
Mfm	Mesoproterozoic	Porphyritic ferromonzonite to ferrodiorite	0.05
Amgps	Neoarchean	Porphyritic metagabbro sill, locally sulfide-bearing	0.05
Mg	Mesoproterozoic	Porphyritic ophitic gabbro	0.05
Mfg	Mesoproterozoic	Porphyritic quartz-ferrogabbro to ferrodiorite	0.05
Mfmd	Mesoproterozoic	Pyroxene ferromonzodiorite	0.05
Mmd	Mesoproterozoic	Pyroxene monzodiorite	0.05
Mfmd	Mesoproterozoic	Pyroxene-prismatic, ferromonzodiorite	0.05
Ampx	Neoarchean	Pyroxenite sill	0.05
Ampxs	Neoarchean	Pyroxenite, weakly sulfide-bearing	0.05
Agp	Neoarchean	Quartz-biotite gabbro	0.05
Amp	Neoarchean	Serpentinized peridotite with chalcopyrite	0.05
Mdb	Mesoproterozoic	Subophitic diabase	0.05
Mmts1	Mesoproterozoic	Sulfide-bearing melatroctolite	0.05
Mtghs	Mesoproterozoic	Sulfide-bearing oxide gabbro	0.05
Amqgs	Neoarchean	Sulfide-bearing to sulfide-rich, quartz gabbro	0.05
Mhtgs	Mesoproterozoic	Sulfide-bearing troctolitic rocks	0.05
Mgas	Mesoproterozoic	Sulfide-bearing, altered anorthositic rocks	0.05
Mmts	Mesoproterozoic	Sulfide-bearing, coarse-grained, layered oxide-bearing troctolite	0.05
Mtghs	Mesoproterozoic	Sulfide-bearing, contaminated noritic rocks	0.05
Mhts	Mesoproterozoic	Sulfide-bearing, heterogeneous troctolite contact zone	0.05
Mtghs	Mesoproterozoic	Sulfide-bearing, heterogeneous troctolitic rocks	0.05
Mlts	Mesoproterozoic	Sulfide-bearing, layered troctolitic rocks	0.05
Amgbs	Neoarchean	Sulfide-bearing, microgabbro (chilled margin)	0.05
Mgas	Mesoproterozoic	Sulfide-bearing, PGE-poor, anorthositic rocks	0.05
Mhts1	Mesoproterozoic	Sulfide-bearing, PGE-poor, heterogeneous troctolitic rocks	0.05
Mmts1a	Mesoproterozoic	Sulfide-poor melatroctolite	0.05
Mhts1b	Mesoproterozoic	Sulfide-poor, weakly heterogeneous troctolitic rocks	0.05
Mts	Mesoproterozoic	Sulfide-rich troctolite	0.05
Amgbs	Neoarchean	Sulfidic metagabbro	0.05
Amgbh	Neoarchean	Taxitic metagabbro	0.05
Mt	Mesoproterozoic	Troctolite	0.05
Mt_a	Mesoproterozoic	Troctolite with abundant anorthosite inclusions	0.05
Mta	Mesoproterozoic	Troctolitic anorthosite	0.05
Mai	Mesoproterozoic	Troctolitic anorthosite xenolith	0.05
Mt	Mesoproterozoic	Troctolitic diabase	0.05
Mt	Mesoproterozoic	Troctolitic rocks	0.05
Mt	Mesoproterozoic	Troctolitic to gabbroic dikes	0.05
Ampxs	Neoarchean	Weakly sulfide-bearing pyroxenite	0.05
Mgs	Mesoproterozoic	Weakly sulfide-bearing, fine to medium-grained gabbro to oxide gabbro	0.05
Mpr	Mesoproterozoic	Weakly sulfide-bearing, fine-grained peridotite	0.05
Mpr	Mesoproterozoic	Weakly sulfide-bearing, peridotite	0.05
Amps	Neoarchean	Weakly sulfide-bearing, serpentinized peridotite	0.05

Mineral occurrences (point data) for mineral species commonly associated with graphite deposits associated with the Metamorphic mineral system were extracted from the Assembling Minnesota mineral occurrence database. Based on the minerals present in this database, the following mineral species were utilized for the model: 1) graphite; 2) garnet plus biotite; and 3) quartz plus potassium feldspar (K-Spar). Graphite was assigned a W.O.E. of 1, and garnet plus biotite and quartz plus K-spar were each assigned a W.O.E. of 0.5. Point locations were given a 1km buffer, and the total number of overlapping mineral polygons present at any one site were summed and normalized to develop the Mineral Factor.

Three types of geological contacts (lines) were distinguished for this model and given W.O.E. based on their relationships to graphite-associated Metamorphic mineral system mineralization. Contacts between intrusive rocks and graphite-bearing sedimentary rocks, intrusive rocks and iron formation/mudstone, and intrusive rocks and siliciclastic sedimentary rocks were each given buffers of 0.1km and assigned W.O.E. of 0.0.3-0.6, 0.1-0.2, and 0.05-0.2, respectively. The buffer polygons with their respective W.O.E. were utilized to develop the Geologic Contacts factor used in the final model.

For the geochemistry component, geochemical data (point data) were extracted from the Assembling Minnesota geologic and drillhole geochemistry databases. These databases were merged to develop the point data utilized in the model. Uranium and carbon contents were rarely observed in the database, therefore potential for graphite mineralization was modeled based on the sum of vanadium and nickel (Robinson et al., 2017; Tichy and Turnovec, 1978 (referenced in Robinson et al., 2017) contents within prospective rocks. Kriging of the normalized sums of the point data was performed to develop the surface raster, and the raster values were classified and converted to polygons for the Geochemistry Factor utilized in the model.

The geophysics factor was determined utilizing airborne and helicopter EM surveys, as graphite-bearing deposits should be electrically conductive (Marjoribanks, 2010). Airborne and helicopter electromagnetic survey (EM) values (point data) were classified into three categories based on the number of channel responses indicated in the survey. Those points with 0 channel responses in both 6-channel surveys and 12-channel surveys were classified as “no conductor” and given a point value of 0. Those points indicating 1–2 channel responses in a 6-channel survey or 1–4 channel responses in a 12-channel survey were classified as “weak conductors” and given a point value of 0.33. Those points indicating 3–4 channel responses in a 6-channel survey or 5–8 channel responses in a 12-channel survey was classified as “moderate conductors” and assigned a point value of 0.67. Those points indicating 5–6 channel responses in a 6-channel survey or 9–12 channel responses in a 12-channel survey were classified as “good conductors” and were assigned a point value of 1. Both the airborne EM points and the helicopter EM points were given a 0.1km buffer, comprising one of the polygon layers for the Geophysics factor. Total magnetics data (Chandler, 1982) were extracted to the bedrock geology boundaries, normalized, and reclassified into 10 quantile classes (1–10) to create the second polygon layer for the Geophysics factor utilized in the model.

The final Metamorphic Mineral System Potential Map was developed by multiplying each of the model factors by their assigned factor weights, and then calculating the fuzzy algebraic sum by means of the following equation (Bonham-Carter, 1994; Peterson, 2001):

$$\mu_{\text{combination}} = 1 - \prod_{i=1}^{n}(\mu i)$$

where μ*i* is the fuzzy membership value for the ith map, and *i* = 1. 2. 3, ….n maps are to be combined.

The factor weights assigned for each of the model factors are as follows:

- Geology Factor Weight = 0.95
- Mineral Factor Weight = 0.0.9
- Geologic Contacts Factor Weight = 0.7
- Geochemistry Factor Weight = 0.5
- Geophysics Factor Weight = 0.85

Results

The Metamorphic Mineral System Potential Map is illustrated in Figure 17 (with a Minnesota geology map underlay) and in Figure 18 (without the Minnesota geology map underlay). Shapefiles for the Metamorphic Mineral System Potential Map can be found in Digital Appendix 5 in the subdirectory labeled "Shapefiles." Model calculations can be found in Digital Appendix 5 in the subdirectory labeled "Model Calculations."

The modeling conducted for this study indicates several regions where elevated potential for Metamorphic mineral systems exist. The highest modeled potential for such a system exists in east-central St. Louis county and northwestern Lake county. This region of modeled high potential may be a false positive as the igneous rocks included in the model have anomalously high contents of nickel (and perhaps vanadium), and these igneous rocks are in contact with Paleoproterozoic and Neoarchean supracrustal rocks. Other small areas with modeled high potential occur within northeastern Koochiching County and are associated with Quetico subprovince high-grade metamorphic rocks that are in proximity to the Rainy Lake – Seine River Fault. An additional area of modeled high potential occurs in northeastern Itaca County, in proximity to the Coon Lake Pluton (Jirsa et al., 2012).

Alkalic Porphyry Mineral System

Deposit Types and Model

Table 11 indicates the various mineral deposit types associated with the Alkalic Porphyry mineral system (Hofstra and Kreiner, 2021). This mineral system comprises a variety of mineral deposit types encompassing base and precious metals as well as critical minerals. The genesis of these deposits involves mineral deposition by fluids exsolved from fractionated alkalic pluton and stocks.

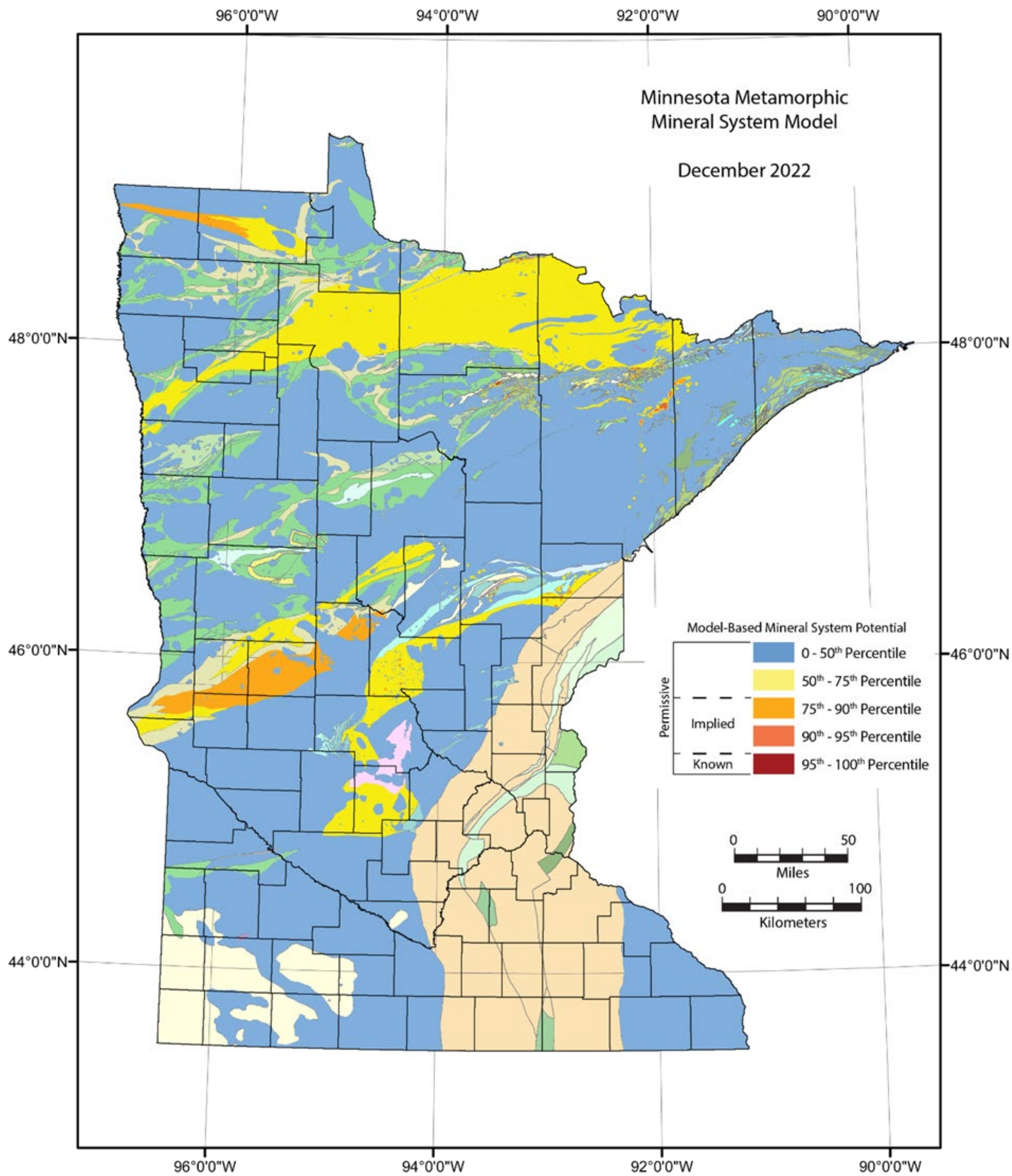

Figure 17. Results of ***Metamorphic*** knowledge-based mineral system model with geology.

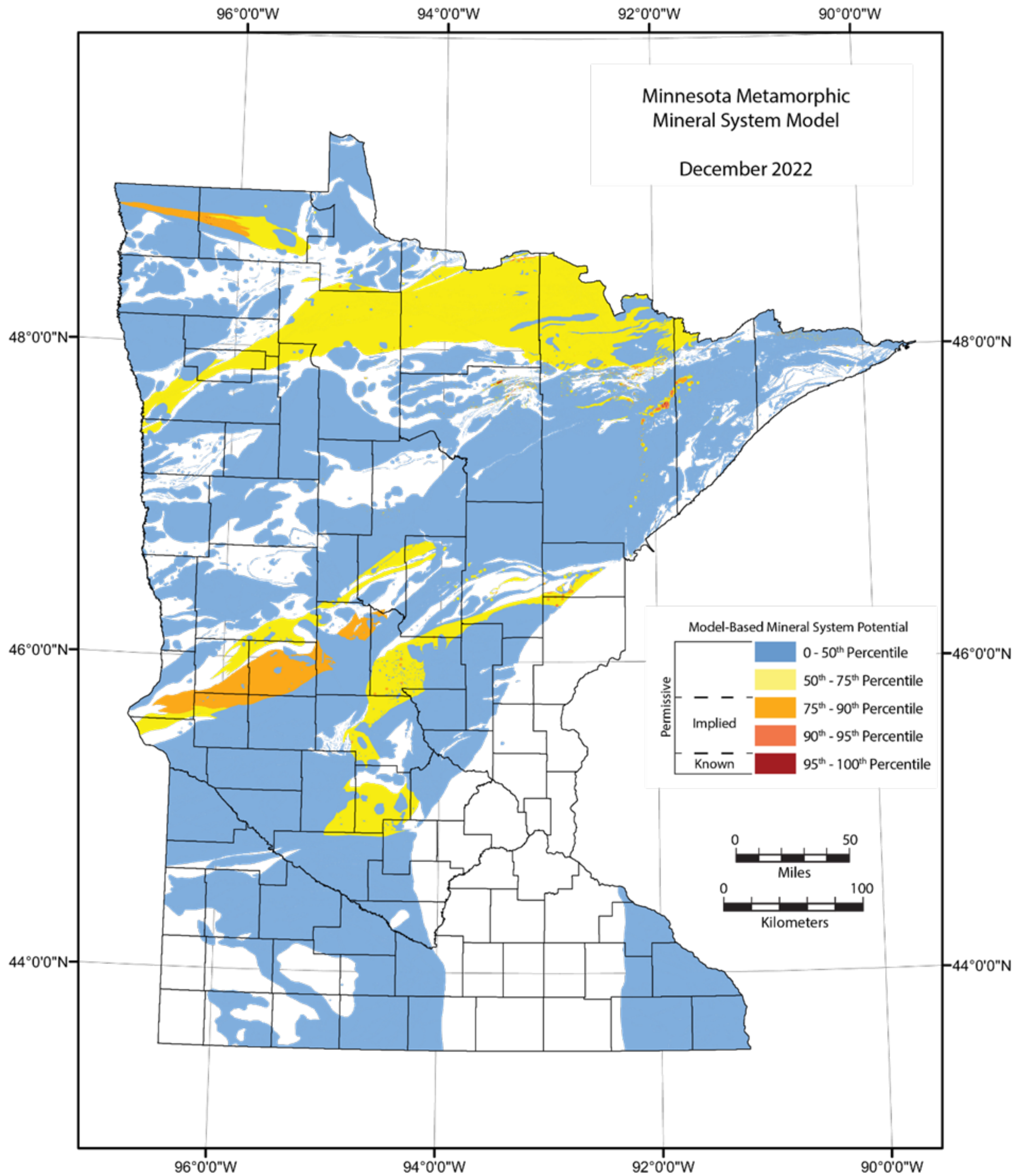

Figure 18. Results of ***Metamorphic*** knowledge-based mineral system model without geology.

Table 11. Systems-Deposits-Commodities-Critical Minerals table for the ***Alkalic Porphyry*** mineral system (modified after Hofstra and Kreiner, 2021). Explanation for table is as follows: ±, present (absent); --, not applicable; ?, maybe; Ag, silver; Al, aluminum; As, arsenic; Au, gold; B, boron; Ba, barium; Be, beryllium; Bi, bismuth; Br, bromine; Ca, calcium; Cd, cadmium; Co, cobalt; CO_2, carbon dioxide; Cs, cesium; Cr, chromium; Cu, copper; F, fluorine; Fe, iron; Ga, gallium; Ge, germanium; Hf, hafnium; Hg, mercury; I, iodine; IAEA, International Atomic Energy Agency; In, indium; IOA, iron oxide-apatite; IOCG, iron oxide-copper-gold; IS, intermediate sulfidation; K, potassium; LCT, lithium-cesium-tantalum; Li, lithium; Mg, magnesium; Mn, manganese; Mo, molybdenum; Na, sodium; Nb, niobium; Ni, nickel; NYF, niobium-yttrium-fluorine; P, phosphorus; Pb, lead; PGE, platinum group elements; R, replacement; Rb, rubidium; Re, rhenium; REE, rare earth elements; S, skarn; Sb, antimony; Sc, scandium; Se, selenium; Sn, tin; Sr, strontium; Ta, tantalum; Te, tellurium; Th, thorium; Ti, titanium; U, uranium; V, vanadium (in "Principal Commodities" column); V, vein (in "Deposit Types" column); W, tungsten; Y, yttrium; Zn, zinc; Zr, zirconium. In the "Critical Minerals" column, elements in **bold** have been produced from the deposit type, whereas element in *italics* are enriched in the deposit type but have not been produced.

System Name	Deposit Types	Principal Commodities	Critical Minerals	References
Alkalic Porphyry	Greisen	Mo, Bi	*Bi*	Jensen and Barton, 2000; Kelley and Spry, 2016; Wang et al., 2021.
	S-R-V Tungsten	W	**W,** *Bi, Mn, Sc*	
	Porphyry/skarn copper-gold	Cu, Mo, Au	*PGE, Te, Bi*	
	Polymetallic sulfide S-R-V-IS	Au, Ag, Pb, Zn, Cu	*Ge, Ga, In, Bi, Te*	
	Fluoprospar	Fluorite	**Fluorite**	
	Distal disseminated silver-gold	Ag, Au	*Sb, As*	
	High sulfidation	Cu, Ag, Au	*Te, Bi, Ass, Sb*	
	Low sulfidation	Au	*Te, Bi, V, F*	
	Lithocap alunite?	Al, K_2SO_4 (potash)	*Al, K_2SO_4, Ga*	
	Lithocap kaolinite	Kaolin	*Ga*	

Most alkaline porphyry deposits are Mesozoic to Neogene in age (Kelley and Spry, 2016) and are associated with low-sulfidation epithermal deposits that are genetically related to alkali element-enriched stocks. These stocks often occur in clusters and can be associated with multiple alkalic magmatic events (Jensen and Barton, 2000). However, gold deposits associated with alkaline intrusions (shoshonitic lamprophyres, syenites) of Archean age have been identified in the western United States, in the Fennoscandian Shield and within the Superior Province of Canada (Jensen and Barton, 2000; Kalinin and Kudryashov, 2021).

Key characteristics of Alkalic Porphyry mineral system-associated intrusions include (Jensen and Barton, 2000; Kelley and Spry, 2016):

- The alkaline igneous rocks can vary from syenite to shoshonite in composition;
- Intrusive rocks that host economic mineral deposits straddle, or sit above, the alkaline-subalkaline boundary when plotted on total alkali – silica diagrams (e.g. Le Bas et al., 1986);
- The rocks are commonly enriched in fluorine, platinum group metals, rare earth elements, tellurium, vanadium, and tungsten;
- Alkaline intrusive rocks associated with gold deposits are light rare earth element (LREE) enriched and have hydrous minerals indicative of formation in environments with high oxygen fugacities (e.g. hornblende, biotite, magnetite, and aegirine);
- Large mineral deposits commonly occur in alkalic porphyries that have a close spatial relationship to first-order geological structures; and
- Alteration and ore minerals associated with gold-producing alkalic porphyries include a variety of silicates, carbonates, sulfosalts, sulfide, oxides, arsenides, and native elements (e.g. Au, Ag).

For more detailed discussions of the characteristics of Alkalic Porphyry mineral system characteristics, see Jensen and Barton, 2000; Seedorf et al., 2005; Kelley and Spry, 2016; Wang et al., 2021; Kalinen and Kudryashov, 2021.

Modeling Methods

The modeling methodology for the Alkalic Porphyry mineral system included four components that could be derived from the Assembling Minnesota dataset (Bartsch et al., 2022; Peterson, 2018). These four components include: 1) bedrock geology; 2) mineral occurrences; 3) geochemistry; and 4) structure. The inference net illustrating the various components used in the Alkalic Porphyry mineral system model are illustrated in Figure 19.

Bedrock geology focused on two main components: 1) alkalic amphibole-pyroxene-bearing intrusions; and 2) other intrusions. Polygons of permissible host rock types were extracted from the Assembling Minnesota bedrock geology database and given W.O.E. based on their prospectivity for hosting alkalic-porphyry-associated mineralization. In summary, the W.O.E. assigned for alkalic amphibole-pyroxene-bearing intrusions was 0.8. The W.O.E. for other intrusions ranged from 0.25–0.7. The W.O.E for the various lithological units utilized in the model is provided in Table 12. The various polygon values represented the Geology Factor utilized in the model.

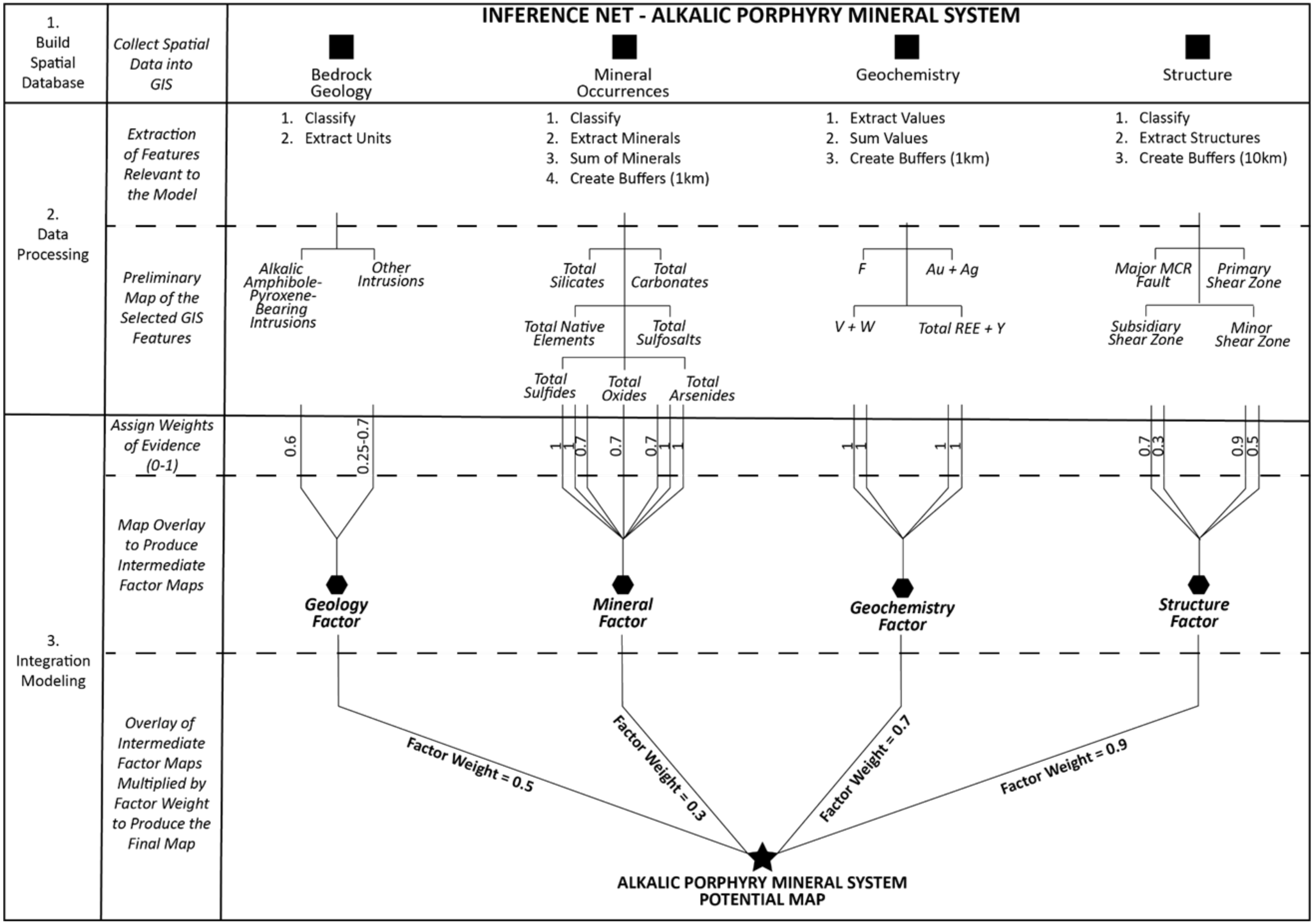

Figure 19. Inference net for ***Alkalic Porphyry*** knowledge-based mineral system model.

Table 12. Weights of evidence for geology polygons in the ***Alkali Porphyry*** mineral system model.

Map Label	Era	Rock Type	W.O.E.
Asd	Neoarchean	Alkalic (syenitic, monzodioritic, dioritic), amphibole & pyroxene-bearing intrusions	0.8
Aqfp	Neoarchean	Quartz-feldspar porphyry, gold bearing	0.8
Am	Neoarchean	Hornblende monzonite	0.7
Asd	Neoarchean	Syenite	0.7
Asd	Neoarchean	Syenitic, monzodioritic, or dioritic pluton	0.65
Asd	Neoarchean	Monzodiorite and syenite	0.6
Mmd	Mesoproterozoic	Monzodioritic rocks	0.6
Am	Neoarchean	Monzonite	0.6
Aqm	Neoarchean	Quartz monzonite	0.6
Aqmm	Neoarchean	Quartz monzonite, variably magnetic and magmatically foliated	0.6
Aqm	Neoarchean	Quartz monzonite, monzonite, and granodiorite, non-magnetic	0.55
Afp	Neoarchean	Feldspar porphyry	0.5
Almp	Neoarchean	Lamprophyre	0.5
Mlamp	Mesoproterozoic	Lamprophyre dike	0.5
Agp	Neoarchean	Lamprophyre dike/plug	0.5
Agp	Neoarchean	Lamprophyre intrusion	0.5
Almp	Neoarchean	Lamprophyric to ultramafic intrusions	0.5
Mmd	Mesoproterozoic	Monzodiorite, granite, and granodiorite	0.5
Mmd	Mesoproterozoic	Pyroxene monzodiorite	0.5
Aqfp	Neoarchean	Quartz-feldspar porphyry	0.5
Mfmd	Mesoproterozoic	Ferromonzodiorite	0.45
Mfmd	Mesoproterozoic	Ferromonzodiorite to ferrogabbro	0.45
Mfm	Mesoproterozoic	Ferromonzonite	0.45
feM	Mesoproterozoic	Ferromonzonite hybrid	0.45
Mfm	Mesoproterozoic	Ferromonzonite to ferrogranite	0.45
Mfm	Mesoproterozoic	Ferromonzonite to ferromonzodiorite	0.45
Mfmd	Mesoproterozoic	Medium- to fine-grained, nonfoliated ferromonzodiorite to ferrodiorite.	0.45
Mfmd	Mesoproterozoic	Pyroxene ferromonzodiorite	0.45
Mfmd	Mesoproterozoic	Pyroxene-prismatic, ferromonzodiorite	0.45
Mfm	Mesoproterozoic	Pyroxene-quartz ferromonzonite	0.45
Mmd	Mesoproterozoic	Pyroxene-quartz Monzodiorite	0.45
Mfmd	Mesoproterozoic	Quartz ferromonzodiorite	0.45
Mfm	Mesoproterozoic	Quartz ferromonzonite to ferromonzodiorite	0.45
Mmd	Mesoproterozoic	Quartz-bearing monzodiorite	0.45
Mfmd	Mesoproterozoic	Sparsely porphyritic quartz-ferromonzodiorite	0.45
Mgr	Mesoproterozoic	Biotite granite	0.4
Afp	Neoarchean	Feldspar porphyry	0.4
Ad	Neoarchean	Hornblende diorite	0.4
Mird	Mesoproterozoic	Inclusion-rich diorite	0.4
Mrn	Mesoproterozoic	Maple Hill Rhyolite	0.4
Mpd	Mesoproterozoic	Porphyritic diorite	0.4
Mfm	Mesoproterozoic	Porphyritic ferromonzonite to ferrodiorite	0.4
Mqd	Mesoproterozoic	Quartz diorite	0.4
Aqfp	Neoarchean	Quartz feldspar porphyry	0.4
Mfmd	Mesoproterozoic	Quartz-ferromonzodiorite	0.4
Mfd	Mesoproterozoic	Sparsely porphyritic, weakly amygduloidal ,quartz-ferrodiorite	0.4
feD	Mesoproterozoic	Plagioclase-porphyritic ferrodiorite	0.35
Mfd	Mesoproterozoic	Apatite-bearing, ferrodiorite	0.3
Pd	Paleoproterozoic	Diorite	0.3
APd	Neoarchean or Paleoproterozoic	Dioritic to granodioritic intrusion of uncertain age	0.3
Mfd	Mesoproterozoic	Ferrodiorite	0.3
Agd	Neoarchean	Granodiorite	0.3
Agn	Neoarchean	Granodiorite gneiss	0.3
Agd	Neoarchean	Granodiorite to diorite	0.3
Agd	Neoarchean	Granodiorite, foliated and synvolcanic	0.3
Pdg	Paleoproterozoic	Granodiorite; variably foliated	0.3
Agd	Neoarchean	Granodioritic intrusion	0.3
Mgr	Mesoproterozoic	Hornblende granite	0.3
Mgrd	Mesoproterozoic	Hornblende granodiorite	0.3

Map Label	Era	Rock Type	W.O.E.
Agr	Neoarchean	Granite	0.25
Mgr	Mesoproterozoic	Granite dike	0.25
Aqpeg	Neoarchean	Granite pegmatite (Kspar-quartz-muscovite-plagioclase)	0.25
Agr	Neoarchean	Granite plug	0.25
Agrm	Neoarchean	Granite to granodiorite, variably magnetic	0.25
Mgr	Mesoproterozoic	Granite to quartz-monzodiorite	0.25
Agr	Neoarchean	Granitic dike	0.25
Agr	Neoarchean	Granitic intrusion	0.25
APgr	Neoarchean or Paleoproterozoic	Granitic intrusion of uncertain age	0.25
Pgm	Paleoproterozoic	Granitic intrusion, variably magnetic	0.25
Amg	Mesoarchean to Paleoarchean	Granitic orthogneiss and migmatite	0.25
Agn	Neoarchean	Granitic to granodioritic orthogneiss	0.25
Agr	Neoarchean	Granitoid	0.25
Agru	Neoarchean	Granitoid intrusion, undifferentiated or poorly constrained by core and outcrop	0.25
Aql	Neoarchean	Lac La Croix Granite; locally pegmatitic and magnetic	0.25
Agrl	Neoarchean	Leucogranite	0.25
Agr	Neoarchean	Leucogranite with 1/3 amphibolite fragments	0.25
Agr	Neoarchean	Leucogranite with 1/3 biotite schist and amphibolite fragments	0.25
Agr	Neoarchean	Leucogranite with 1/3 biotite schist fragments	0.25
Pgp	Paleoproterozoic	Llamprophyric intrusion	0.25
Amn	Mesoarchean to Paleoarchean	Amphibolitic to dioritic gneiss	0.2
Ad	Neoarchean	Diorite, synvolcanic intrusion	0.2
Afp	Neoarchean	Feldspar porphyry	0.2
Agr	Neoarchean	Granite	0.2
Agr	Neoarchean	Granite	0.2
Aqfp	Neoarchean	Quartz-feldspar porphyry	0.2
Mrn	Mesoproterozoic	Devil's Kettle porphyritic rhyolite	0.1
Mrn	Mesoproterozoic	Devil's Kettle rhyolite	0.1
Mrn	Mesoproterozoic	Devil's Track rhyolite	0.1
Mrp	Mesoproterozoic	Porphyritic rhyolite	0.1
Mrp	Mesoproterozoic	Porphyritic Rhyolite lava flow	0.1
Mrn	Mesoproterozoic	Porphyritic rhyolite lava flows, normally polarized	0.1
Mrn	Mesoproterozoic	Rhyolite	0.1
Mrn	Mesoproterozoic	Rhyolite crystal tuff	0.1
Mrn	Mesoproterozoic	Rhyolite lava flow	0.1
Mrn	Mesoproterozoic	Rhyolite lava flows, normally polarized	0.1
Mrr	Mesoproterozoic	Rhyolite lava flows, reverse polarity	0.1
Afvm	Neoarchean	Rhyolite to latite lava flows	0.1

Mineral occurrences (point data) for mineral species commonly associated with mineral deposits associated with the Alkalic Porphyry mineral system were extracted from the Assembling Minnesota mineral occurrence database. Based on the minerals present in this database, the following mineral species were utilized for the model: 1) total silicates (the sum of amphibole + hornblende + biotite + aegirine + K-spar + sericite + fuchsite); 2) total carbonates (the sum of ankerites + calcite + dolomite + rhodochrosite); 3) total native elements (native gold); 4) total sulfosalts (tetrahedrite); 5) total sulfides (pyrite + pyrrhotite + galena + chalcopyrite + sphalerite); 6) total oxides (magnetite); and 7) total arsenides (arsenopyrite). W.O.E. assigned to the different mineral groups were as follows:

- Total Silicates W.O.E. = 0.7
- Total Carbonates W.O.E. = 0.7
- Total Native Elements W.O.E. = 1
- Total Sulfosalts W.O.E. = 1

- Total Sulfides W.O.E. = 1
- Total Oxides W.O.E. = 0.7
- Total Arsenides W.O.E. = 1

Point locations were given a 1km buffer. The total number of overlapping mineral polygons present at any one site were summed and normalized to develop the Mineral Factor.

Geochemical data (point data) were extracted from Hauck et al. (2014) were utilized for the Alkalic Porphyry model as samples had previously been classified as alkaline or subalkaline utilizing the total alkali – silica diagram (Figure 20; after Le Bas et al., 1986). Key parameters utilized in the geochemistry component included: 1) fluorine contents; 2) the sum of gold plus silver; 3) the sum of vanadium plus tungsten; and 4) the sum of total rare earth element plus yttrium. All four parameters were assigned W.O.E. of 1. Kriging of the normalized sums for each of the point datasets was performed to develop surface rasters, and the raster values were classified and converted to polygons for the Geochemistry Factor utilized in the model.

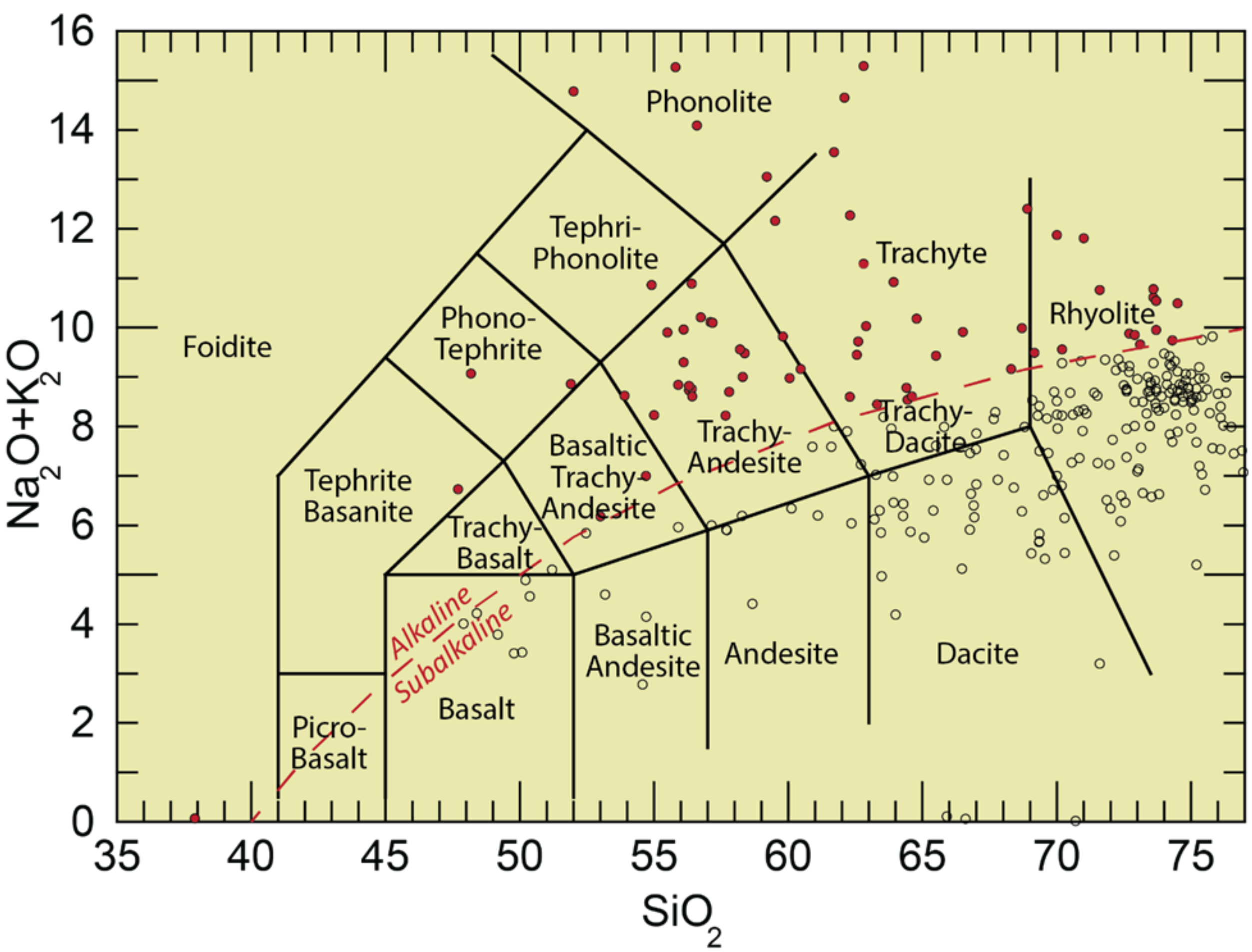

Figure 20. Total alkali – silica (TAS) diagram (Le Bas et al., 1986) illustrating classification of Hauck et al. (2014) lithogeochemistry. Samples indicated in red were utilized in the ***Alkalic Porphyry*** mineral system model.

The structure component of the Alkali Porphyry model included four types of geological structures: 1) major Midcontinent Rift associated faults; 2) primary shear zones; 3) subsidiary shear zones; and 4) minor shear zones. These structures were extracted from the geoline dataset associated with the Assembling Minnesota database (Bartsch et al., 2022; Peterson, 2018), provided a 1km buffer, and the resulting polygons were assigned W.O.E. based on the structure type. WOE values used for the various structure types include: 1) W.O.E. of 0.3 for major Midcontinent Rift associated faults; 2) W.O.E. of 0.9 for primary shear zones; 3) W.O.E. of 0.7 for subsidiary shear zones; and 4) W.O.E. of 0.5 for minor shear zones. The resulting polygon layer was utilized in the calculation of the Alkali Porphyry mineral system model.

The final Metamorphic Mineral System Potential Map was developed by multiplying each of the model factors by their assigned factor weights and then calculating the fuzzy algebraic sum by means of the following equation (Bonham-Carter, 1994; Peterson, 2001):

$$\mu_{\text{combination}} = 1 - \prod_{i=1}^{n}(\mu i)$$

where μ*i* is the fuzzy membership value for the ith map, and *i* = 1. 2. 3, ….n maps are to be combined.

The factor weights assigned for each of the Alkalic Porphyry model factors are as follows:

- Geology Factor Weight = 0.5
- Mineral Factor Weight = 0.3
- Geochemistry Factor Weight = 0.7
- Structure Factor Weight = 0.9

Results

The Alkali Porphyry Mineral System Potential Map is illustrated in Figure 21 (with a Minnesota geology map underlay) and in Figure 22 (without the Minnesota geology map underlay). Shapefiles for the Alkali Porphyry Mineral System Potential Map can be found in Digital Appendix 6 in the subdirectory labeled “Shapefiles.” Model calculations can be found in Digital Appendix 6 in the subdirectory labeled “Model Calculations.”

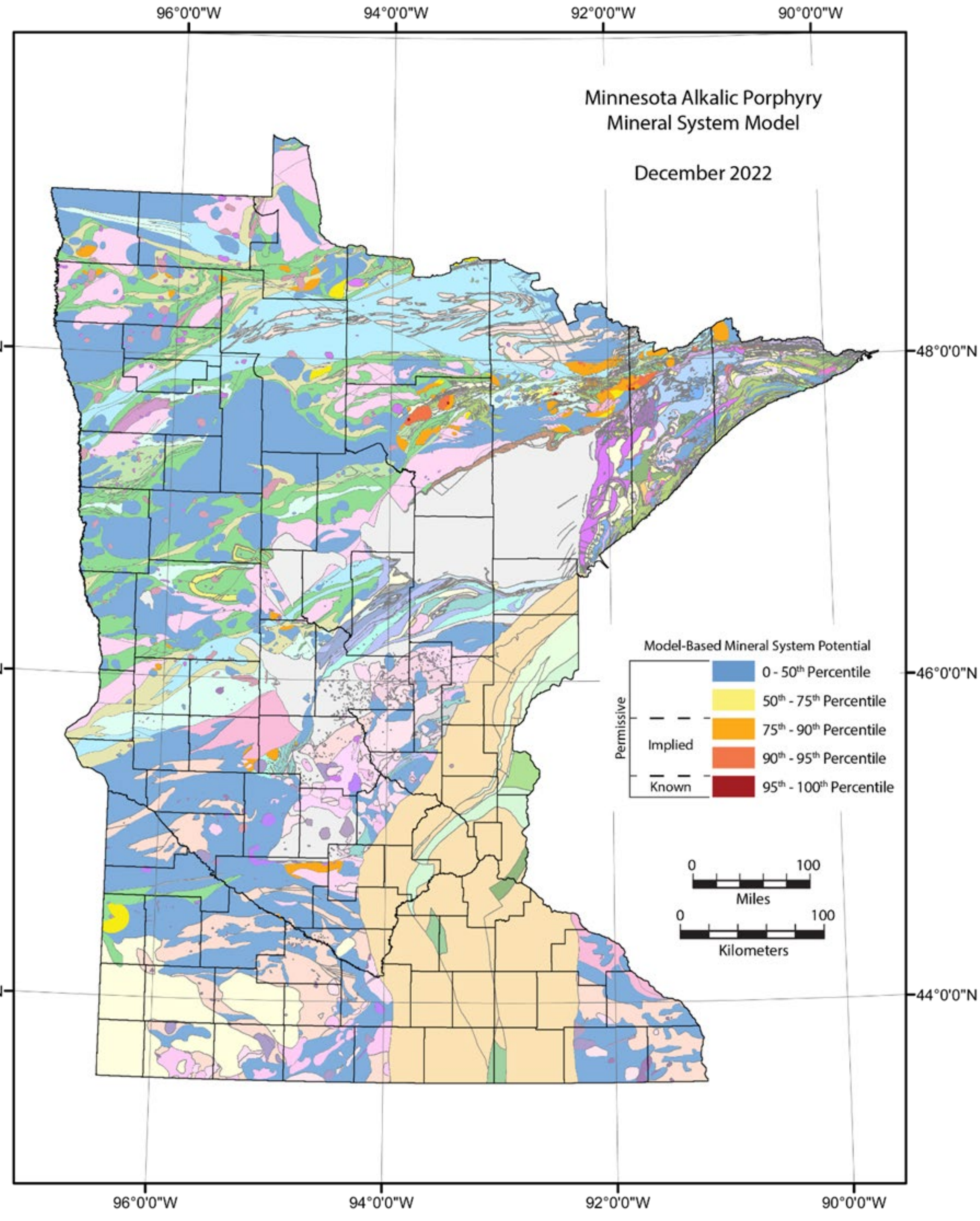

Figure 21. Results of ***Alkalic Porphyry*** knowledge-based mineral system model with geology.

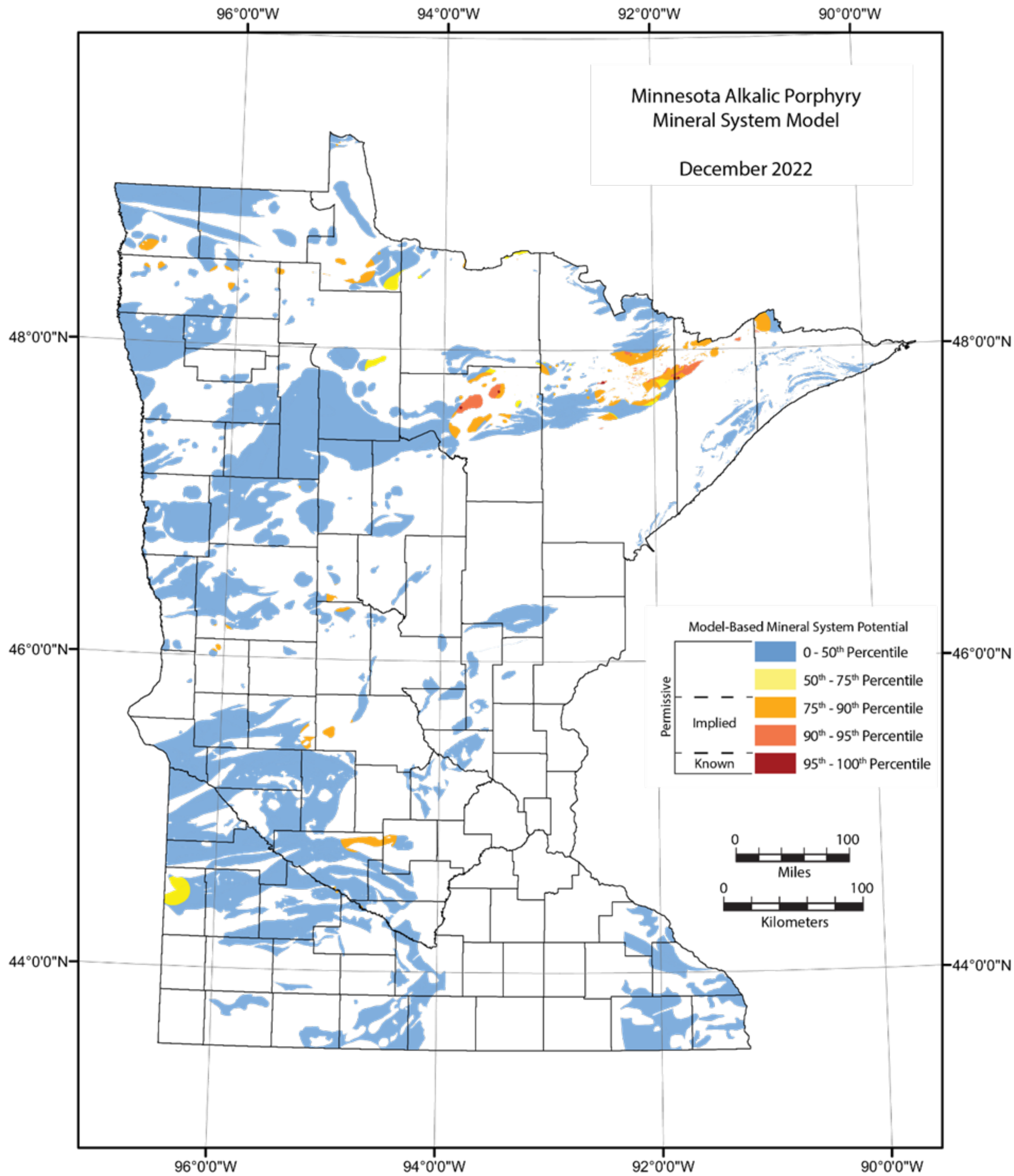

Figure 22. Results of ***Alkalic Porphyry*** knowledge-based mineral system model without geology.

GIS-based fuzzy logic modeling conducted for this study indicates several regions where elevated potential for Alkalic Porphyry mineral systems exist. The areas with the highest modeled probability for having Alkalic Porphyry mineral systems occur in northeastern Minnesota with Lake, St. Louis, and Itasca counties. In northwestern Lake County, the highest modeled potential for Alkalic Porphyry mineral systems resides within the Giants Range Batholith. In St. Louis County, the highest potential lies within syenite, monzonite, granodiorites and diorites that contain both hornblende and pyroxed (geologic unit "Asd" of Jirsa et al., 2011). In Itasca County, the highest modeled potential for Alkalic Porphyry mineral systems also occurs within "Asd" units, including the Coon Lake Pluton.

Magmatic REE Mineral System

Deposit Types and Model

Table 13 indicates the various mineral deposit types associated with the Magmatic REE mineral system (Hofstra and Kreiner, 2021). Mineral deposits associated with the Magmatic REE mineral system typically occur in highly-evolved alkaline and peralkaline rocks that can span a wide range of compositions, including silica-undersaturated rocks (e.g. nepheline syenites) to silica oversaturated rocks (e.g. granites) that can subdivided into three types: 1) those associated with nepheline syenites in large, layered alkaline intrusions; 2) those associated with pegmatites, felsic dikes, and minor granitic intrusions within peralkaline granitic rocks; and 3) those associated with peralkaline trachytic volcanic and volcaniclastic rocks (Dostal, 2016). They are commonly spatially associated with within-plate or continental anorogenic tectonic settings associated with faulting, rifting, and crustal extension (Dostal, 2016; Dostal, 2017). Carbonatites also are primary sources of rare earth elements (Verplanck et al., 2014).

Table 13. Systems-Deposits-Commodities-Critical Minerals table for the ***Magmatic REE*** mineral system (modified after Hofstra and Kreiner, 2021). Explanation for table is as follows: ±, present (absent); --, not applicable; ?, maybe; Ag, silver; Al, aluminum; As, arsenic; Au, gold; B, boron; Ba, barium; Be, beryllium; Bi, bismuth; Br, bromine; Ca, calcium; Cd, cadmium; Co, cobalt; CO_2, carbon dioxide; Cs, cesium; Cr, chromium; Cu, copper; F, fluorine; Fe, iron; Ga, gallium; Ge, germanium; Hf, hafnium; Hg, mercury; I, iodine; IAEA, International Atomic Energy Agency; In, indium; IOA, iron oxide-apatite; IOCG, iron oxide-copper-gold; IS, intermediate sulfidation; K, potassium; LCT, lithium-cesium-tantalum; Li, lithium; Mg, magnesium; Mn, manganese; Mo, molybdenum; Na, sodium; Nb, niobium; Ni, nickel; NYF, niobium-yttrium-fluorine; P, phosphorus; Pb, lead; PGE, platinum group elements; R, replacement; Rb, rubidium; Re, rhenium; REE, rare earth elements; S, skarn; Sb, antimony; Sc, scandium; Se, selenium; Sn, tin; Sr, strontium; Ta, tantalum; Te, tellurium; Th, thorium; Ti, titanium; U, uranium; V, vanadium (in "Principal Commodities" column); V, vein (in "Deposit Types" column); W, tungsten; Y, yttrium; Zn, zinc; Zr, zirconium. In the "Critical Minerals" column, elements in **bold** have been produced from the deposit type, whereas element in *italics* are enriched in the deposit type but have not been produced.

System Name	Deposit Types	Principal Commodities	Critical Minerals	References
Magmatic REE	Peralkaline syenite/granite/ Rhyolite/alaskite/ pegmatites	REE, Y, Zr, Hf, Nb, Ta, Be, U, Th, Cu	**REE, Zr, Hf, Nb, Ta, Be, U,** *V, Te, fluorite*	Verplanck et al., 2014; Verplanck et al., 2016; Dostal, 2016; Wang et al., 2021.
	Carbonatite	REE, P, Y, Nb, Ba, Sr, U, Th, Cu	**REE, Nb, Sc, U, Sr, Ba, P, Cu, Zr, magnetite, vermiculite, fluorite**	
	Phosphate	REE, P	*REE*	
	Fluorospar	Fluorite	**Fluorite,** *barite, Ti, Nb, Zr, REE, Sc, U, Be*	

Key characteristics of Magmatic REE mineral systems include (Černý et al., 2005; Verplanck et al., 2014; Dostal, 2016; London, 2016; Bradley et al., 2017; Dostal, 2017):

- They include a wide range of alkaline to peralkaline rocks, ranging from carbonatites to silica-saturated to undersaturated felsic intrusive rocks;
- The intrusive rocks associated with this mineral system are commonly associated with major extensional structures;
- Gangue minerals associated with REE deposits comprising this mineral system include alkali feldspar, alkali amphiboles, alkali pyroxenes, nepheline, phlogopite, carbonate minerals, beryl, and iron oxides;
- Geochemically, REE mineral deposits have high concentrations of total REE plus yttrium, total high field strength elements, and heavy rare earth elements, with an absence of europium anomalies (Eu/Eu*) in carbonatites and an Eu/Eu* value ranging from 0.21–0.23 associated with peralkaline intrusions hosting REE deposits; and
- Alkaline igneous rocks may produce magnetic anomalies due to the magnetic characteristics of the intrusions and adjacent rocks.

Carbonatites have yet to be identified in Minnesota (Jirsa et al., 2011), so modeling conducted for this study focused on evaluating silicate-bearing intrusive rocks that may be associated with the Magmatic REE mineral system within the state.

The reader is referred to the references cited above and references cited within these articles to obtain more information regarding the Magmatic REE mineral system. The reader is also referred to a recent study regarding rare earth element mineral potential in Minnesota (Hauck et al., 2014).

Modeling Methods

The fuzzy logic modeling methodology for the Magmatic REE mineral system included five components that could be ascertained from the Assembling Minnesota dataset (Bartsch et al., 2022; Peterson, 2018). These five components include: 1) bedrock geology; 2) mineral occurrences; 3) geochemistry; 4) geophysics; and 5) geochronology. The inference net illustrating the various components used in the Placer Mineral System model are illustrated in Figure 23.

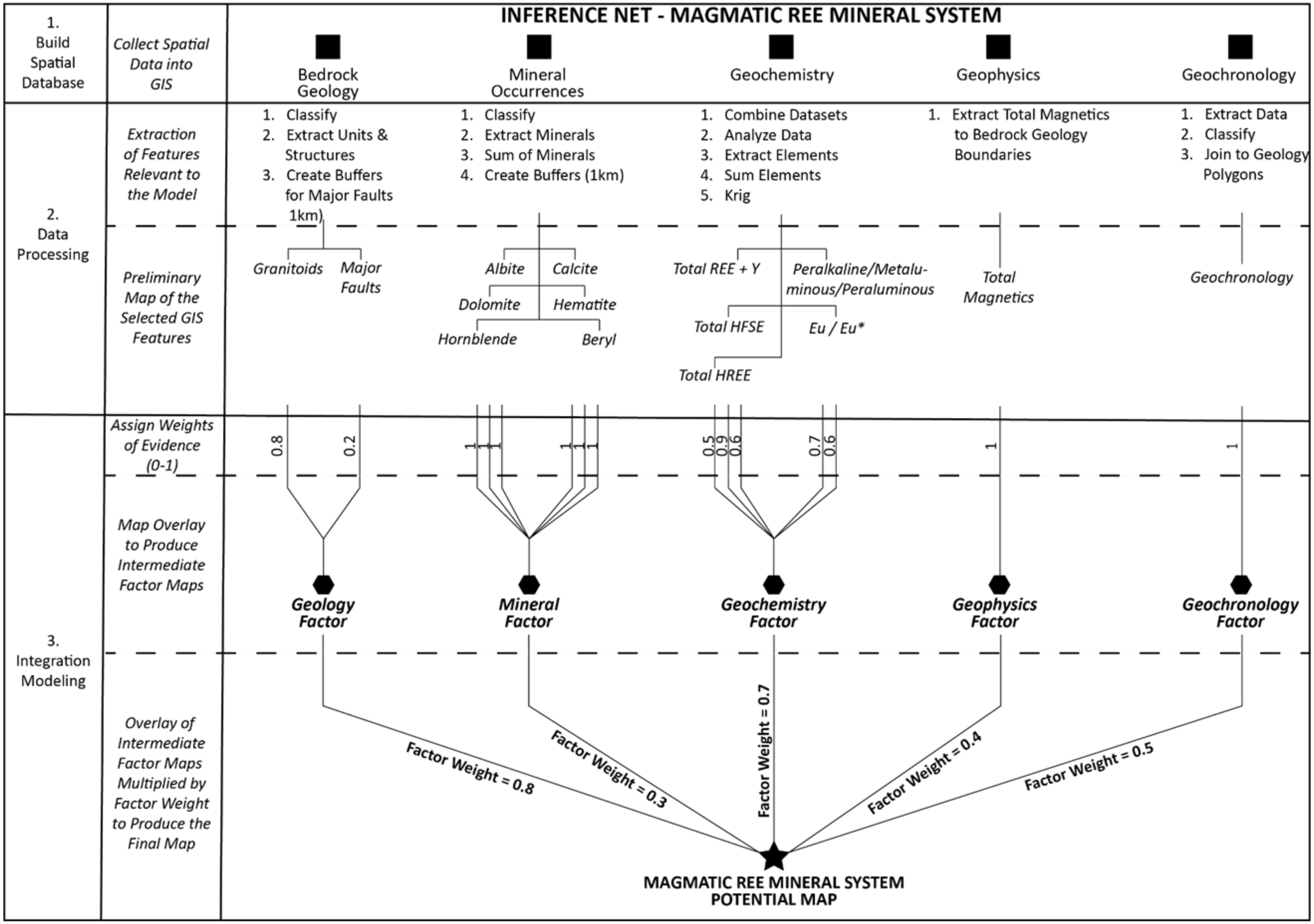

Figure 23. Inference net for ***Magmatic REE*** knowledge-based mineral system model.

Bedrock geology focused on two main features: 1) the presence of granitoid intrusive rocks (polygons); and 2) the locations of major faults (lines). Polygons of permissible host rock types (schist/gneiss/ migmatite, felsic intrusions, graywacke/shale/slate, intermediate intrusions, graphitic argillite, and mafic/ultramafic intrusions) were extracted from the Assembling Minnesota bedrock geology database and given W.O.E. based on their prospectivity for hosting metamorphic graphite mineralization. The W.O.E. for the various lithological units utilized in the model are provided in Table 14. In addition, major faults were extracted from the Assembling Minnesota geology lines dataset, provided with a 1km buffer, and assigned W.O.E. of 0.2. These two polygon layers representing granitoid intrusive rocks and major faults were summed and normalized to develop the Geology Factor utilized in the model.

Table 14. Weights of evidence for geology polygons in the ***Magmatic REE*** mineral system model.

Map Label	Era	Rock Type	W.O.E.
Asd	Neoarchean	Alkalic (syenitic, monzodioritic, dioritic), amphibole & pyroxene-bearing intrusions	0.7
Asd	Neoarchean	Syenite	0.66
Asd	Neoarchean	Syenitic, monzodioritic, or dioritic pluton	0.63
Mfd	Mesoproterozoic	Apatite-bearing, ferrodiorite	0.6
Pgp	Paleoproterozoic	Gabbro, pyroxenite, diorite, and lamprophyre intrusion	0.6
Aqpeg	Neoarchean	Granite pegmatite (Kspar-quartz-muscovite-plagioclase)	0.6
Mfg	Mesoproterozoic	Apatitic ferrogabbro	0.57
Afp	Neoarchean	Feldspar-hornblende porphyry	0.55
Aqg	Neoarchean	Granite-rich migmatite, locally magnetic	0.55
Amg	Mesoarchean to Paleoarchean	Granitic orthogneiss and migmatite	0.55
Amd	Mesoarchean to Paleoarchean	Granitoid gneiss with amphibolitic to dioritic enclaves	0.55
Phpn	Paleoproterozoic	Hornblendite, pyroxenite and nelsonite	0.55
Aql	Neoarchean	Lac La Croix Granite; locally pegmatitic and magnetic	0.55
Almp	Neoarchean	Lamprophyre	0.55
Agp	Neoarchean	Lamprophyre dike	0.55
Agp	Neoarchean	Lamprophyre dike/plug	0.55
Agp	Neoarchean	Lamprophyre intrusion	0.55
Almp	Neoarchean	Lamprophyric to ultramafic intrusions	0.55
Agr	Neoarchean	Leucogranite with 1/3 amphibolite fragments	0.55
Agr	Neoarchean	Leucogranite with 1/3 biotite schist and amphibolite fragments	0.55
Pgn	Paleoproterozoic	Quartzofeldspathic orthogneiss and schist	0.55
Aqs	Neoarchean	Schist-rich migmatite	0.55
Mbr	Mesoproterozoic	Strongly porphyritic trachyandesite	0.53
Atv	Neoarchean	Trachyandesite	0.53
Ma	Mesoproterozoic	Trachyandesite lava flows	0.53
Ma	Mesoproterozoic	Trachyandesite, grey, fine- to locally medium-grained, variably porphyritic.	0.53
Mgr	Mesoproterozoic	Hornblende granite	0.52
Asd	Neoarchean	Monzodiorite and syenite	0.52
Agrl	Neoarchean	Muscovite-biotite leucogranite	0.52
Agn	Neoarchean	Granitic to granodioritic orthogneiss	0.51
Mrn	Mesoproterozoic	Aphryic rhyolite inclusion	0.5
Mrn	Mesoproterozoic	Aphyric rhyolite	0.5
Mrn	Mesoproterozoic	Aphyric rhyolite, rare feldspar phenocrysts	0.5
Aszb	Neoarchean	BIF-Inclusion Schist	0.5
Mgr	Mesoproterozoic	Biotite granite	0.5
Mrn	Mesoproterozoic	Devil's Kettle porphyritic rhyolite	0.5
Mrn	Mesoproterozoic	Devil's Kettle rhyolite	0.5
Mrn	Mesoproterozoic	Devil's Track rhyolite	0.5
Afp	Neoarchean	Feldspar porphyry	0.5
Agr	Neoarchean	Granite	0.5
Mgr	Mesoproterozoic	Granite dike	0.5
Mgr	Mesoproterozoic	Granite dike	0.5
Mgr	Mesoproterozoic	Granite xenolith in the BRD	0.5

Map Label	Era	Rock Type	W.O.E.
Pgr	Paleoproterozoic	Granite, red to pink, variably porphyritic, massive	0.5
Pgu	Paleoproterozoic	Granite, undifferentiated	0.5
Agr	Neoarchean	Granitic dike	0.5
Agr	Neoarchean	Granitic intrusion	0.5
APgr	Neoarchean or Paleoproterozoic	Granitic intrusion of uncertain age	0.5
Pgm	Paleoproterozoic	Granitic intrusion, variably magnetic	0.5
Agr	Neoarchean	Granitoid	0.5
Agru	Neoarchean	Granitoid intrusion, undifferentiated or poorly constrained by core and outcrop	0.5
Mgy	Mesoproterozoic	Granophyre	0.5
Agrl	Neoarchean	Leucogranite	0.5
Mrn	Mesoproterozoic	Maple Hill Rhyolite	0.5
Mmgy	Mesoproterozoic	Melagranophyre	0.5
Aszc	Neoarchean	Mylonite	0.5
Aszu	Neoarchean	Mylonite zone	0.5
Pmy	Paleoproterozoic	Mylonitic, gneissic, schistose rocks of plutonic and volcanic protolith	0.5
Mgr	Mesoproterozoic	Porphyritic felsite, contains glomerophenocrystic plag-augite-Fe-Ti oxides-apatite in matrix	0.5
Mrr	Mesoproterozoic	Porphyritic rhyolite	0.5
Mrp	Mesoproterozoic	Porphyritic Rhyolite lava flow	0.5
Mrn	Mesoproterozoic	Porphyritic rhyolite lava flows, normally polarized	0.5
Afvm	Neoarchean	Quartz-eye rhyolite lava flow with sphalerite veining	0.5
Aqfp	Neoarchean	Quartz-feldspar porphyry	0.5
Aqfp	Neoarchean	Quartz-feldspar porphyry, gold bearing	0.5
Mrn	Mesoproterozoic	Rhyolite	0.5
Mrn	Mesoproterozoic	Rhyolite crystal tuff	0.5
Mrn	Mesoproterozoic	Rhyolite lava flow	0.5
Mrn	Mesoproterozoic	Rhyolite lava flows, normally polarized	0.5
Mrr	Mesoproterozoic	Rhyolite lava flows, reverse polarity	0.5
Mrn	Mesoproterozoic	Rhyolits lava flow	0.5
Pgk	Paleoproterozoic	Rockville porphyritic granite	0.5
Aqfp	Neoarchean	Sheared quartz-feldspar porphyry	0.5
Mrn	Mesoproterozoic	Tuffaceous rhyolite	0.5
Agru	Neoarchean	Undifferentiated granitoid pluton defined magnetically	0.5
Mgr	Mesoproterozoic	Granite to quartz-monzodiorite	0.49
Mgrd	Mesoproterozoic	Hornblende granodiorite	0.49
Mmd	Mesoproterozoic	Monzodiorite, granite, and granodiorite	0.49
Agd	Neoarchean	Foliated granodioritic intrusion	0.48
Agrm	Neoarchean	Granite to granodiorite, variably magnetic	0.48
Agrm	Neoarchean	Granite to granodiorite, variably magnetic, locally magmatically foliated	0.48
Agd	Neoarchean	Granodiorite	0.48
Agn	Neoarchean	Granodiorite gneiss	0.48
Agd	Neoarchean	Granodiorite to diorite	0.48
Agd	Neoarchean	Granodiorite, foliated and synvolcanic	0.48
Pdg	Paleoproterozoic	Granodiorite; variably foliated	0.48
Agd	Neoarchean	Granodioritic intrusion	0.48
Pgd	Paleoproterozoic	Gray granodioritic to dioritic intrusion	0.48
Am	Neoarchean	Monzonite	0.48
Aqm	Neoarchean	Quartz monzonite	0.48
Aqm	Neoarchean	Quartz monzonite, monzonite, and granodiorite, non-magnetic	0.48
Aqmm	Neoarchean	Quartz monzonite, variably magnetic and magmatically foliated	0.48
Atf	Mesoarchean to Paleoarchean	Foliated to gneissic granodiorite to tonalite	0.45
Atf	Neoarchean	Foliated to gneissic tonalite	0.45
Atf	Neoarchean	Foliated to gneissic tonalite, diorite and granodiorite	0.45
APd	Neoarchean or Paleoproterozoic	Dioritic to granodioritic intrusion of uncertain age	0.37
Ad	Neoarchean	Diorite	0.35
Aqfp	Neoarchean	Quartz feldspar porphyry	0.1

Mineral occurrences (point data) for mineral species commonly associated with the Magmatic REE mineral system were extracted from the Assembling Minnesota mineral occurrence database. Based on the minerals present in this database, the following mineral species were utilized for the model: 1) albite; 2) calcite; 3) dolomite; 4) hematite; 5) hornblende; and 6) beryl. Each of the mineral species was assigned a W.O.E. of 1. Point locations were given a 1km buffer, and the total number of overlapping mineral polygons for each group was summed and normalized to develop the polygon layers for the mineral factor.

For the geochemistry component, geochemical data (point data) were extracted from the Assembling Minnesota geologic geochemistry and drillhole geochemistry databases (Bartsch et al., 2022; Peterson, 2018) and the Hauck et al. (2014) dataset. These three databases were merged to develop the point dataset utilized in the model. Components of the geochemisty included: 1) total rare earth element (REE) plus yttrium (W.O.E. = 0.9); 2) total high field strength (HFSE) elements (W.O.E. = 0.6); 3) total heavy rare earth elements (W.O.E. = 0.5); 5) the europium anomaly (Eu/Eu*, W.O.E. = 0.6); and 6) from the Hauck et al. (2014) dataset, only peraluminous rocks (W.O.E. = 0.6) based on Shand's classification (see Figure 24). Kriging of the normalized sums for each of the point datasets was performed to develop surface rasters, and the raster values were classified and converted to polygon layers for the Geochemistry Factor utilized in the model.

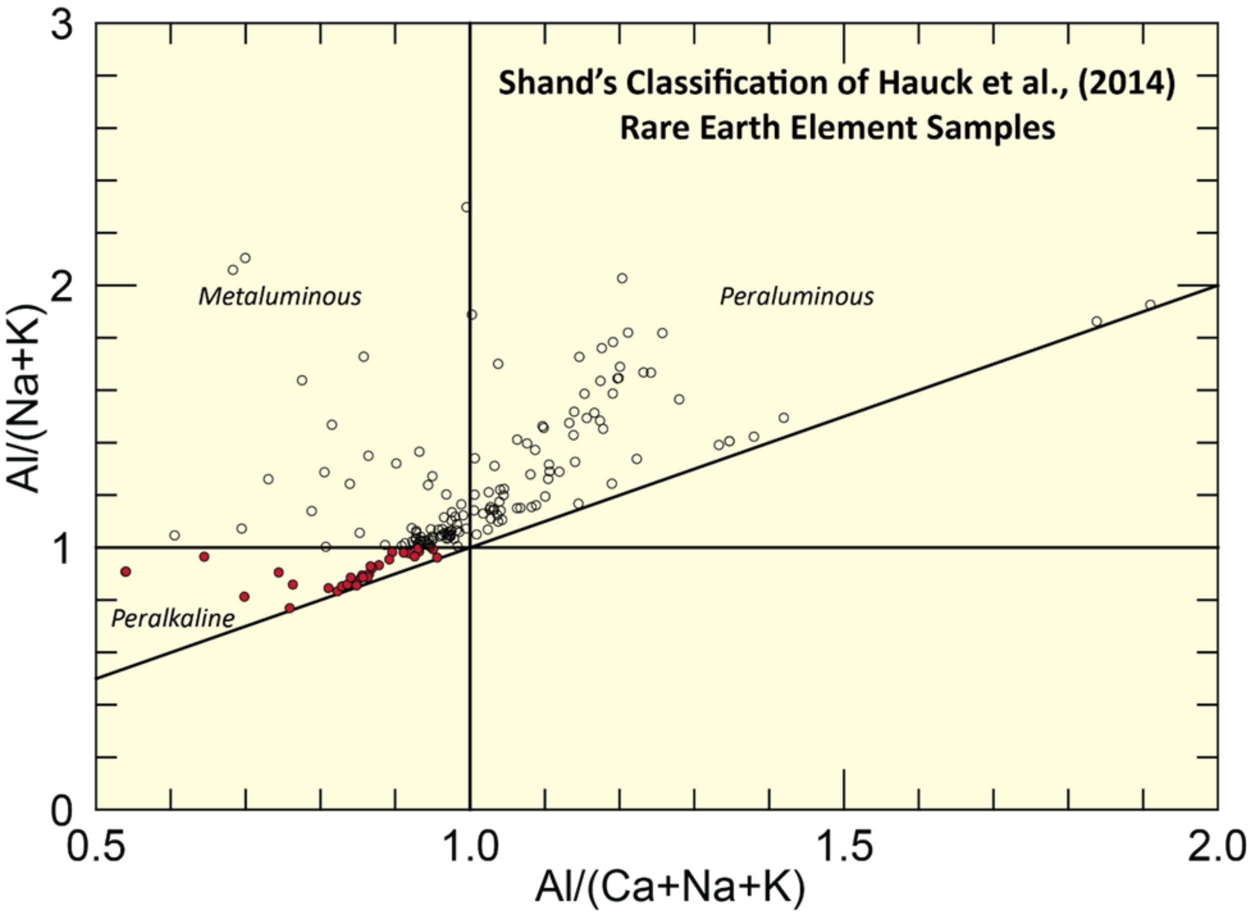

Figure 24. Shand's classification (after Maniar and Piccoli, 1989) of Hauck et al. (2014) lithogeochemistry. Samples indicated in red were classified as "peralkaline" in the ***Magmatic REE*** mineral system model.

The geophysics factor was determined utilizing total magnetics data (Chandler, 1982). This data was extracted to the bedrock geology boundaries and subsequently normalized and reclassified into 10 quantile classes (1–10) to create the polygon layer for the Geophysics factor utilized in the model.

The geochronology factor (point data) was composed of two components: 1) Neoarchean rocks (W.O.E. = 0.4); and Proterozoic rocks with dates ranging from 1400–1500 Ma (W.O.E. = 0.6; similar in age to the Wolf River Batholith in Wisconsin: Dewane and Van Schmus, 2007). Geochronological data was obtained from the Minnesota Geological Survey (Boerboom, 2021). Geochronological data points were assigned 1km buffers and values equal to their W.O.E. as the polygon layer for the Geochronology Factor.

The final Magmatic REE System Potential Map was developed by multiplying each of the model factors by their assigned factor weights and then calculating the fuzzy algebraic sum by means of the following equation (Bonham-Carter, 1994; Peterson, 2001):

$$\mu_{\text{combination}} = 1 - \prod_{i=1}^{n}(\mu i)$$

where μi is the fuzzy membership value for the i^{th} map, and *i* = 1. 2. 3, ….n maps are to be combined.

The factor weights assigned for each of the model factors are as follows:

- Geology Factor Weight = 0.8
- Mineral Factor Weight = 0.3
- Geochemistry Factor Weight = 0.7
- Geophysics Factor Weight = 0.4
- Geochronology Factor Weight = 0.5

Results

The Magmatic REE Mineral System Potential Map is illustrated in Figure 25 (with a Minnesota geology map underlay) and in Figure 26 (without the Minnesota geology map underlay). Shapefiles for the Magmatic REE Mineral System Potential Map can be found in Digital Appendix 7 in the subdirectory labeled “Shapefiles.” Model calculations can be found in Digital Appendix 7 in the subdirectory labeled “Model Calculations.”

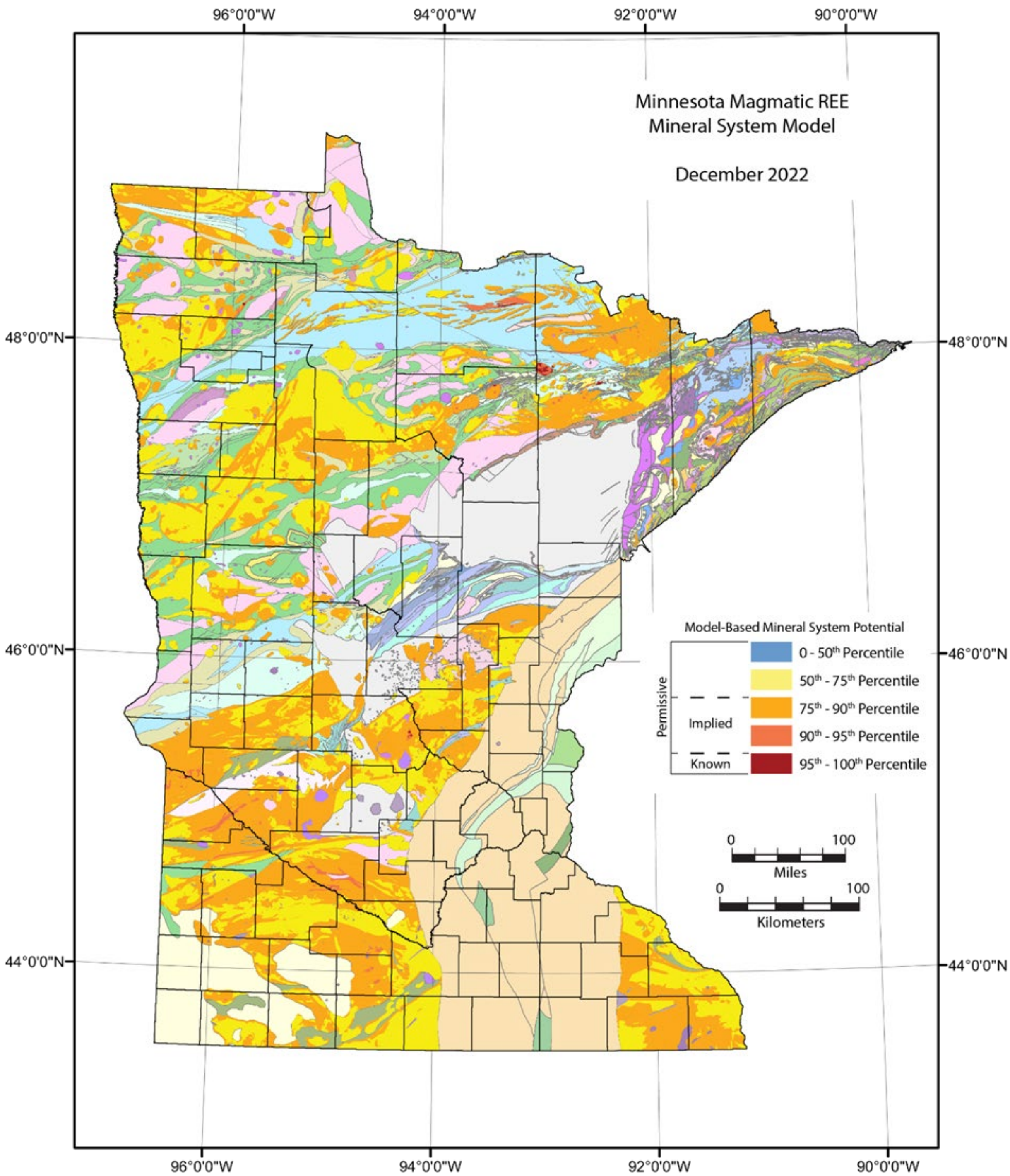

Figure 25. Results of ***Magmatic REE*** knowledge-based mineral system model with geology.

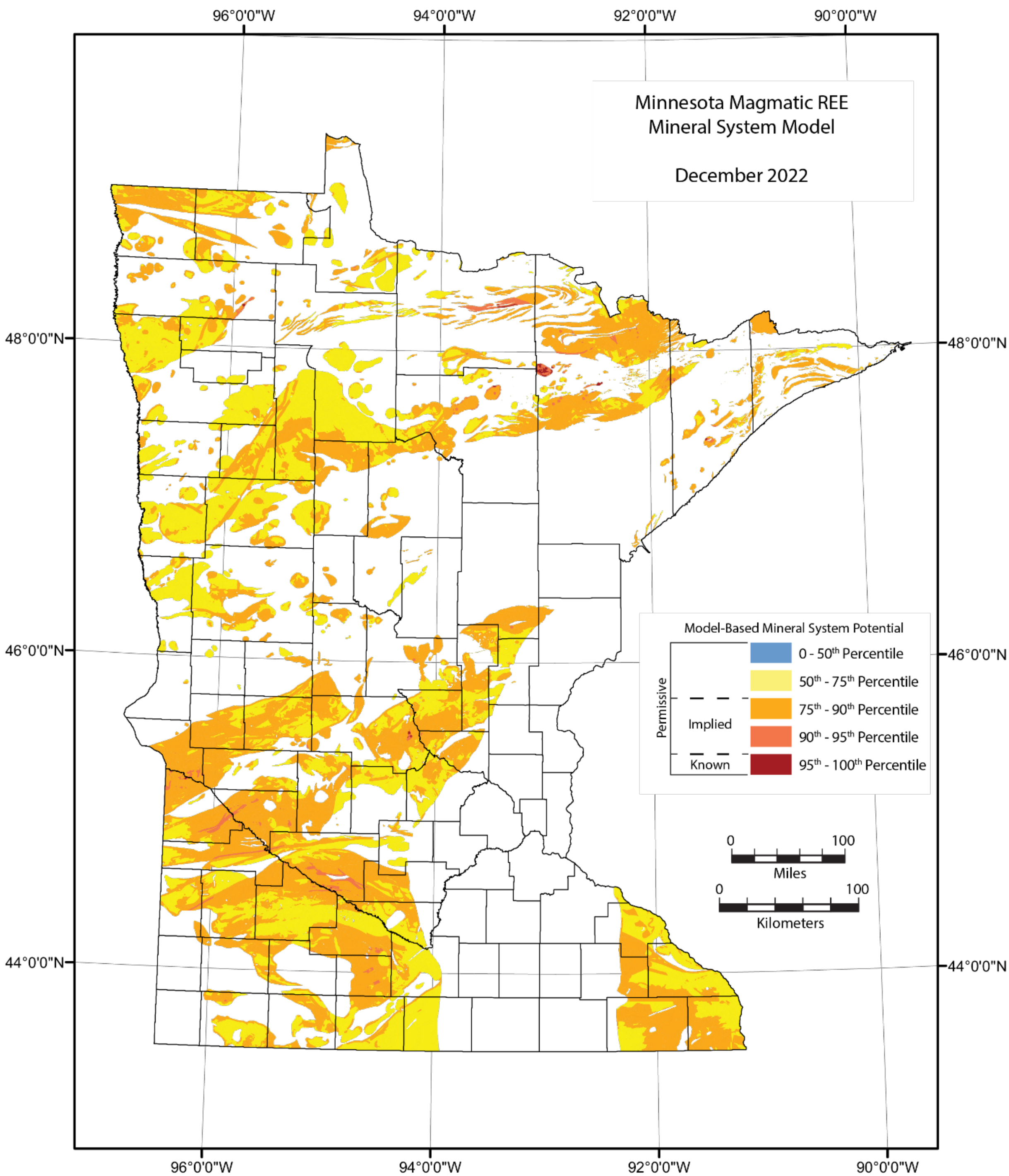

Figure 26. Results of ***Magmatic REE*** knowledge-based mineral system model without geology.

As illustrated in Figures 25 and 26, Minnesota possesses an abundance of igneous rocks and meta-igneous rocks that have elevated potential to be associated with Magmatic REE mineral systems. Based on our modeling, regions with the highest potential to be associated with the mineral system occur in south-central Lake County, north-central and northwestern St. Louis County, northeastern Itasca County, east-central Koochiching County, southeastern Marshall County, and east-central Stearns County. Within south-central Lake County, the highest modeled potential occurs within Mesoproterozoic age granophyric and granitic rocks (unit "Mbf" of Jirsa et al., 2011). High modeled potential for Magmatic REE mineral systems in St. Louis County is associated with syenite, monzodiorite, granodiorite, and diorite (rock unit "Asd" of Jirsa et al., 2011), including the Linden Pluton in northwestern St. Louis County. High potential in Itasca County is associated with syenite, monzodiorite, granodiorite, and diorite associated with the Coon Lake Pluton, and high modeled potential in east-central Koochiching County is associated with granite-rich migmatites (unit "Aqg" of Jirsa et al., 2011) within the Quetico subprovince. High modeled potential for Magmatic REE-associated mineral systems in southern Marshall County is associated with Neoarchean gabbro, peridotite, pyroxenite, lamprophyre and metamorphic equivalents (unit "Agp" of Jirsa et al., 2011), and reddish, variably porphyritic granites of Paleoproterozoic age (unit "Pgr" of Jirsa et al., 2011) host the highest potential for a Magmatic REE mineral system in east-central Stearns County.

Mafic Magmatic Mineral System

<u>*Deposit Types and Model*</u>

Table 15 indicates the various mineral deposit types associated with the Mafic Magmatic mineral system (Hofstra and Kreiner, 2021). Mafic magmatic systems commonly form in large igneous provinces that may be associated with extensional tectonic environments (Schulz et al., 2014) and may be associated with the impingement of mantle plumes on the crust (Ernst and Jowitt, 2013; Ciborowski et al., 2017). Mafic Magmatic minerals systems can also occur as a result of meteorite impacts, as is the case with the Sudbury mineral district (Barnes and Lightfoot, 2005). Sulfur saturation of the magma results in the precipitation of sulfide minerals that contain the metals extracted from these resources (Arndt et al., 2005; Virtanen et al., 2022). Ultramafic oxide-rich intrusions and anorthositic rocks associated with these systems may host economic iron-titanium-(vanadium) oxide deposits (Severson and Hauck, 1990; Severson, 1995; Woodruff et al., 2013) associated with semi-massive to massive ilmenite-titanomagnetite-magnetite mineralization.

Table 15. Systems-Deposits-Commodities-Critical Minerals table for the ***Mafic Magmatic*** mineral system (modified after Hofstra and Kreiner, 2021). Explanation for table is as follows: ±, present (absent); --, not applicable; ?, maybe; Ag, silver; Al, aluminum; As, arsenic; Au, gold; B, boron; Ba, barium; Be, beryllium; Bi, bismuth; Br, bromine; Ca, calcium; Cd, cadmium; Co, cobalt; CO_2, carbon dioxide; Cs, cesium; Cr, chromium; Cu, copper; F, fluorine; Fe, iron; Ga, gallium; Ge, germanium; Hf, hafnium; Hg, mercury; I, iodine; IAEA, International Atomic Energy Agency; In, indium; IOA, iron oxide-apatite; IOCG, iron oxide-copper-gold; IS, intermediate sulfidation; K, potassium; LCT, lithium-cesium-tantalum; Li, lithium; Mg, magnesium; Mn, manganese; Mo, molybdenum; Na, sodium; Nb, niobium; Ni, nickel; NYF, niobium-yttrium-fluorine; P, phosphorus; Pb, lead; PGE, platinum group elements; R, replacement; Rb, rubidium; Re, rhenium; REE, rare earth elements; S, skarn; Sb, antimony; Sc, scandium; Se, selenium; Sn, tin; Sr, strontium; Ta, tantalum; Te, tellurium; Th, thorium; Ti, titanium; U, uranium; V, vanadium (in "Principal Commodities" column); V, vein (in "Deposit Types" column); W, tungsten; Y, yttrium; Zn, zinc; Zr, zirconium. In the "Critical Minerals" column, elements in **bold** have been produced from the deposit type, whereas element in *italics* are enriched in the deposit type but have not been produced.

System Name	Deposit Types	Principal Commodities	Critical Minerals	References
Mafic Magmatic	Chromite	Cr	**Cr**	Ash, 1996; Schulte et al., 2012; Ernst and Jowitt, 2013; Woodruff et al., 2013; Zientek et al., 2017; Mondal and Griffin, 2018
	Nickel-copper-PGE sulfide	Ni, Cu, Co, PGE, Ag, Au, Se, Te	**Co, PGE,** *Te*	
	PGE (low sulfide)	PGE	**PGE**	
	Iron-titanium oxide	Fe, Ti, V, P	**Ti, V,** *REE*	

Key criteria for understanding and exploring for Mafic Magmatic mineral systems can be found in Arndt et al. (2005), Barnes and Lightfoot (2005), Cawthorne et al. (2005), Ernst and Jowitt (2013), Woodruff et al. (2013), Schulz et al. (2014), Ciborowski et al. (2017), Le Vaillant et al. (2018), Thakurta et al. (2022), and Virtanen et al. (2022). For the Mafic Magmatic mineral system, these criteria include:

- Ultramafic to mafic igneous rocks commonly associated with a large igneous province;
- Contacts between ultramafic and mafic igneous rocks that can allow assimilation of sulfur into the magmatic system;
- Ore minerals include a wide variety of sulfide minerals, and in the case of Fe-Ti-(V) deposits, oxide minerals;
- Sulfide-bearing mineral deposits are enriched in Cu and Ni, and commonly platinum group elements (Pt, Pd, Os, Ir, Rh, Ru); oxide-bearing mineral deposits are enriched in Fe and Ti, and sometimes V and Cr;
- Within the Lake Superior district, deposits are most likely to occur in extensional tectonic settings associated with Mesoproterozoic and Neoarchean terranes; and
- Sulfide-based mineral systems may be identified using a variety of electromagnetic geophysical techniques, whereas oxide-based mineral deposits may be identified utilizing magnetics.

Modeling Methods

Modeling for the Mafic Magmatic mineral system included six components that could be derived from the Assembling Minnesota dataset (Bartsch et al., 2022; Peterson, 2018). These six components include: 1) bedrock geology; 2) mineral occurrences; 3) geochemistry; 4) geochronology; 5) known deposits; and 6) geophysics. The inference net illustrating the various components used in the Mafic Magmatic mineral system model are illustrated in Figure 27.

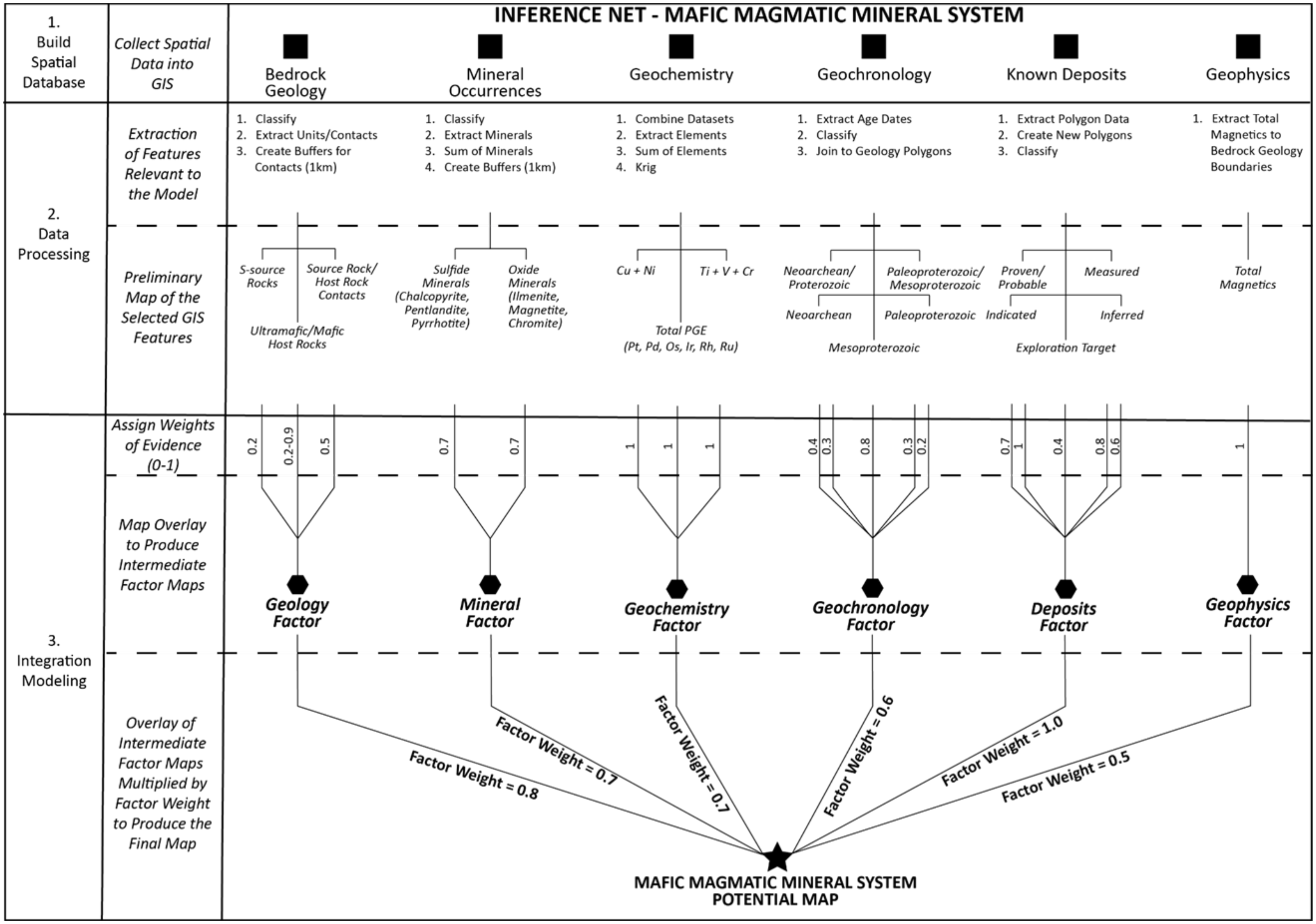

Figure 27. Inference net for ***Mafic Magmatic*** knowledge-based mineral system model.

Bedrock geology focused on three components: 1) lithological units that have potential to be sulfur source rocks via magmatic assimilation; 2) ultramafic/mafic mineral deposit host rocks; and 3) the contacts between potential sulfur source rocks and ultramafic/mafic mineral deposit host rocks. Polygons of permissible sulfur source rocks and ultramafic/mafic mineral deposit host rock types were extracted from the Assembling Minnesota bedrock geology database and given W.O.E. based on their prospectivity for hosting Mafic Magmatic mineral system-associated mineralization. Potential sulfur source rock polygons were assigned a W.O.E. of 0.2, and ultramafic/mafic host rock polygons were assigned W.O.E. ranging from 0.2–0.9 (Table 16). Geological contacts between potential sulfur source rocks and potential ultramafic/mafic host rocks were extracted from the geoline dataset associated with the Assembling Minnesota database, provided a 1km buffer, and the resulting polygons were assigned W.O.E. of 0.5. These two sets of polygons, with their respective W.O.E., were merged to develop the Geology Factor utilized in the model.

Table 16. Weights of evidence for geology polygons in the ***Mafic Magmatic*** mineral system model.

Map Label	Era	Rock Type	W.O.E.
Mprms	Mesoproterozoic	Net-textured to massive Ni-Cu-PGE sulfide ore	1
Mtpeg	Mesoproterozoic	Pegmatitic troctolite, locally sulfide-bearing	1
Mprs	Mesoproterozoic	Coarse-grained, Ni-Cu sulfide-bearing peridotite	0.9
Pmi	Paleoproterozoic	Mafic intrusion; pyroxenite, peridotite, gabbro, lamprophyre	0.9
Mmi	Mesoproterozoic	Mafic intrusive stock; diabase, diorite, pyroxenite, gabbro	0.9
Amp	Neoarchean	Metaperidotite and pyroxenite sill	0.9
Amp	Neoarchean	Metaperidotite sill	0.9
Mnt	Mesoproterozoic	Norite	0.9
Agp	Neoarchean	Olivine-rich gabbro and peridotite	0.9
Moui	Mesoproterozoic	Oxide-rich pyroxenite	0.9
Mgpeg	Mesoproterozoic	Pegmatitic gabbro	0.9
Amp	Neoarchean	Peridotite	0.9
Mpr	Mesoproterozoic	Peridotite of the Tamarack Bowl	0.9
Ampx	Neoarchean	Pyroxenite	0.9
Ampx	Neoarchean	Pyroxenite sill	0.9
Ampxs	Neoarchean	Pyroxenite, weakly sulfide-bearing	0.9
Amp	Neoarchean	Serpentinized peridotite with chalcopyrite	0.9
Amp	Neoarchean	Serpentinized, strongly magnetic peridotite	0.9
Almp	Neoarchean	Ultramafic Fragmental Rocks	0.9
Auv	Neoarchean	Ultramafic to mafic volcanic and hypabyssal intrusive rocks	0.9
Ampxs	Neoarchean	Weakly sulfide-bearing pyroxenite	0.9
Mgs	Mesoproterozoic	Weakly sulfide-bearing, fine to medium-grained gabbro to oxide gabbro	0.9
Mpr	Mesoproterozoic	Weakly sulfide-bearing, fine-grained peridotite	0.9
Mpr	Mesoproterozoic	Weakly sulfide-bearing, peridotite	0.9
Amps	Neoarchean	Weakly sulfide-bearing, serpentinized peridotite	0.9
Mpth	Mesoproterozoic	Heterogeneous Augite Troctolite	0.8
Mpth	Mesoproterozoic	Heterogeneous troctolite to augite troctolite	0.8
Mltmt	Mesoproterozoic	Latered troctolite	0.8
Mdn	Mesoproterozoic	Layered dunite	0.8
Mmt	Mesoproterozoic	Layered melatroctolite	0.8
Pxgl	Paleoproterozoic	Layered oxide-rich melaggabbro	0.8
Mcr_t	Mesoproterozoic	Layered troctolite and chromitite	0.8
Mltmt	Mesoproterozoic	Layered troctolite to melatroctolite	0.8
Mt	Mesoproterozoic	Layered, fine-grained troctolite dike	0.8
Aag	Neoarchean	Mafic to ultramafic hypabyssal intrusive complexes; gabbro, anorthosite	0.8
Ami	Neoarchean	Mafic to ultramafic intrusions	0.8
Auv	Neoarchean	Mafic to ultramafic volcanic rocks	0.8
Mmts2	Mesoproterozoic	Sulfide-bearing melatroctolite	0.8
Mtghs	Mesoproterozoic	Sulfide-bearing oxide gabbro	0.8
Mmts1a	Mesoproterozoic	Sulfide-poor melatroctolite	0.8
Mpth	Mesoproterozoic	Heterogeneous, inclusion-rich troctolite to olivine-oxide gabbro	0.7

Map Label	Era	Rock Type	W.O.E.
Mhtgs	Mesoproterozoic	Heterogeneous, locally sulfide-bearing, gabbroic to troctolitic rocks	0.7
Mltg	Mesoproterozoic	Interlayered gabbro and troctolite	0.7
Mlts	Mesoproterozoic	Sulfide-bearing, layered troctolitic rocks	0.7
Amgbs	Neoarchean	Sulfide-bearing, microgabbro (chilled margin)	0.7
Mhts1b	Mesoproterozoic	Sulfide-poor, weakly heterogeneous troctolitic rocks	0.7
Mhts1b	Mesoproterozoic	Sulfide-poor, weakly heterogeneous troctolitic rocks	0.7
feMD	Mesoproterozoic	Augite ferromonzodiorite, coarse-grained, prismatic ferromonzodiorite	0.6
Mpt	Mesoproterozoic	Augite troctolite	0.6
Mtpt	Mesoproterozoic	Augite troctolite to troctolite	0.6
Mht	Mesoproterozoic	Heterogeneous troctolitic rocks	0.6
Mpth	Mesoproterozoic	Heterogeneous troctolitic to gabbroic rocks	0.6
Mpth	Mesoproterozoic	Heterogeneous, augite troctolite	0.6
Mcc	Mesoproterozoic	Highly magnetic, Colvin Creek type meta-interflow sandstone	0.6
Mpt	Mesoproterozoic	Homogeneous augite troctolite with pegmatoidal oxide-augite patches	0.6
Mog	Mesoproterozoic	Olivine (oxide) gabbro and troctolite transition zone	0.6
Mdb	Mesoproterozoic	Olivine diabase	0.6
Mog	Mesoproterozoic	Olivine gabbro	0.6
Mxt	Mesoproterozoic	Oxide-rich troctolite	0.6
Mxog	Mesoproterozoic	Oxide-rich, coarse-grained, gabbro to olivine gabbro	0.6
Mxmts	Mesoproterozoic	Oxide-rich, sulfide-bearing, melatroctolite	0.6
Mhtgs	Mesoproterozoic	Sulfide-bearing troctolitic rocks	0.6
Mgas	Mesoproterozoic	Sulfide-bearing, altered anorthositic rocks	0.6
Mmts	Mesoproterozoic	Sulfide-bearing, coarse-grained, layered oxide-bearing troctolite	0.6
Mtghs	Mesoproterozoic	Sulfide-bearing, contaminated noritic rocks	0.6
Mhts	Mesoproterozoic	Sulfide-bearing, heterogeneous troctolite contact zone	0.6
Mtghs	Mesoproterozoic	Sulfide-bearing, heterogeneous troctolitic rocks	0.6
Mhts1	Mesoproterozoic	Sulfide-bearing, PGE-poor, heterogeneous troctolitic rocks	0.6
Mhts4	Mesoproterozoic	Sulfide-bearing, PGE-rich, heterogeneous augite troctolite	0.6
Mts	Mesoproterozoic	Sulfide-rich troctolite	0.6
Mt	Mesoproterozoic	Troctolite	0.6
Mt_a	Mesoproterozoic	Troctolite with abundant anorthosite inclusions	0.6
Mt	Mesoproterozoic	Troctolitic rocks	0.6
Mt	Mesoproterozoic	Troctolitic to gabbroic dikes	0.6
Mhbx	Mesoproterozoic	Unknown magnetic inclusion in troctolitic intrusion	0.6
Mfmd	Mesoproterozoic	Pyroxene ferromonzodiorite	0.5
Mmd	Mesoproterozoic	Pyroxene monzodiorite	0.5
Mfmd	Mesoproterozoic	Pyroxene-prismatic, ferromonzodiorite	0.5
Mmd	Mesoproterozoic	Pyroxene-quartz Monzodiorite	0.5
Mta	Mesoproterozoic	Troctolitic anorthosite	0.5
Mai	Mesoproterozoic	Troctolitic anorthosite xenolith	0.5
Mt	Mesoproterozoic	Troctolitic diabase	0.5
Mat	Mesoproterozoic	Anorthositic troctolite	0.3
Mat	Mesoproterozoic	Anorthositic troctolite to troctolite	0.3
Mg	Mesoproterozoic	Coarse-grained gabbro	0.2
Mgg	Mesoproterozoic	Coarse-grained, granophyric gabbro	0.2
Mai	Mesoproterozoic	Coarse-grained, ophitic gabbroic anorthosite	0.2
Mxn	Mesoproterozoic	Contaminated, oxide-rich, noritic contact zone	0.2
Mfg	Mesoproterozoic	Cumulate-textured ferrogabbro	0.2
Mbrd	Mesoproterozoic	Diabase	0.2
Mdb	Mesoproterozoic	Diabase dike	0.2
Mdb	Mesoproterozoic	Diabase dike (?)	0.2
Mdbm	Mesoproterozoic	Diabase dike, highly magnetic	0.2
Mdbn	Mesoproterozoic	Diabase Dike, normally polarized	0.2
Mdb	Mesoproterozoic	Diabase dike, sill	0.2
Mdb	Mesoproterozoic	Diabase dike, sill and/or plug-like intrusion	0.2
Ami	Neoarchean	Diabase plug	0.2
Pdb	Paleoproterozoic	Diabase sill	0.2
Mbrd	Mesoproterozoic	Diabase-gabbro	0.2
Mdb	Mesoproterozoic	Ferrodiabase	0.2
Mdb	Mesoproterozoic	Fine to medium-grained, locally plag-phyric, ophitic olivine diabase	0.2
Mpt	Mesoproterozoic	Fine to medium-grained, poorly to moderately foliated, subophitc augite troctolite to troctolite	0.2

Map Label	Era	Rock Type	W.O.E.
Mg	Mesoproterozoic	Fine-grained, foliated gabbro	0.2
Mmg	Mesoproterozoic	Fine-medium-grained, oxide-bearing microgabbro	0.2
Mg	Mesoproterozoic	Foliated gabbro	0.2
Mxg	Mesoproterozoic	Foliated, oxide-bearing (lenses), gabbro	0.2
Amgb	Neoarchean	Gabbro	0.2
PMm	Paleoproterozoic or Mesoproterozoic	Gabbro and anorthosite	0.2
Mg	Mesoproterozoic	Gabbro sill	0.2
Pgp	Paleoproterozoic	Gabbro, pyroxenite, diorite, and lamprophyre intrusion	0.2
Mdb	Mesoproterozoic	Granophyric, ophitic, poikilitic olivine-diabase	0.2
Mdb	Mesoproterozoic	Intergranular diabase	0.2
Mdb	Mesoproterozoic	Intergranular diabase sill	0.2
Mdb	Mesoproterozoic	Mafic intrusion ?	0.2
Mdb	Mesoproterozoic	Mafic intrusion inferred	0.2
Ami	Neoarchean	Mafic intrusion, defined magnetically	0.2
Ami	Neoarchean	Mafic intrusion, undifferentiated	0.2
Pmv	Paleoproterozoic	Mafic metavolcanic and hypabyssal intrusive rocks	0.2
Ami	Neoarchean	Mafic plug-like intrusion; typically magnetic	0.2
Agp	Neoarchean	Marginal oxide-rich gabbro	0.2
Amgb	Neoarchean	Meta Orthopyroxene gabbro	0.2
Pmdb	Paleoproterozoic	Metadiabase hypabyssal intrusive rocks	0.2
Amgb	Neoarchean	Meta-diabase sill	0.2
Pmdb	Paleoproterozoic	Metadiabase/metagabbro sill-like intrusive	0.2
Amgb	Neoarchean	Metadiorite/gabbro	0.2
Amgb	Neoarchean	Metagabbro	0.2
Amgb	Neoarchean	Metagabbro intrusion	0.2
Amgb	Neoarchean	Metagabbro sill	0.2
Amgb	Neoarchean	Metagabbro sill in basaltic rocks	0.2
Amgps	Neoarchean	Metagabbro sill, locally sulfide-bearing	0.2
Amgbs	Neoarchean	Metagabbro sill, weakly (0-3%) sulfide-bearing	0.2
Amgb	Neoarchean	Metagabbro sill, weakly sulfide-bearing	0.2
Aag	Neoarchean	Metagabbro, commonly chloritized	0.2
Agp	Neoarchean	Metagabbro, locally brecciated	0.2
Amgb	Neoarchean	Metagabbro/metadiabase	0.2
Amgb	Neoarchean	Metagabbroic sill	0.2
Mg	Mesoproterozoic	Mg - Gabbroic rocks	0.2
Mmg	Mesoproterozoic	Microgabbro	0.2
Mmg	Mesoproterozoic	Micro-gabbro	0.2
Mdb	Mesoproterozoic	Mixed diabase and granophyre	0.2
Mmzg	Mesoproterozoic	Mixed monzogabbro, gabbronorite, and gabbro	0.2
Mpth	Mesoproterozoic	Mixed troctolitic and anorthositic rocks	0.2
Mdb	Mesoproterozoic	Monker Lake diabase	0.2
Mdb	Mesoproterozoic	Monker Lake diabase	0.2
Mdb	Mesoproterozoic	Ophitic diabase	0.2
Mdb	Mesoproterozoic	Ophitic diabase dike	0.2
Mg	Mesoproterozoic	Ophitic gabbro	0.2
Mag	Mesoproterozoic	Ophitic gabbroic anorthosite	0.2
Mdb	Mesoproterozoic	Ophitic olivine diabase	0.2
Mgn	Mesoproterozoic	Ophitic olivine gabbronorite	0.2
Mdb	Mesoproterozoic	Ophitic olivine-diabase	0.2
Mdb	Mesoproterozoic	Ophitic olvine gabbro to diabase	0.2
Mbn	Mesoproterozoic	Ophitic to intergranular pigeonitic basalt	0.2
Mbn	Mesoproterozoic	Ophitic to pigeonitic basaltic rocks	0.2
Mdb	Mesoproterozoic	Ophitic troctolitic diabase	0.2
Mdbg	Mesoproterozoic	Ophitic, olivine-bearing diabase-gabbro sill	0.2
Mxog	Mesoproterozoic	Oxide and altered-oliving bearing ophitic gabbro	0.2
Mxog	Mesoproterozoic	Oxide-olivine leucogabbro / leucotroctolite	0.2
Mdb	Mesoproterozoic	Plagioclase-porphyritic diabase	0.2
feD	Mesoproterozoic	Plagioclase-porphyritic ferrodiorite	0.2
Amgp	Neoarchean	Porphyritic (opx) melagabbro	0.2
Mdb	Mesoproterozoic	Porphyritic diabase	0.2
Amgps	Neoarchean	Porphyritic metagabbro sill, locally sulfide-bearing	0.2

Map Label	Era	Rock Type	W.O.E.
Mg	Mesoproterozoic	Porphyritic ophitic gabbro	0.2
Agp	Neoarchean	Quartz-biotite gabbro	0.2
Afvm	Neoarchean	Quartz-eye rhyolite lava flow with sphalerite veining	0.2
Amqgs	Neoarchean	Sulfide-bearing to sulfide-rich, quartz gabbro	0.2
Amgbh	Neoarchean	Taxitic metagabbro	0.2
Amvpv	Neoarchean	Variolitic pillowed flows	0.2
Mhg	Mesoproterozoic	Vari-textured gabbro	0.2
Mfg	Mesoproterozoic	Apatitic ferrogabbro	0.15
Mfg	Mesoproterozoic	Ferrogabbro	0.15
Mfg	Mesoproterozoic	Ferrogabbro to ferromonzonite	0.15
Mfg	Mesoproterozoic	Ferrogabbro to ferromonzonite	0.15
Mfg	Mesoproterozoic	Ferrogabbro to quartz ferromonzodiorite	0.15
Mfg	Mesoproterozoic	Foliated ferrogabbro	0.15
Mfg	Mesoproterozoic	Foliated ferrogabbro	0.15
Mfmd	Mesoproterozoic	Medium- to fine-grained, nonfoliated ferromonzodiorite to ferrodiorite.	0.15
Mltg	Mesoproterozoic	Medium-grained, layered gabbro	0.15
Mgd	Mesoproterozoic	Medium-grained, well-foliated, apatitic olivine oxide gabbro/diorite	0.15
Mxog	Mesoproterozoic	Medium-to coarse-grained, well-foliated and modally layered, intergranular olivine oxide gabbro	0.15
Mmlg	Mesoproterozoic	Melagabbro	0.15
Amgps	Neoarchean	Melagabbro sill, locally sulfide-bearing	0.15
Mga	Mesoproterozoic	Olivine-bearing gabbroic anorthosite	0.15
Mog	Mesoproterozoic	Olivine-bearing gabbroic rocks	0.15
Man	Mesoproterozoic	Anorthosite	0.1
Maat	Mesoproterozoic	Anorthosite with troctolitic rocks	0.1
Mai	Mesoproterozoic	Anorthosite xenolith	0.1
Magh	Mesoproterozoic	Anorthosite, gabbro, and hornfels undivided	0.1
Mag	Mesoproterozoic	Anorthositic gabbro	0.1
Mag	Mesoproterozoic	Anorthositic gabbro to gabbro	0.1
Mags	Mesoproterozoic	Anorthositic gabbro, locally altered and sulfide-bearing	0.1
Mant	Mesoproterozoic	Anorthositic norite	0.1
Mau	Mesoproterozoic	Anorthositic rocks, undivided	0.1
Mai	Mesoproterozoic	Anorthositic xenolith	0.1
Mgd	Mesoproterozoic	Gabbro-diorite	0.1
Mga	Mesoproterozoic	Gabbroic anorthosite	0.1
Mga	Mesoproterozoic	Gabbroic anorthosite pegmatite	0.1
Mfg	Mesoproterozoic	Gabbroic rock with mottled granophyric zones	0.1
Mg	Mesoproterozoic	Gabbroic rocks	0.1
APgb	Neoarchean or Paleoproterozoic	Gabbroic to dioritic intrusion and metamorphic equivalent	0.1
Pga	Paleoproterozoic	Gabbroic, noritic, and anorthositic intrusion	0.1
Mgn	Mesoproterozoic	Gabbronorite	0.1
Mgn	Mesoproterozoic	Gabbronorite hornfels, highly magnetic	0.1
Mai	Mesoproterozoic	Magnetic Anorthosite and Gabbroic rocks, Magnetic	0.1
Mcc	Mesoproterozoic	Magnetite-rich, metamorphosed interflow sandstone and basalt	0.1
Amvm	Neoarchean	Massive metabasaltic rocks and/or metagabbroic sill-like intrusive	0.1
Pms	Paleoproterozoic	Massive pyrite-pyrrhotite, locally saprolitic and siliceous	0.1
Mgas	Mesoproterozoic	Ophitic anorthositic rocks, locally altered and sulfide-bearing	0.1
Mgas	Mesoproterozoic	Sulfide-bearing, PGE-poor, anorthositic rocks	0.1
Mdb	Mesoproterozoic	Basalt dike	0.03
Mhb	Mesoproterozoic	Basalt hornfels	0.03
Mhbx	Mesoproterozoic	Basalt hornfels, magnetic	0.03
Mbn	Mesoproterozoic	Basalt lava flow	0.03
Mbn	Mesoproterozoic	Basalt lava flows, normal polarity	0.03
Mbr	Mesoproterozoic	Basalt lava flows, reverse polarity	0.03
Ma	Mesoproterozoic	Basalt or andesite	0.03
Amvm	Neoarchean	Basalt sheet flow in small iron formation	0.03
Mbn	Mesoproterozoic	Basalt sill or dike	0.03
Mbn	Mesoproterozoic	Basalt xenolith	0.03
Mrn	Mesoproterozoic	Basaltic andesite	0.03
Ma	Mesoproterozoic	Basaltic andesite lava flows	0.03
Ma	Mesoproterozoic	Basaltic andesite to andesite	0.03

Map Label	Era	Rock Type	W.O.E.
Mhbx	Mesoproterozoic	Basaltic hornfels, magnetic	0.03
Mhb	Mesoproterozoic	Basaltic hornfels, typically non-magnetic	0.03
Amvu	Neoarchean	Basaltic lava flows	0.03
Amvpb	Neoarchean	Basaltic pillow breccia and hyaloclastite deposits	0.03
Amvu	Neoarchean	Basaltic rocks, massive & pillowed undifferentiated	0.03
Mbn	Mesoproterozoic	Basaltic rocks, undifferentiated	0.03
Amvs	Neoarchean	Basaltic Scoria Deposit	0.03
Mbn	Mesoproterozoic	Basaltic trachyandesite	0.03
Amvt	Neoarchean	Basaltic tuff	0.03
Amvt	Neoarchean	Basaltic tuff and epiclastic sediments	0.03
Amvu	Neoarchean	Basaltic volcanic rocks	0.03
Mbx	Mesoproterozoic	Basaltic volcaniclastic rocks	0.03
Amvs	Neoarchean	Bedded basaltic scoria deposits	0.03
APmvu	Neoarchean or Paleoproterozoic	Mafic volcanic and hypabyssal intrusive rocks of uncertain age	0.03
Amvm	Neoarchean	Massive basalt lava flows with thin iron formation horizons	0.03
Amvm	Neoarchean	Massive basalt with thin iron formation horizons	0.03
Mbn	Mesoproterozoic	ophitic basalt	0.03
Mbn	Mesoproterozoic	Ophitic basalt lava flow	0.03
Mbn	Mesoproterozoic	Ophitic basalt with fine-grained ophites from 2 to 4 millimeters in diameter	0.03
Mbn	Mesoproterozoic	Ophitic basalt with plagioclase phenocrysts	0.03
Mbn	Mesoproterozoic	Ophitic basalt, normal polarity	0.03
Mbn	Mesoproterozoic	Ophitic basalt, weakly porphyritic, normal polarity	0.03
Aifc	Neoarchean	Chert and lean iron formation	0.02
Aifc	Neoarchean	Chert-rich iron formation	0.02
Aifc	Neoarchean	Cherty interflow exhalite with pyrite	0.02
Avms	Neoarchean	Cherty interpillow exhalite	0.02
Aifc	Neoarchean	Cherty iron formation	0.02
Aifc	Neoarchean	Cherty iron formation with pyrite	0.02
Aifo	Neoarchean	Iron Formation	0.02
Aifo	Neoarchean	Iron formation interlayered with green sandstone	0.02
Aifo	Neoarchean	Iron formation, defined magnetically	0.02
Aifo	Neoarchean	Iron Formation, defined via linear positive magnetic anomaly	0.02
Aifo	Neoarchean	Iron Formation, inferred from aeromagnetic data	0.02
Aifo	Neoarchean	Iron Formation, inferred from positive magnetic anomaly	0.02
Aifo	Neoarchean	Iron-formation	0.02
Auv	Neoarchean	Komatiitic basalt lava flows	0.02
Auv	Neoarchean	Komatiitic metavolcanic rocks, strongly foliated to tremolitic schists	0.02
Avms	Neoarchean	Massive sulfide	0.02
Avms	Neoarchean	Massive sulfide (VMS-type)	0.02
Avms	Neoarchean	Massive sulfide is felsic breccias	0.02
Avms	Neoarchean	Massive sulfide to Semi-massive sulfide breccia with felsic fragments in flowed iron sulfide	0.02
Avms	Neoarchean	Massive sulfide, pyrite-rich	0.02
Mfg	Mesoproterozoic	Massive, intergranular ferrogabbro	0.02
Aifo	Neoarchean	Oxide facies banded iron formation	0.02
Aifo	Neoarchean	Oxide Facies Iron Formation	0.02
Mxg	Mesoproterozoic	Oxide gabbro	0.02
Mxg	Mesoproterozoic	Oxide gabbro of the Tamarack Intrusion Bowl	0.02
Mxt	Mesoproterozoic	Oxide rich troctolite	0.02
Moui	Mesoproterozoic	Oxide Ultramafic Intrusion	0.02
Mxog	Mesoproterozoic	Oxide-bearing, olivine gabbro	0.02
Aifo	Neoarchean	Oxide-facies iron formatiom	0.02
Aifo	Neoarchean	Oxide-facies iron formation, highly magnetic	0.02
Aifs	Neoarchean	Sulfide facies iron formation	0.02
Aifs	Neoarchean	Sulfide-facies iron formation	0.02
Avms	Neoarchean	Sulfide-facies iron fromation, ie., bedded massive sulfide	0.02
Psi	Paleoproterozoic	Sulfidic and graphitic iron-formation	0.02
Aifs	Neoarchean	Sulfidic interpillow exhalitive deposits	0.02
Mfd	Mesoproterozoic	Apatite-bearing, ferrodiorite	0.01
Aszu	Neoarchean	Banded ultramylonite with local heavy pyrite	0.01
Mbss	Mesoproterozoic	Basal sandstone/quartzite	0.01

Map Label	Era	Rock Type	W.O.E.
Mbn	Mesoproterozoic	Basalt	0.01
Amvm	Neoarchean	Basalt & BIF	0.01
Mfd	Mesoproterozoic	Ferrodiorite	0.01
Mfd	Mesoproterozoic	Foliated ferrodiorite	0.01
Aga	Neoarchean	Graphitic & pyritic argillite	0.01
Aga	Neoarchean	Graphitic and pyritic argillite	0.01
Aga	Neoarchean	Graphitic and pyritic sedimentary rocks intercalated with felsic tuffs	0.01
Aga	Neoarchean	Graphitic and tuffaceous metasediments	0.01
Aga	Neoarchean	Graphitic argillite	0.01
Aga	Neoarchean	Graphitic argillite with minor pyrite	0.01
Aga	Neoarchean	Graphitic sediment with 0.5-2% pyrite	0.01
Ags	Neoarchean	Graywacke and mudstone; typically greenschist facies metamorphism	0.01
Pgs	Paleoproterozoic	Graywacke, slate with graphitic and sulfidic zones	0.01
Ags	Neoarchean	Greywacke and slate	0.01
Pag	Paleoproterozoic	Greywacke slate	0.01
Pvf	Paleoproterozoic	Greywacke, mudstone, and argillite	0.01
Prf	Paleoproterozoic	Greywacke, siltstone and argillite	0.01
Ags	Neoarchean	Greywacke-slate	0.01
Ags	Neoarchean	Greywacke-slate, mixed sourced	0.01
Aifo	Neoarchean	Inferred iron formation	0.01
Aifo	Neoarchean	Inferred iron formation, defined magnetically	0.01
Ags	Neoarchean	Interbedded greywacke-slate	0.01
Aas	Neoarchean	Lithic sandstone, mudstone, and siliceous siltstone with detrital hbld and plag	0.01
Aas	Neoarchean	Lithic sandstone, mudstone, and siliceous siltstone with detrital hbld and plag	0.01
Aas	Neoarchean	Lithic sandstone, mudstone, and siliceous siltstone with detrital hbld and plag	0.01
Pmv	Paleoproterozoic	Mafic metavolcanic and hypabyssal intrusive rocks, argillite, slate, graywacke	0.01
Amvu	Neoarchean	Mafic metavolcanic rocks; minor volcaniclastic and hypabyssal intrusions	0.01
Pifs	Paleoproterozoic	Manganiferous, thin bedded Virginia Formation Iron Formation associated w/ graphitic argillites	0.01
Pd	Paleoproterozoic	Mesocratic Diorite	0.01
Amgb	Neoarchean	Meta hornblende-gabbro sill	0.01
Amgb	Neoarchean	Meta hornblende-gabbro, amphibolite-grade	0.01
Pm	Paleoproterozoic	Mudstone, quartzite, graywacke, phyllite, graphitic argillite	0.01
Aszp	Neoarchean	Pyrite-rich Phyllite / Schist	0.01
Asza	Neoarchean	Quartz-Ankerite Schist (+/- Pyrite)	0.01
Aqv	Neoarchean	Quartz-pyrite vein	0.01
Aszs	Neoarchean	Quartz-Sericite Schist (+/- Pyrite)	0.01
Aga	Neoarchean	Sheared graphitic and pyritic argillite	0.01
Aifo	Neoarchean	Sheared iron formation, Quartz-calcite-magnetite schist	0.01
Aifo	Neoarchean	Sheared Iron-formation	0.01
Aifsl	Neoarchean	Silicate facies iron formation	0.01
Pag	Paleoproterozoic	Slate, graywacke	0.01
Aks	Neoarchean	Slate, siltstone, lithic sandstone, and conglomerate	0.01
Aifo	Neoarchean	Stretched iron formation	0.01
Psi	Paleoproterozoic	Sulfidic iron-formation	0.01
Amgbs	Neoarchean	Sulfidic metagabbro	0.01
Pifs	Paleoproterozoic	Superior type iron formation	0.01
Mcc	Mesoproterozoic	Thermally metamorphosed, cross-bedded, interflow sandstone	0.01
Aifo	Neoarchean	Thin BIF horizon in mafic tuff	0.01
Aifo	Neoarchean	Thin iron formation horizon in massive basalt	0.01
Aifo	Neoarchean	Thin iron formation in altered mafic tuff	0.01
Avms	Neoarchean	Thin zones of massive sulfide in altered felsic tuff	0.01
Ags	Neoarchean	Tuffaceous metasediment (greywacke-slate?)	0.01
Mrn	Mesoproterozoic	Tuffaceous rhyolite	0.01
Pvfg	Paleoproterozoic	Virginia Formation graphitic argillite w/ argillite, chert, and carbonate-silicate iron formation	0.01
Pifs	Paleoproterozoic	Virginia Formation Iron Formation associated w/ graphitic argillites	0.01
Pac	Paleoproterozoic	Virginia Formation slate with thin limestone interbeds	0.01

Mineral occurrences (point data) for mineral species commonly associated with Mafic Magmatic mineral system mineralization were extracted from the Assembling Minnesota mineral occurrence database. Two mineral species groups were utilized for the model: 1) total sulfide minerals (the sum of chalcopyrite + pentlandite + pyrrhotite); and 2) total oxide minerals (the sum of ilmenite, magnetite, and chromite). W.O.E. of 0.7 were assigned to each of the mineral species groups and the point locations were given a buffer of 1km. The total number of overlapping minerals polygons present at any one site for each group were summed and normalized to develop the Mineral Factor.

Geochemical data (point data) were extracted from the Assembling Minnesota geologic geochemistry and drillhole geochemistry databases (Bartsch et al., 2022; Peterson, 2018). Three sums were calculated from the datasets: 1) copper plus nickel; 2) titanium + vanadium + chromium; and 3) total platinum group elements (platinum + palladium + osmium + Iridium + rhenium + ruthenium). Kriging of normalized sums was performed to develop surface rasters, and the raster values were classified and converted to polygon layers for the Geochemistry Factor utilized in the model.

Geochronological data for the Mafic Magmatic mineral system model was obtained from the Minnesota Geological Survey (Boerboom, 2021). The geochronology factor (polygons) was composed of five components: 1) Neoarchean/Proterozoic age rocks (W.O.E. = 0.3); 2) Paleoproterozoic/Mesoproterozoic age rocks (W.O.E. = 0.3); 3) Neoarchean age rocks (W.O.E. = 0.4); 4) Paleoproterozoic age rocks (W.O.E. = 0.2); and 5) Mesoproterozoic age rocks (W.O.E. = 0.8). Mesoproterozoic age rocks were given W.O.E. significantly higher than other age rocks, as it is well known that these rocks host significant Mafic Magmatic mineral system-associated mineral deposits in the Lake Superior region. Geochronological data points were assigned 1km buffers with values equal to their W.O.E. as polygon layers utilized to construct the Geochronology Factor. Geochronological polygons were extracted from the Assembling Minnesota bedrock geology database and assigned W.O.E, comprising the polygon layer for the Geochronology factor.

Polygons for known NI 43-101 compliant mineral resources were digitized. These polygons were assigned various W.O.E. based on the Canadian Institute of Mining, Metallurgy and Petroleum mineral resource and mineral reserve classification (CIM, 2014). Polygons of Proven/Probable mineral reserves were assigned a W.O.E. of 1. Measured, indicated, and inferred mineral resources were assigned W.O.E. of 0.8, 0.7, and 0/6, respectively. Deposits classified as exploration targets were assigned W.O.E. of 0.4. The polygons with their respective W.O.E. made up the Deposits Factor utilized in the model.

The geophysics factor was determined utilizing total magnetics data (Chandler, 1982). This data was extracted to the bedrock geology boundaries, and subsequently normalized and reclassified into 10 quantile classes (1–10) to create the polygon layer shapefile for the Geophysics factor utilized in the model.

The final Mafic Magmatic mineral system Potential Map was developed by multiplying each of the model factors by their assigned factor weights and then calculating the fuzzy algebraic sum by means of the following equation (Bonham-Carter, 1994; Peterson, 2001):

$$\mu_{combination} = 1 - \prod_{i=1}^{n}(\mu i)$$

where μ*i* is the fuzzy membership value for the i^{th} map, and *i* = 1. 2. 3, ….n maps are to be combined.

The factor weights assigned for each of the Mafic Magmatic mineral system model factors are as follows:

- Geology Factor Weight = 0.8
- Mineral Factor Weight = 0.7
- Geochemistry Factor Weight = 0.7
- Geochronology Factor Weight = 0.6
- Deposits Factor Weight = 1
- Geophysics Factor Weight = 0.5

Results

The Mafic Magmatic Mineral System Potential Map is illustrated in Figure 28 (with a Minnesota geology map underlay) and in Figure 29 (without the Minnesota geology map underlay). Shapefiles for the Mafic Magmatic Mineral System Potential Map can be found in Digital Appendix 8 in the subdirectory labeled "Shapefiles." Model calculations can be found in Digital Appendix 8 in the subdirectory labeled "Model Calculations."

Fuzzy-logic modeling indicates the highest probability for the presence of Mafic Magmatic mineral systems occurs in northeastern Lake County, east-central St. Louis County, and within eastern Aitkin County. The model clearly has identified known disseminated to massive Cu-Ni-PGM deposits that occur in ultramafic and mafic rocks at the base of the Duluth Complex in Lake and St. Louis counties, as well as Ti-V-oxide deposits and prospects associated with oxide ultramafic intrusions (peridotites, pyroxenites) that occur along the western margin of the Duluth Complex in central St. Louis County. As well, the model identified the Tamarack intrusion in eastern Itasca County, the host of the Tamarack Ni-Cu-Co deposit. Identification of these resources is not surprising, as the geological, mineralogical, geochemical, geochronological, geophysical, and resource confidence characteristics will all score highly for these regions based on model parameters.

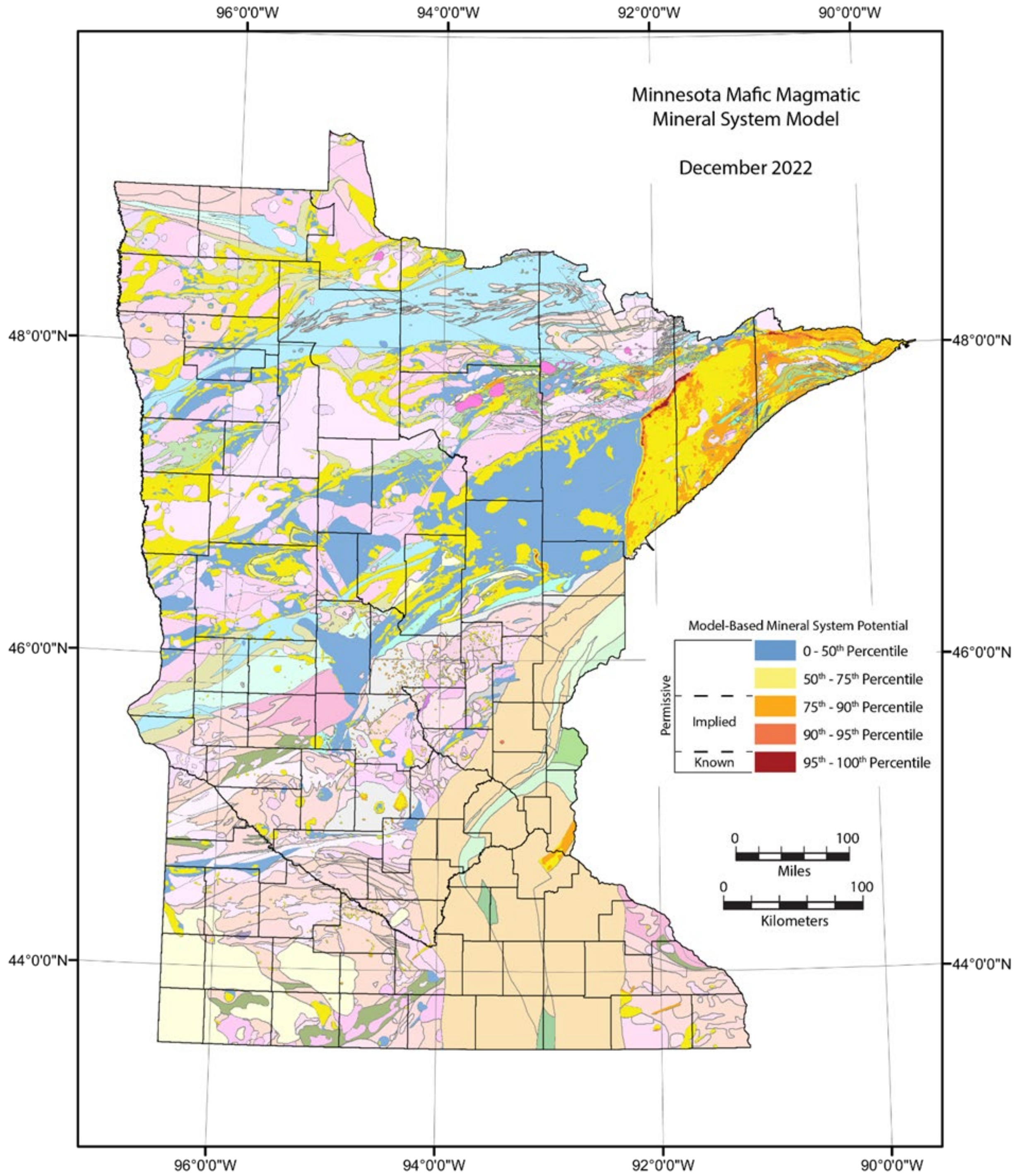

Figure 28. Results of ***Mafic Magmatic*** knowledge-based mineral system model with geology.

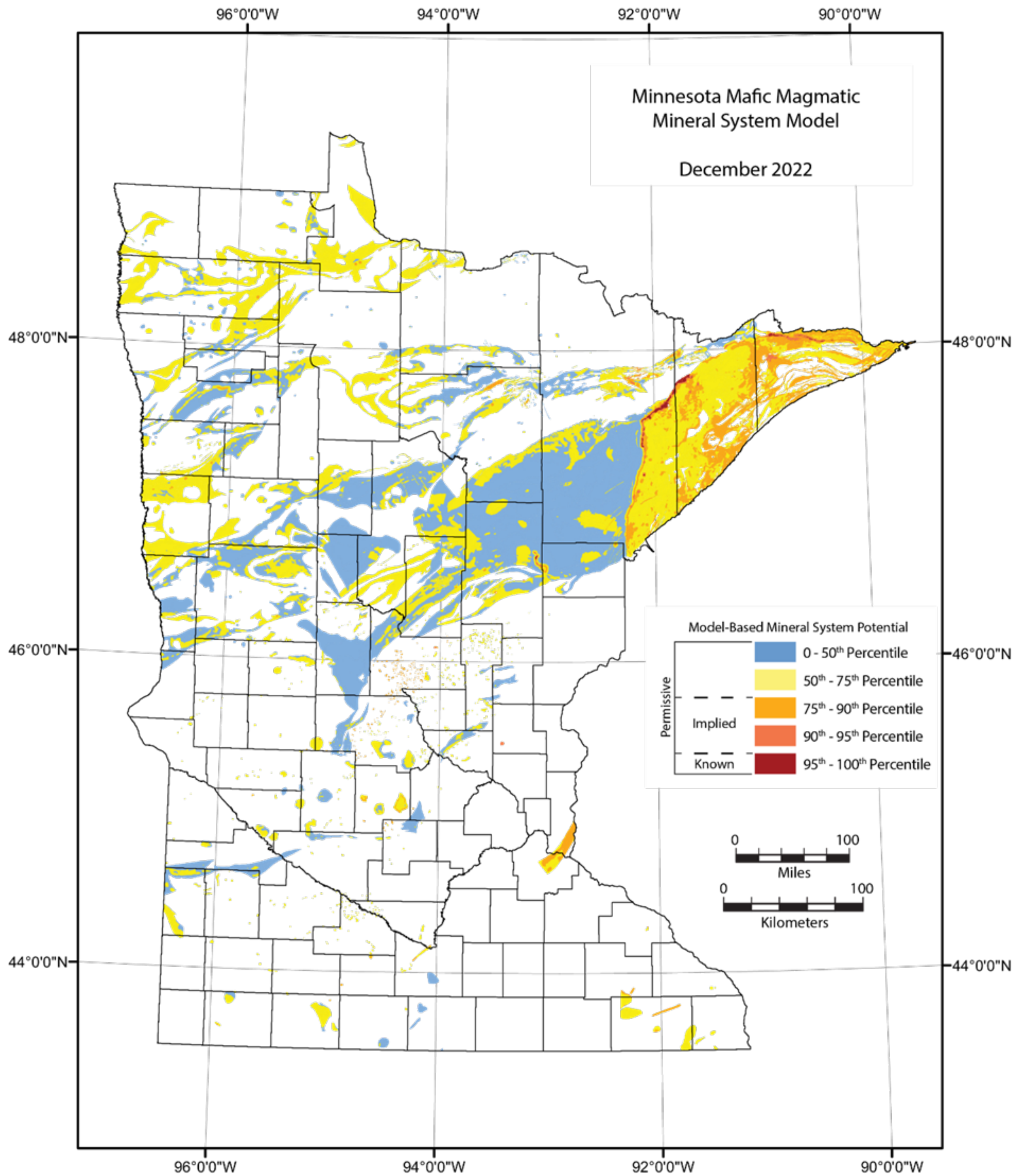

Figure 29. Results of ***Mafic Magmatic*** knowledge-based mineral system model without geology.

Several other areas within the state score highly (90th–95th percentile scores in the model). These include: 1) numerous regions in Cook, Lake, and St. Louis counties associated with the Mesoproterozoic Midcontinent Rift Intrusive Supersuite (Jirsa et al., 2011); 2) regions associated with ultramafic and mafic intrusive rocks associated with the Neoarchean Vermilion District; and 3) a small region in northeastern Itasca County comprising Neoarchean ultramafic to mafic hypabyssal intrusive complexes (Unit "Aag" of Jirsa et al., 2011). A few notable areas that scored moderately highly (75th–90th percentile scores in the model) including a region in north-central Polk County (associated with the Neorchean Mentor Mafic Igneous Complex (Jirsa et al., 2011) and a region that extends northeast-southwest through Dakota and Washington counties that is associated with Midcontinent-rift related rocks.

DISCUSSION

Regions with high potential to host the eight mineral systems modeled in this have been identified by means of fuzzy-logic modeling utilizing ArcMap® software. In general, the models have confirmed our general understanding of where these mineral systems may exist in Minnesota, and in some cases the models have identified new regions worthy of further study.

It is important to keep in mind that the mineral system models conducted in this study were limited by:

- Existing data in the Assembling Minnesota dataset: Although the Assembling Minnesota dataset is currently the most comprehensive seamless collection of geoscience-related geospatial data in the state known to the authors, it is *not a fully comprehensive collection of geospatial geoscience data for the state*. For example, rock type lithogeochemical classification is not part of the existing database, and this can hamper evaluations of mineral systems based on this type of data. The mineral occurrence database associated with the Assembling Minnesota dataset is based solely on hand sample identification – no petrographic analyses are included in the current mineral occurrence database. This can hamper evaluation of mineral systems, as petrographic analyses are more likely to provide accurate and more detailed mineralogical data than hand sample mineral identification alone. Also, the current Assembling Minnesota dataset does not include mineral chemistry data (e.g. electron microprobe data) – it is well known that the compositions of many solid-solution minerals can change in proximity to mineralization, and such changes could not be modeled given the data limitations.
- Time and Budget: The comprehensive development of fuzzy logic-based mineral system models takes a large amount of time. Sufficient time and budget were not available to add significant amounts of data to the existing Assembling Minnesota dataset. Given both time and budgetary constraints, the mineral system models developed in this study are relatively simple, and in many cases have focused on limited mineral deposit types within individual mineral systems. More complex models inclusive of all mineral deposit types within individual mineral systems may produce different results. As well, confirmation of the models could not be achieved with the time and budgetary constraints.

SUMMARY AND CONCLUSIONS

Eight mineral systems potentially present in Minnesota have been evaluated using fuzzy-logic modeling utilizing ArcMap® software. Data used to develop the models was derived from the NRRI Assembling Minnesota dataset. The eight mineral systems modeled include: 1) Placer; 2) Marine Chemocline; 3) Volcanogenic Seafloor; 4) Orogenic; 5) Metamorphic; 6) Alkalic Porphyry; 7) Magmatic REE; and 8) Mafic Magmatic. Inference nets have been developed and illustrate the fuzzy logic and components of each of the mineral system models.

Results of the modeling are summarized below by mineral system:

Placer Mineral System: Based on the modeling, the highest probabilities for the presence of a Placer mineral system occur in northeastern Minnesota and in southwestern Minnesota. In northeastern Minnesota, placer mineral system probabilities are highest within footwall rocks to the Biwabik iron formation, along with rocks immediately up-section from the Biwabik iron formation in the Virginia formation. Elevated potential for Placer mineral systems occurs in metasedimentary rocks associated with the Penokean Orogeny in northern and southern Crow Wing County and the southwestern part of Aitkin County. In southwestern Minnesota, elevated potential for Placer mineral systems occurs in southern Lincoln County, southwestern Lyon County, southern Nobles County, and in Cottonwood, Watonwan, and Martin counties. These areas correspond to the margins of the Paleoproterozoic Sioux Quartzite.

Marine Chemocline: Based on the modeling, the highest probabilities for the presence of Marine Chemocline mineral systems occur in northeastern and north-central Minnesota in rocks associated with the Animikie Basin and Penokean Orogeny strata. This modeling is consistent with the presence of the Biwabik iron formation in St. Louis and Itasca counties as well as the various iron formations associated with Penokean Orogeny strata in Aitkin and Crow Wing counties. As well, the model indicates high probabilities for the presence of the Marine Chemocline mineral system in western and southwestern Stearns County associated with interlayered volcanic, volcaniclastic, sedimentary, and hypabyssal intrusive rocks that comprise the Mille Lacs Group, North and South Range Groups, and Glen Township Formation (Jirsa et al., 2011).

Volcanogenic Seafloor: High potential for the presence of Volcanogenic Seafloor mineral systems was identified in both the Abitibi-Wawa and Wabigoon subprovinces. In the Abitibi-Wawa subprovince, this includes regions in St. Louis County associated with the Vermilion district and areas in northeastern Itasca County associated with the Wilson Lake sequence (Jirsa, 1990). Within the Wabigoon subprovince, enhanced potential for Volcanogenic Seafloor mineral systems occurs in east-central Lake of the Woods County and in northwestern Beltrami County. These findings are consistent with the presence of massive sulfide mineralization documented within the Assembling Minnesota database (Figure 12). A single region of high potential for the presence of a Volcanogenic Seafloor mineral system also occurs in north-central Marshall County.

Orogenic: Based on the modeling, the highest probabilities for the presence of Orogenic mineral system-associated orogenic gold deposits occur within the Abitibi-Wawa and Wabigoon subprovinces within the northernmost one-third of Minnesota. Within the Abitibi-Wawa subprovince, the highest probabilities for Orogenic mineral systems occur in the nortwestern and east-central part of St. Louis County, the northern one-third of Itasca County, the southernmost part of Koochiching County, western Hubbard County, and east-central Becker County. Within the Wabigoon subprovince, the highest probabilities for Orogenic mineral system-related mineralization occur in the northwestern part of Koochiching County, the southern one-third of Lake of the Woods County, the northwestern part of Beltrami County, the west-central part of Polk County, and within the east-central and northwestern parts of Marshall County. The modeled regions correlate well with the six areas of gold exploration identified by Severson (2011) as well as a weights of evidence model developed by Hartley (2014).

Metamorphic: The modeling conducted for this study indicates several regions where elevated potential for Metamorphic mineral systems exists. The highest modeled potential for such a system exists in east-central St. Louis County and northwestern Lake County. This region of modeled high potential may be a false positive, as the igneous rocks included in the model have anomalously high contents of nickel (and perhaps vanadium), and these igneous rocks are in contact with Paleoproterozoic and Neoarchean supracrustal rocks. Other small areas with modeled high potential occur within northeastern Koochiching County and are associated with Quetico subprovince high-grade metamorphic rocks that are in proximity to the Rainy Lake – Seine River Fault. An additional area of modeled high potential occurs in northeastern Itaca County, in proximity to the Coon Lake Pluton.

Alkalic Porphyry: GIS-based fuzzy-logic modeling conducted for this study indicates several regions where elevated potential for Alkalic Porphyry mineral systems exists. The areas with the highest modeled probability for having Alkalic Porphyry mineral systems occur in northeastern Minnesota with Lake, St. Louis, and Itasca counties. In northwestern Lake County, the highest modeled potential for Alkalic Porphyry mineral systems resides within the Giants Range Batholith. In St. Louis County, the highest potential lies within syenite, monzonite, granodiorites, and diorites that contain both hornblende and pyroxed (geologic unit "Asd" of Jirsa et al., 2011). In Itasca County, the highest modeled potential for Alkalic Porphyry mineral systems also occurs within "Asd" units, including the Coon Lake Pluton.

Magmatic REE: Based on our modeling, regions with the highest potential to be associated with the mineral system occur in south-central Lake County, north-central and northwestern St. Louis County, northeastern Itasca County, east-central Koochiching County, southeastern Marshall County, and east-central Stearns County. Within south-central Lake County, the highest modeled potential occurs within Mesoproterozoic age granophyric and granitic rocks (unit "Mbf" of Jirsa et al., 2011). High modeled potential for Magmatic REE mineral systems in St. Louis County is associated with syenite, monzodiorite, granodiorite, and diorite (rock unit "Asd" of Jirsa et al., 2011), including the Linden Pluton in northwestern St. Louis County. High potential in Itasca County is associated with syenite, monzodiorite, granodiorite, and diorite associated with the Coon Lake Pluton, and high modeled potential in east-central Koochiching County is associated with granite-rich migmatites (unit "Aqg" of Jirsa et al., 2011) within the Quetico subprovince. High modeled potential for Magmatic REE-associated mineral systems in southern Marshall County is associated with Neoarchean gabbro, peridotite, pyroxenite, lamprophyre, and metamorphic equivalents (unit "Agp" of Jirsa et al., 2011), and reddish, variably porphyritic granites of Paleoproterozoic age (unit “Pgr” of Jirsa et al., 2011) host the highest potential for a Magmatic REE mineral system in east-central Stearns County.

Mafic Magmatic: Fuzzy-logic modeling indicates the highest probability for the presence of Mafic Magmatic mineral systems occurs in northeastern Lake County, east-central St. Louis County, and within eastern Aitkin County. The model clearly has identified known disseminated to massive Cu-Ni-PGM deposits that occur in troctolitic rocks at the base of the Duluth Complex in Lake and St. Louis counties as well as Ti-V-oxide deposits and prospects associated with oxide ultramafic intrusions (peridotites, pyroxenites) that occur along the western margin of the Duluth Complex in central St. Louis County. As well, the model identified the Tamarack intrusion in eastern Itasca County, the host of the Tamarack Ni-Cu-Co deposit. Identification of these resources is not surprising, as the geological, mineralogical, geochemical, geochronological, geophysical, and resource confidence characteristics have all scored highly based on model parameters. Other areas with moderately-high potential for the presence of the Mafic Magmatic mineral system include: include: 1) numerous regions in Cook, Lake, and St. Louis counties associated with the Mesoproterozoic Midcontinent Rift Intrusive Supersuite (Jirsa et al., 2011); 2) regions associated with ultramafic and mafic intrusive rocks associated with the Neoarchean Vermilion District; and 3) a small region in northeastern Itasca County comprising Neoarchean ultramafic to mafic hypabyssal intrusive complexes (Unit “Aag” of Jirsa et al., 2011). A few notable areas scored moderately highly (75^{th}–90^{th} percentile scores in the model), including a region in north-central Polk County (associated with the Neorchean Mentor Mafic Igneous Complex (Jirsa et al., 2011) and a region that extends northeast-southwest through Dakota and Washington counties that is associated with Midcontinent-rift related rocks.

REFERENCES

Abedi, M, Norouzi, G-H., and Fathianpour, N., 2013, Fuzzy outranking approach: a knowledge-driven model for mineral prospectivity mapping: International Journal of Applied Earth Observation and Geoinformation, v. 21, p. 556-567.

Arndt, N. T., Lesher, C. M., and Cxamanske, G. K., 2005, Mantle-derived magmags and magmatic Ni-Cu-(PGE) deposits: Society of Economic Geologists, 100th Anniversary Volume, Littleton, CO, p. 5-23.

Ash, C., 1996, Podiform chromite: in Lefebure, D. V., and Hoy, T., (eds.), Selected British Columbia mineral deposit profiles, volume 2 – Metallic deposits: British Columbia Ministry of Employment and Investment, Open File 1996-13, p. 109-112.

Barnes, S.-J., and Lightfoot, P. C., 2005, Formation of magmatic nickel sulfide deposits and processes affecting their copper and platinum group element contencts: Society of Economic Geologists, 100th Anniversary Volume, Littleton, CO, p. 179-213.

Bartsch, W., Hudak, G., Kne, L., Wiringa, P., Ilyushkin, S., Post, S., and Nixon, K., 2022, Assembling Minnesota: NRRI Report submitted to Dr. James Wilgenbusch, Director of Computing at the University of Minnesota, 40 p.

Behera, S., and Panigrahi, M. K., 2021, Gold Prospectivity: Mapping in the Sonakhan Greenstone Belt, Central India: A Knowledge-Driven Guide for Target Delineation in a Region of Low Exploration Maturity: Natural Resources Research, v. 30, no. 6, p. 4009-4045.

Blatt, H. and Tracy, R. J., 1997, Petrology – Igneous, Sedimentary, and Metamorphic, 2nd Edition: W. H. Freeman and Company, New York, 529 p.

Bleeker, W., 2012, Targeted Geoscience Initiative (TGI-4) Lode Gold Deposits in Ancient Deformed and Metamorphosed Terranes: The role of extension in the formation of Timiskaming basins and large gold deposits, Abitibi greenstone belt–A discussion: in Summary of field work and other activities 2011; Ontario Geological Survey, Open File Report 6280, p. 47-1 to 47-12.

Bleeker, W., 2015, Syn-orogenic gold mineralization in granite-greenstone terranes: the deep onnection between extension, major faults, syn-orogenic clastic basins, magmatism, thrust inversion and long-term preservation: in Targeted Geoscience Initiative 4: Contributions to the Understanding of Precambrian Lode Gold Deposits and Implications for Exploration, B. Dube and P. Mercier-Langevin (eds.),Geological Survey of Canada, Open File 7852, p. 25–47.

Boerboom, T. J., 2021, D-07 Geochronology Database: Minnesota Geological Survey Open Data Site.

Bonham-Carter, G.F., 1994, Geographic Information Systems for Geoscientists: Modelling with GIS Computer Methods in the Geosciences 13, Elsevier, New York, NY, 397 p.

Bonham-Carter, G.F., Agterberg, F.P. and Wright, D.F., 1989, Weights of evidence modelling: a new approach to mapping mineral deposits: *in* Agterberg, F.P. and Bonham-Carter, G.F., (Eds.), 1989. Statistical Applications in Earth Sciences, Geological Survey of Canada , Paper 89-9, pp. 171-183.

Bonham-Carter, G.F., Galley, A.G. and Hall, G.E.M., (ed.) 1996, EXTECH I: A multidisciplinary approach to massive sulfide research in the Rusty Lake-Snow Lake greenstone belts, Manitoba: Geological Survey of Canada, Bulletin 426.

Bonham-Carter, G.F., Reddy, R.K.T. and Galley, A.G., 1993, Knowledge-driven Modeling of Volcanogenic Massive Sulfide Potential with a Geographic Information System: *in* Kirkham, R.V., Sinclair, W.D., Thorpe, R.I., and Duke, J.M., 1993, Mineral Deposit Modeling, Geological association of Canada, Special Paper 40, p. 735-749.

Bradley, D. C., McCauley, A. D., and Stillings, L. M., 2017, Mineral-deposit model for lithium-cesium-tantalum pegmatites: U. S. Geological Survey Scientific Investigations Report 2010-5070-O, 48 p.

Cannon, W. F., Kimball, B. E., and Corathers, L. A., 2017, Chapter L – Manganese; in Schulz, K. J., DeYoung, J. H., Jr., Seal, R. R., II, and Bradley, D. C., (eds.), Critical mineral resources of the United States – Economic and environmental geology and prospects for future supply: U. S. Geological Survey Professional Paper 1802, p. L1-L28.

Cawthorne, R. G., Barnes, S. J., Ballhaus, C., and Malitch, K. N., 2005, Platinum Group Element, Chromium, and Vanadium Deposits in Mafic and Ultramafic Rocks: Society of Economic Geologists, 100th Anniversary Volume, Littleton, CO, p. 215-249.

Černý, P., Blevin, P. L., Cuney, M., and London, D., 2005, Granite-Related Ore Deposits: Society of Economic Geologists, 100th Anniversary Volume, Littleton, CO, p. 337-370.

Chandler, V. W., 1982, S-11 Aeromagnetic anomaly map of Minnesota: Minnesota Geological Survey, retrieved from the University of Minnesota Digital Conservancy.

Chandler, V. W., and Lively, R. S., 2011, Upgrade of the Gravity Database: Minnesota Geological Survey, retrieved from the University of Minnesota Digital Conservancy.

Ciborowski, T. J. R., Minifie, M. J., Kerr, A. C., Ernst, R. E., Baragar, B., and Millar, I. L., 2017, A mantle plume origin for the Paleoproterozoic Circum-Superior Large Igneous Province: Precambrian Research, v. 294, p. 189-213.

CIM, 2014, CIM Definition Standards for Mineral Resources and Mineral Reserves: Canadian Institute of Mining, Metallurgy, and Petroleum.

Clout, J. M. F., and Simonson, B. M., 2005, Precambrian Iron Formations and Iron Formation-Hosted Iron Ore Deposits: Society of Economic Geologists, 100th Anniversary Volume, Littleton, CO, p. 643-679.

Dewane, T. J., and Van Schmus, W.R., 2007, U-Pb geochronology of the Wolf River batholith, north-central Wisconsin: Evidence for successive magmatism between 1484 Ma and 1468 Ma: Precambrian Research, v. 157, p. 215-234, dx.doi.org/10.1016/j.precamres.2007.02.018.

Dhinesh, S., Udayaganessan, P., Ramakrishnan, D., Rajani, R., and Xavier Ignaci Muthu, J., 2021, An integrated strategy for the exploration of palaeofluvial placer deposits: Applied Geomatics, v. 13, p. 165-177.

Dostal, J., 2016, Chapter 2 - Rare metal deposits associated with alkaline/peralkaline igneous rocks: in Verplanck, P. L., and Hitzman, M. W., (eds.), Reviews in Economic Geology, v. 18 - Rare earth and critical elements in ore deposits, p. 33-54.

Dostal, J., 2017, Rare earth element deposits of alkaline igneous rocks: Resources, v. 6, no. 34.

DSM Observer, 2020, Beyond batteries – Exploring the demand for scandium and tellurium from the deep ocean: Deep Sea Mining News & Resources.

Dubé, B., Mercier-Langevin, P., Castonguay, S., McNicoll, V.J., Bleeker, W., Lawley, C.J.M., De Souza, S., Jackson, S.E., Dupuis, C., Gao, J.-F., Bécu, V., Pilote, P., Goutier, J., Beakhouse, G.P., Yergeau, D., Oswald, W., Janvier, V., Fontaine, A., Pelletier, M., Beauchamp, A.-M., Katz, L.R., Kontak, D.J., Tóth, Z., Lafrance, B., Gourcerol, B., Thurston, P.C., Creaser, R.A., Enkin, R.J., El Goumi, N., Grunsky, E.C., Schneider, D.A., Kelly, C.J., and Lauzière, K., 2015, Precambrian lode gold deposits — a summary of TGI-4 contributions to the understanding of lode gold deposits, with an emphasis on implications for exploration, In: Targeted Geoscience Initiative 4: Contributions to the Understanding of Precambrian Lode Gold Deposits and Implications for Exploration: B. Dubé and P. Mercier- Langevin (eds.), Geological Survey of Canada, Open File 7852, p. 1–24.

Emsbo, P., 2000, Gold in SEDEX deposits: Reviews in Economic Geology, v. 13, p. 427-437.

Emsbo, P, McLaughlin, P. I., Breit, G. N., du Bray, E. A., and Koenig, A. E., 2015, Rare earth elements in sedimentary phosphate deposits – Solution to the global REE crisis?: Gondwana Research, v. 27, p. 776-785.

Ernst, R. E., and Jowitt, S. M., 2013, Chapter 2 - Large igneous provinces (LIPs) and metallogeny: in Colpron, M., Bissing, T., Rusk, B. G., and Thomson, J. F. H., (eds.), Tectonics, metallogeny, and discovery – The North American Cordillera and similar accretionary settings: Society of Economic Geologists, Special Publications Volume 17, p. 17-51.

Force, E. R., Paradis, S., and Simandl, G. J., 1999, Sedimentary manganese: in Simandl, G. J., Hora, Z. D., and Lefebure, D. V., (eds.), Selected British Columbia mineral deposit profiles, v. 3 – Industrial Minerals: British Columbia Ministry of Energy and Mines, Open File 1999-10, p. 47-50.

Franklin, J. M., Gibson, H. L., Jonasson, I. R., and Galley, A. G., 2005, Volcanogenic massive sulfide deposits: Society of Economic Geologists, 100th Anniversary Volume, Littleton, CO, p. 523-560.

Franklin, J. M., Lydon, J. W., and Sangster, D. M., 1981, Volcanic-associated massive sulfide deposits: Society of Economic Geologists, 75th Anniversary Volume, Littleton, CO, p. 485-627.

Franklin, J. M., Sangster, D. M., and Lydon, J. W., 1981, Volcanic-associated massive sulfide deposits: Society of Economic Geologists, 75th Anniversary Volume, Littleton, CO, p. 485-627.

Galetakis, M., and Vasiliou, A., 2012, Chapter 10 - Applications of Fuzzy Inference Systems in Mineral Industry – Overview: in Segura, J. M., and Reiter, A. C. (eds), Expert System Software, Nova Science Publishers, Inc., Hauppauge, N.Y., p. 211-226.

Garnett, R. H. T. and Bassett, N. C., 2005, Placer Deposits: Society of Economic Geologists, 100th Anniversary Volume, Littleton, CO, p. 813-843.

Gibson , H. L., Allen, R. L., Riverin, G., and Lane, T. E., 2007, The VMS Model: Advances and Application to Exploration Targeting: in Milkereit, B. (ed.), Proceedings of Exploration 07: Fifth Decennial International Conference on Mineral Exploration, p. 713-730.

Gibson, H. L., Morton, R. L., and Hudak, G. J., 1999, Submarine volcanic processes, deposits, and environments favorable for the location of volcanic-associated massive sulfide deposits: Reviews in Economic Geology, v. 8, p. 13-51.

Goldfarb, R. J., Baker, T., Dubé, B., Groves, D. I., Hart, C. J. R., and Gosselin, P., 2005, Distribution, character and genesis of gold deposits in metamorphic terranes: Society of Economic Geologists, 100th Anniversary Volume, Littleton, CO, p. 407-450

Goldfarb, R. J., Hofstra, A. H., and Simmons, S. F., 2016, Chapter 10 - Critical elements in Carlin, epithermal and orogenic gold deposits; in Verplank, P. L., and Hitzman, M. W., (eds.), Reviews in Economic Geology, v. 18 – Rare earth and critical elements in ore deposits, p. 217-244.

Groves, D. I., Goldfarb, R. J., Gebre-Mariam, M., Hageman, S. G., and Robert, F., 1998, Orogenic gold deposits – A proposed classification in the context of their crustal distribution and relationship to other gold deposit types: Ore Geology Reviews, v. 13, no 1-5, p. 7-27.

Groves, D. I., Santosh, M., and Zhang, L., 2020, A scale-integrated exploration model for orogenic gold deposits based on a mineral system approach: Geoscience Frontiers, v. 11, p. 719-738.

Gumsley, A. P., Chamberlain, K. R., Bleeker, W., Söderlund, U., de Kock, M. O., Larsson, E. R., and Bekker, A., 2017, Timing and tempo of the Great Oxidation Event: Proceedings of the National Academy of Sciences, v. 114, no. 8, p. 1811-1816.

Hannington, M. D., de Ronde, C. E. J., and Petersen, S., 2005, Sea-floor tectonics and submarine hydrothermal systems: Society of Economic Geologists, 75th Anniversary Volume, Littleton, CO, p. 111-141.

Hartley, B. K., 2014, Evaluation of weights of evidence to predict gold occurrences in northern Minnesota's Archean greenstone belts: unpublished M. S. Thesis, University of Southern California, 55 p.

Hauck, S.A., Heine, J.J., Severson, M.J., Post, S.P., Chlebecek, S., Monson Geerts, S.D., Oreskovich, J.A., Gordee, S.M., and Hudak, G., 2014, Geological and Geochemical Reconnaissance for Rare Earth Element Mineralization in Minnesota: Natural Resources Research Institute, University of Minnesota Duluth, Technical Report NRRI/TR-2014/39, 572 p.

Hofstra, A. H. and Kreiner, D. C., 2021, Systems-Deposits-Commodities-Critical Minerals Table for the Earth Mapping Resources Initiative (ver. 1.1, May 2021): U. S. Geological Survey Open-File Report 2020-1042, 26 p.

Hofstra, A., Lisitsin, V., Corriveau, L., Paradis, S., Peter, J., Lauziére, K., Lawley, C., Gadd, M., Pilote, J., Honsberger, I, Bastrakov, E., Champion, D., Cxarnota, K., Doublier, M., Houston, D., Raymond, O., VanDerWielen, S., Emsbo, P., Granitto, M., and Kreiner, D., 2021, Deposit classification scheme for the Critical Minerals Mapping Initiative Global Geochemical Database: U. S. Geological Survey Open-File Report 2021-1049, 60 p.

Hudak, G. J., Morton, R. L., Franklin, J. M., and Peterson, D. M., 2003, Morphology, distribution, and estimated eruption volumes for intracaldera tuffs associated with volcanic-hosted massive sulfide deposits in the Archean Sturgeon Lake Caldera Complex, northwestern Ontario: in White, J. D. L., Smellie, J. L, and Clague, D. A., (eds) Explosive Submarine Volcanism: American Geophysical Union Monograph Series, v. 140, p. 345-360.

Hudak, G.J., and Peterson, D., 2014, Non-Ferrous Mineralization Associated with the Wawa Abitibi Terrane and Duluth Complex Cu-Ni-PGM Deposits, NE Minnesota: Society of Economic Geologists, SEG Guidebook Series Guidebook 47, 150 p.

International Atomic Energy Agency (IAEA), 2020, Descriptive uranium deposit and mineral system models: Vienna, Austria, International Atomic Energy Association, 313 p.

James, H. L., 1954, Sedimentary facies of iron-formations: Economic Geology, v. 49, p. 235-293.

Jensen, E. P., and Barton, M. D., 2000, Chapter 8 – Gold deposits related to alkaline magmatism; in Hagemann, S. G., and Brown, P. E., (eds.), Reviews in Economic Geology, v. 13, p. 279-314.

Jirsa, M. A., 1990, Bedrock geologic map of northeastern Itasca County, Minnesota: Minnesota Geological Survey, Miscellaneous Map Series Map M-068, retrieved from the University of Minnesota Digital Conservancy.

Jirsa, M. A., Boerboom, T. J., Chandler, V. W., 2012, S-22 Geologic Map of Minnesota, Precambrian Bedrock Geology: Minnesota Geological Survey, retrieved from the University of Minnesota Digital Conservancy,.

Jirsa, M. A., Boerboom, T. J., Chandler, V. W., Mossler, J. H., Runkel, A. C., and Setterholm, D. R., 2011, S-21 Geologic Map of Minnesota – Bedrock Geology: Minnesota Geological Survey, retrieved from the University of Minnesota Digital Conservancy.

Jones, J. V., III, Piatak, N. M., and Bedinger, G. M., 2017, Chapter V - Zirconium and hafnium: in Schulz, K. J., DeYoung, J. H., Jr., Seal, R. R., II, and Bradley, D. C., (eds.), Critical mineral resources of the United States – Economic and environmental geology and prospects for future supply: U. S. Geological Survey Professional Paper 1802, p. D1-D18.

Kalinin, A. A., and Kudryashov, N. M., 2021, Porphyry-related metamorphosed Au-Ag and Cu-Mo deposits in the Precambrian of the Fennoscandian Shield: Minerals, v. 11, 139.

Kelley, K. D., and Spry, P. G., 2016, Chapter 9 - Critical elements in alkaline igneous rock-related epithermal gold deposits: in Verplanck, P. L., and Hitzman, M. W., (eds.), Reviews in Economic Geology, v. 18, Rare Earth earth and critical elements in ore deposits, p[. 195-216.

Le Bas, M. J., Le Maitre, R. W., Streckeisen, A., and Zenettin, B., 1986, A chemical classification of volcanic rocks based on the total alkali-silica diagram: Journal of Petrology, v. 27, p. 745-750.

Le Valliant, M., Fiorentini, M. L., and Barnes, S. J., 2018, Chapter 2 - Review of predictive and detective exploration tools for magmatic Ni-Cu-(PGE) deposits, with a focus on komatiite-related systems in Western Australia: in Mondal, S. K. and Griffen, W. L., (eds.), Processes and Ore Deposits of Ultramafic-Mafic Magmas through Space and Time, p. 47-78.

Lefebure, D. V., and Coveny, R. M., Jr., 1995, Shale-hosted Ni-Zn-Mo-PGE: in Lefebure, D. V. and Ray, G. E., (eds.), Selected British Columbia mineral deposit profiles, v. 1 – Metallics and coal: British Columbia Ministry of Employment and Investment, Open File 1995-20, p. 45-48.

Levson, V. M., 1995, Marine placers: in Lefebure, D. V. and Ray, G. E., (eds.), Selected British Columbia mineral deposit profiles, v. 1 – Metallics and coal: British Columbia Ministry of Employment and Investment, Open File 1995-20, p. 29-31.

Li, C., Yue, J., and Zhang, Y., 1985, Research on geological background and origin of Liu Mao graphite deposits, Heilongjiang Province: in Cheng, Y., (ed.), International Symposium on Metallogeny of the Early Precambrian: Abstracts, Organizational Committee of the International Symposium of Metallogeny, China, p. 108-109.

Lindsay, M. D., Betts, P. G., and Ailleres, L., 2014, Data fusion and porphyry copper prospectivity models, southeastern Arizona: Ore Geology Reviews, v. 61, p. 120-140.

London, D., 2016, Rare-element granitic pegmatites: Reviews in Economic Geology, v. 18, p. 165-193.

Luque, F. J., Huizenga, J. M., Crespo-Feop, E., Wada, H., Ortega, L., and Barrenechea, J. F., 2014, Vein graphite deposits – Geological settings, origin, and economic significance: Mineralium Deposita, v. 49, no. 2, p. 261-277.

Ma, Y., Zhao, J., Sui, Y., Liao, S., Zhang, Z., 2020, Application of Knowledge-Driven Methods for Mineral Prospectivity Mapping of Polymetallic Sulfide Deposits in the Southwest Indian Ridge between 46° and 52°E: Minerals, volume 10, 970.

Maniar, P. D., and Piccoli, P. M., 1989, Tectonic discrimination of granitoids: Geological Society of America Bulletin, v. 101, p. 635-643.

Marjoribanks, R., 2010, Geological Methods in Mineral Exploration and Mining, 2nd Edition: Springer, Heidelberg, 238 p.

McKinney, S. T., Cottle, J. M., and Lederer, G. W., 2015, Evaluating rare earth element (REE) mineralization mechanisms in Proterozoic gneiss, Music Valley, California: Geological Society of America Bulletin, v. 127, p. 1135-1152.

McSwiggen, P. L., Morey, G. B., and Cleland, J. M., 1995, Iron-formation protolith and genesis, Cuyuna Range, Minnesota: Minnesota Geological Survey Report of Investigations 45, 54 p.

Menzel, M. D., Garrido, C. J., Sánchez-Vizcaíno, V. L., Marchesi, C, Hidas, K., Escayola, M. P., and Huertas, A. D., 2018, Carbonation of mantle peridotite by CO2-rich fluids – The formation of listvenites in the Advocate ophiolite complex (Newfoundland, Canada): Lithos, v. 323, p. 238-261.

Mondal, S. K., and Griffin, W. L., (eds.), 2018, Processes and ore deposits of ultramafic-mafic magmas through space and time: Elsevier, Amsterdam, 364 p.

Monecke, T., Peterson, S., Hannington, M. D., Grant, H., and Samson, S. I., 2016, Chapter 11 - The minor element endowment of modern sea-floor massive sulfides in comparison with deposits hosted in ancient volcanic successions; in Verplanck, P. L., and Hitzman, M. W., (eds.), Reviews in Economic Geology, v. 18 – Rare earth and critical elements in ore deposits, p. 245-306.

Morton, R.L. and Franklin, J.M. 1987. Two-fold classification of Archean volcanic-associated massive sulfide deposits. Economic Geology, v. 82, p. 1057-1063.

Nicholson, S.W., Cannon, W.F., Schulz, K.J., 1992, Metallogeny of the Midcontinent Rift System of North America: Precamb. Res. 58, 355-386.

Niiränen, T., Nykänen, V., Lahti, I., 2019, Scalability of the mineral prospectivity modelling – An orogenic gold case study from northern Finland: Ore Geology Reviews, v. 109, p. 11-25.

Ojakangas, R. W., 2009, Roadside Geology of Minnesota: Mountain Press Publishing Company, Misoula, Montana, 353 p.

Orris, G. J., and Bliss, J. D., (eds.), 1991, Some industrial mineral deposit models – Descriptive deposit models: U. S. Geological Survey Open-File Report 91-11A, 73 p.

Patyk-Kara, N. G., 1976, Forms and features of zoning in placers: Geology and Mineral Resources, v. 11, part 2, p. 204-210.

Percival, J. A., and Bleeker, W., 2019, Orogenic gold systems in 3-D space and time: Acta Geologica Sinica, v. 93, p. 226-227.

Peterson, D. M., 2001, Development of Archean lode-gold and massive sulfide deposit exploration models using geographic information system applications: targeting mineral exploration in northeastern Minnesota from analysis of analog Canadian mining camps: unpublished Ph. D. dissertation, University of Minnesota, 503 p.

Peterson, D. M., 2018, Assembling Minnesota: Integration of 140 Years of Government, Academic, and Industry Geologic Studies into a Seamless Statewide GIS Database: 64th Annual Meeting, Institute on Lake Superior Geology, Proceedings Volume 64, Part 1 – Program and Abstracts, p. 81-82.

Porwal, A., Carranza, E. J. M., and Hale, M., 2003, Knowledge-driven and Data-driven Fuzzy Models for Predictive Mineral Potential Mapping: Natural Resources Research, v. 12, no. 11, p. 1-25.

Robert, F., Poulsen, K. H., Cassidy, K. F., and Hodgson, C. J., 2005, Gold metallogeny of the Superior and Yilgarn cratons: Society of Economic Geologists, 100th Anniversary Volume, Littleton, CO, p. 1001-1033.

Robinson, G. R., Jr., Hammarstrom, J. M., and Olson, D. W., 2017, Chapter J – Graphite, in Schulz, K. J., DeYoung, J. H., Jr., Seal, R. R., II, and Bradley, D. C., (eds.), Critical mineral resources of the United States – Economic and environmental geology and prospects for future supply: U. S. Geological Survey Professional Paper 1802, p. J1-J24.

Saljoughi, B. S., Hezarkhani, A., and Farahbakhsh, E., 2018, A comparison between knowledge-driven fuzzy and data-driven artificial neural network approaches for prospecting porphyry Cu mineralization: a case study of Shahr-e-Babak area, Kerman Province, SE Iran: Journal of Mining & Environment, v. 9, no. 4, p. 917-940, DOI: 10.22044/jme.2018.6752.1495.

Schulte, R. F., Taylor, R. D., Piatak, N. M, and Seal, R. R., II, 2012, Chapter E – Stratiform chromite deposit model: Mineral deposit models for resource assessment, U. S. Geological Survey Scientific Investigations Report 2010-5070-E, 131 p.

Schulz, K. J., Woodruff, L. G., Nicholson, S. W., Seal, R. R., Piatak, N. M., Chandler, V. W., and Mars, J. L., 2014, Occurrence model for magmatic sulfide-rich nickel-copper-(platinum group element) deposits related to mafic and ultramafic dike-sill complexes: U.S. Geological Survey Scientific Investigations Report 2010-5070-I, 80 p.

Seedorf, E., Dilles, J. H., Proffett, J. M. Jr., Einaudi, M. T., Zurcher, L., Stavast, W. J. A., Johnson, D. A., and Barton, M. D., 2005, Porphyry deposits: characteristics and origin of hypogene features: Society of Economic Geologists, 100th Anniversary Volume, Littleton, CO, p. 251-298.

Sengupta, D., and Van Gosen, B. S., 2016, Chapter 4 – Placer-type rare earth element deposits: in Verplanck, P. L., and Hitzman, M. W., Reviews in Economic Geology, v. 18 – Rare earth and critical elements in ore deposits, p. 81-100.

Severson, M. J., 1995, Geology of the southern portion of the Duluth Complex: Natural Resources Research Institute Technical Report NRRI/GMIN-TR-95/26, 217 p.

Severson, M. J., 2011, The history of gold exploration in Minnesota: Natural Resources Research Institute Technical Report NRRI/TR-2011/43, 171 p.

Severson, M. J., and Hauck, S. A., 1990, Geology, geochemistry, and stratigraphy of a portion of the Partridge River intrusion: Natural Resources Research Institute Technical Report NRRI/GMIN-TR-89-11, 236 p.

Severson, M. J., and Heine, J., 2003, Sedimentary Exhalative (SEDEX) Potential of the Cuyuna North Range, Cuyuna South Range, Emily District, and Portions of Aitkin County – Old Drill Log Searches: Natural Resources Research Institute Technical Report NRRI/TR-2003/13, 37 pages.

Severson, M. J., Zanko, L. M., Hauck, S. A., and Oreskovich, J. A., 2003, Geology and SEDEX Potential of Early Proterozoic Rocks, East Central Minnesota: Natural Resources Research Institute Technical Report NRRI/TR-2003/35, 160 p.

Shanks, W. C., III, and Thurston, R., 2012, Volcanogenic massive sulfide occurrence model: U. S. Geological Survey Scientific Investigations Report 2010-5070-C, 345 p.

Sloan, R. E., 1964, The Cretaceous system in Minnesota: Minnesota Geological Survey, Report of Investigations 5, 64 p.

Sutherland, W. M., and Cola, E. C., 2016, A comprehensive report on rare earth elements in Wyoming: Wyoming State Geological Survey Report of Investigations 71, 137 p.

Sutphin, D. M., 1991a, Descriptive model of amorphous graphite (Model 18k): in Orris, G. J., and Bliss, J. D., (eds.), Some industrial mineral deposit models – Descriptive deposit models: U. S. Geological Survey Open-File Report 91-11A, p. 9-10.

Sutphin, D. M., 1991b, Descriptive model of disseminated flake graphite (Model 37f): in Orris, G. J., and Bliss, J. D., (eds.), Some industrial mineral deposit models – Descriptive deposit models: U. S. Geological Survey Open-File Report 91-11A, p. 55-57.

Sutphin, D. M., 1991c, Descriptive model of graphite veins (Model 37g): in Orris, G. J., and Bliss, J. D., (eds.), Some industrial mineral deposit models – Descriptive deposit models: U. S. Geological Survey Open-File Report 91-11A, p. 58-60.

Tichy, L., and Turnovec, I., 1978, On possible geochemical identification of graphite in south Bohemia [in Czech]: Geologicky Pruzkum, v. 20, p. 73-75.

Thakurta, J., Rupp, K., and Haag, B., 2022, Episodic nature of magmatic ascent in a dynamic conduit system: evidence from a late gabbroic intrusion associated with the Eagle Ni-Cu sulfide deposit in northern Michigan, USA: Economic Geology, v. 117, no. 5, p. 1105-1130.

Trendall, A. F. and Blockley, J. G., 2004, 5.4 Precambrian Iron-Formation: in Eriksson, P. G., Altermann, W., Nelson, D. R., Mueller, W. U., and Catuneanu, O., (eds.), Developments in Precambrian Geology 12 – The Precambrian Earth: Tempos and Events: Elsevier, Amsterdam, p. 403-421.

Van Gosen, B. S., Fey, D. L., Shah, A. K., Verplanck, P. L., and Hoefen, T. M., 2014, Deposit model for heavy-mineral sands in coastal environments: U. S. Geological Survey Scientific Investigations Report 2010-5070-L, 51 p.

Verplanck, P. L., Mariano, A. N., and Mariano, A., Jr., 2016, Chapter 1 - Rare earth elements in carbonatites: in Verplanck, P. L., and Hitzman, M. W., (eds.), Reviews in Economic Geology, v. 18 – Rare earth and critical elements in ore deposits, p. 5-32.

Verplanck, P. L., Van Gosen, B. S., Seal, R. R., and McCafferty, A. E., 2014, A deposit model for carbonatite and peralkaline intrusion-related rare earth element deposits: U. S. Geological Survey Scientific Investigations Report 2010-5070-J, 58 p.

Virtanen, V. J., Heinonen, J. S., Barber, N. D., and Molnár. F., 2022, Complex effects of assimilation of sulfide saturation revealed by modeling with the magma chamber simulator: A case study on the Duluth Complex, Minnesota, USA: Economic Geology, v. 117, no 8, p. 1881-1899.

Wang, Z., Li, M. Y. H., Liu, Z. R. R., and Zhou, M. F., 2021, Scandium – Ore deposits, the pivotal role of magmatic enrichment and future exploration: Ore Geology Reviews, v. 128, article no. 103906.

Warke, M. R., Di Rocco, T., Zerkle, A. L., Lepland, A., Prave, A. R., Martin, A. P., Ueno, Y., Condon, D. J., and Claire, M. W., 2020, The Great Oxidation Event preceded a Paleoproterozoic "snowball Earth": Proceedings of the National Academy of Sciences, v. 117, no. 24, p. 13314-13320.

Woodruff, L. G., Nicholson, S. W., and Fey, D. L., 2013, A deposit model for magmatic iron-titanium-oxide deposits related to Proterozoic massif anothosite plutonic suites: U. S. Geological Survey Scientific Investigations Report 2010-5070-K, 47 p.

Zalenski, E., and Peterson, V. L., 1995, Depositional setting and deformation of massive sulfide deposits, iron formation, and associated alteration in the Manitouwadge Greenstone Belt, Superior Province, Ontario: Economic Geology, v. 90, p. 2244-2261.

Zientek, M. L., Loferski, P. J., Parks, H. L., Schulte, R. F., and Seal, R. R., II, 2017, Chapter N - Platinum-group elements: in Schulz, K. J., DeYoung, J. H., Seal, R. R., II, and Bradley, D. C., (eds.), Critical mineral resources of the United States – Economic and environmental geology and prospects for future supply: U. S. Geological Survey Professional Paper 1802, p. N1-N91.

DIGITAL APPENDICES

Digital Appendix 1: Shapefiles and Model Calculations – Placer Mineral System Model

Digital Appendix 2: Shapefiles and Model Calculations – Marine Chemocline Mineral System Model

Digital Appendix 3: Shapefiles and Model Calculations – Volcanogenic Seafloor Mineral System Model

Digital Appendix 4: Shapefiles and Model Calculations – Orogenic Mineral System Model

Digital Appendix 5: Shapefiles and Model Calculations – Metamorphic Mineral System Model

Digital Appendix 6: Shapefiles and Model Calculations – Alkalic Porphyry Mineral System Model

Digital Appendix 7: Shapefiles and Model Calculations – Magmatic REE Mineral System Model

Digital Appendix 8: Shapefiles and Model Calculations – Mafic Magmatic Mineral System Model